NOTE TO USERS

This reproduction is the best copy available.

UMI®

uOttawa

L'Université canadienne
Canada's university

FACULTÉ DES ÉTUDES SUPÉRIEURES ET POSTOCTORALES

uOttawa

L'Université canadienne
Canada's university

FACULTY OF GRADUATE AND POSDOCTORAL STUDIES

Yun Lin

AUTEUR DE LA THÈSE / AUTHOR OF THESIS

Ph.D. (Chemical Engineering)

GRADE / DEGREE

Department of Chemical and Biological Engineering

FACULTÉ, ÉCOLE, DÉPARTEMENT / FACULTY, SCHOOL, DEPARTMENT

Improving the Production of High Molecular Weight Pullulan Using a New Radial Reciprocating Plate Impeller

TITRE DE LA THÈSE / TITLE OF THESIS

Jules Thibault

DIRECTEUR (DIRECTRICE) DE LA THÈSE / THESIS SUPERVISOR

Jason Zhang

CO-DIRECTEUR (CO-DIRECTRICE) DE LA THÈSE / THESIS CO-SUPERVISOR

Xudong Cao

Arturo Macchi

David Taylor

Alberto Tecante (UNAM – Mexico)

Gary W. Slater

Le Doyen de la Faculté des études supérieures et postdoctorales / Dean of the Faculty of Graduate and Postdoctoral Studies

IMPROVING THE PRODUCTION OF HIGH MOLECULAR WEIGHT PULLULAN USING A NEW RADIAL RECIPROCATING PLATE IMPELLER

Yun Lin

Thesis Submitted to the
Faculty of Graduate and Postdoctoral Studies
In Partial Fulfillment of the Requirements for the Degree of
Doctorate in Philosophy

In

Department of Chemical and Biological Engineering
UNIVERSITY OF OTTAWA

©Yun Lin, Ottawa, Canada, 2010

Library and Archives Canada

Published Heritage Branch

395 Wellington Street
Ottawa ON K1A 0N4
Canada

Bibliothèque et Archives Canada

Direction du Patrimoine de l'édition

395, rue Wellington
Ottawa ON K1A 0N4
Canada

Your file Votre référence
ISBN: 978-0-494-69126-7
Our file Notre référence
ISBN: 978-0-494-69126-7

NOTICE:

The author has granted a non-exclusive license allowing Library and Archives Canada to reproduce, publish, archive, preserve, conserve, communicate to the public by telecommunication or on the Internet, loan, distribute and sell theses worldwide, for commercial or non-commercial purposes, in microform, paper, electronic and/or any other formats.

The author retains copyright ownership and moral rights in this thesis. Neither the thesis nor substantial extracts from it may be printed or otherwise reproduced without the author's permission.

AVIS:

L'auteur a accordé une licence non exclusive permettant à la Bibliothèque et Archives Canada de reproduire, publier, archiver, sauvegarder, conserver, transmettre au public par télécommunication ou par l'Internet, prêter, distribuer et vendre des thèses partout dans le monde, à des fins commerciales ou autres, sur support microforme, papier, électronique et/ou autres formats.

L'auteur conserve la propriété du droit d'auteur et des droits moraux qui protège cette thèse. Ni la thèse ni des extraits substantiels de celle-ci ne doivent être imprimés ou autrement reproduits sans son autorisation.

In compliance with the Canadian Privacy Act some supporting forms may have been removed from this thesis.

While these forms may be included in the document page count, their removal does not represent any loss of content from the thesis.

Conformément à la loi canadienne sur la protection de la vie privée, quelques formulaires secondaires ont été enlevés de cette thèse.

Bien que ces formulaires aient inclus dans la pagination, il n'y aura aucun contenu manquant.

Canada

ABSTRACT

Pullulan is a natural biopolymer with many useful traits. It has been produced commercially through fermentation with *Aureobasidium pullulans* at a fairly stable level for decades. Yet, the use of pullulan has been largely limited to the food industry due to its relatively high price. This research project was carried out in order to improve the cost efficiency in the mass production of high molecular weight pullulan and hopefully render it more economically available for many of its potential applications. One of the main challenges in its production is the mixing of viscous non-Newtonian broth that is formed gradually through fermentation. A new radial reciprocating plate impeller was designed based on the axial reciprocating plate impeller, which was shown to be efficient when dealing with highly viscous non-Newtonian media. The new design was focused on making the mechanism of the axial reciprocation more adaptable to existing industrial mixing devices. A prototype of this new impeller was built and tested to determine its power requirement and mass transfer characteristics in a laboratory scale bioreactor. Compared to a triple Rushton impeller and an axial reciprocating plate impeller, the new impeller proved to be efficient in different media with a wide range of rheological properties. Simulation using computational fluid dynamics also confirmed that mixing using this new impeller was more uniform compared to the triple Rushton impeller.

Experimental designs were employed to optimize the mass production of high molecular weight pullulan using this new impeller. An exopolysaccharide productivity of 0.30 $gL^{-1}h^{-1}$ was obtained while maintaining the molecular weight of pullulan, which is indicated by the broth viscosity, at a high level. The findings of this study provide a new way to adequately mix viscous broth of aerobic fermentations. Also, this new radial reciprocating plate impeller should be easily adapted to large scale industrial bioreactors to achieve more uniform mixing in rheologically-evolving fermentation broths.

RÉSUMÉ

Le pullulan est biopolymère naturel possédant des caractéristiques très intéressantes. Il a été produit commercialement par fermentation en utilisant le microorganisme *Aureobasidium pullulans* depuis de nombreuses années. Pourtant, l'utilisation du pullulan a été grandement limitée à l'industrie alimentaire en raison de son prix relativement élevé. Ce projet de recherche avait pour objectif d'améliorer la production de pullulan à haut poids moléculaire et le rendre plus économiquement acceptable pour favoriser une plus grande utilisation dans un plus grand nombre d'applications. Un des principaux défis lors de sa production est le mélange du milieu visqueux et non-Newtonien qui apparaît progressivement lors de la fermentation. Un nouveau mélangeur rotatif à plaques perforées a été conçu basé sur le mélangeur axial à plateaux perforés, qui a démontré de bonnes performances pour le mélange de milieux visqueux non-Newtoniens. Les efforts de la conception de ce mécanisme de mélange ont été mis afin de l'adapter aux systèmes industriels actuels de mélange. Un prototype de ce nouveau mécanisme de mélange a été construit et évalué pour déterminer sa consommation énergétique et sa performance pour le transfert de matière dans un bioréacteur à l'échelle de laboratoire. Comparé au mécanisme de mélange utilisant trois turbines de Rushton et au mélangeur axial à plateaux perforés, ce nouveau mécanisme de mélange s'est avéré être particulièrement bien adapté pour différents milieux montrant des changements importants de ses propriétés rhéologiques. Les études de simulations numériques par volume de contrôle ont aussi confirmé que le mélange résultant de ce nouveau mécanisme était plus uniforme comparé aux trois turbines de Rushton.

Deux plans d'expérience ont été utilisés pour optimiser la production du pullulan à haut poids moléculaire avec ce nouveau type de mélangeur. Une productivité d'exo polysaccharide de 0.30 $gL^{-1}h^{-1}$ a été obtenue tout en maintenant le poids moléculaire du pullulan, indiqué par la viscosité élevée du bouillon de fermentation, à un niveau élevé. Les résultats de cette étude suggèrent que le nouveau mécanisme de mélange est adéquat pour mélanger les bouillons visqueux de fermentations aérobies. Aussi, ce nouveau mélangeur rotatif à plaques perforées pourrait être facilement adapté aux bioréacteurs

industriels de grand volume pour permettre un mélange plus uniforme des bouillons de fermentation dont la rhéologie évolue grandement en fonction du temps.

谨以此文献给我的父母

Dedicated to my parents

STATEMENT OF CONTRIBUTIONS OF COLLABORATORS

I hereby declare that I am the sole author of this thesis. I have performed the experimental design, all experiments, and the associated data analysis. I have written all papers contained in this thesis with editorial comments and corrections performed by my supervisors, Dr. Jules Thibault and Dr. Jason Zhang.

The review on the pullulan production methods (Chapter 2) was done in collaboration with Dr. Anh LeDuy (Laval University) and one of my supervisors.

The first few bioreactor tests using triple Rushton impellers were performed with the guidance of Nilesh Patel who had abundant experience on the operation of the two bioreactors in our laboratory with his own research project.

Signature: _____ Date: May 13th, 2010

ACKNOWLEDGEMENT

I wish to express my grateful appreciation and respect to my supervisors, Dr. Jules Thibault and Dr. Jason Zhang, for their guidance, invaluable advices, support as well as constructive criticism throughout the course of my postgraduate program.

I would like to thank all professors and support staff at the Department of Chemical and Biological Engineering, especially our technicians, Louis Tremblay, Gérard Nina and Franco Ziroldo for their invaluable technical help and suggestions.

I sincerely appreciate the friendship of my lab mates and friends in the department: Nilesh Patel, Philippe Malouf, Viviane Choy, Xin Li, Caoyang Feng, and Liang Li.

Finally, I wish to thank my wife, Juan, for her love, support and patience while I worked on my thesis.

TABLE OF CONTENTS

LIST OF TABLES

LIST OF FIGURES

CHAPTER 1

INTRODUCTION

The polysaccharide production by *Aureobasidium pullulans* was first observed and documented by Bauer (1938). This polysaccharide was first isolated and characterized by Bernier (1958). It was named as "Pullulan" by Bender et al. (1959), who did more investigation on this novel polysaccharide. The basic structure of pullulan was revealed due to the discovery of the enzyme pullulanase, which converts pullulan almost quantitatively into maltotriose (Bender and Wallenfels, 1961).

The industrialization of pullulan production was promoted not only by the oil crisis in the 1970s but also by the public awareness on the pollution caused by the petrochemical polymers (Sugimoto, 1978). Pullulan's commercial production was pioneered by Hayashibara Biochemical Laboratories, in Okayama, Japan since 1976 (Tsujisaka and Mitsuhashi, 1993). However, application of pullulan had been limited to the food industry for many years due to the relatively high price of pullulan. Few of its potential applications have been widely adopted. Only until recently, the interest in pullulan has been reignited mostly for higher value pharmaceutical and biomedical applications (Leathers, 2003). In fact, this research project is a small part of a collaboration that involved the University of Ottawa, the Biotechnology Research Institute in Montreal, the University of Sherbrooke, Laval University, and Biomatera Inc in a NSERC strategic project trying to develop 3-D scaffolds based on pullulan and polyhydroxyalkanoate (PHA) as directional guides for engineering microvessel networks.

Pullulan is sold at three times the price of dextran and xanthan, two of the most popular microbial gums produced by fermentation (Leathers, 2003). There are many reasons for the higher price of pullulan, including economic factors such as production scale, demand and supply, and profits. In addition to the economical issues, several technical challenges also contribute to the higher price. Compared to dextran and xanthan production, pullulan production requires longer fermentation time. *A. pullulans*, also known as black yeasts, usually produce melanin during the later stage of the fermentation. Removal of the melanin would increase the cost to pullulan production. The most critical

problem of all is probably the high viscosity of the fermentation broth. The highly viscous non-Newtonian broth creates major difficulties in sampling, mass and heat transfer, mixing, and product separation and recovery (Thibault and LeDuy, 1999). Usually, a significant amount of energy is consumed to mix the fermentation broth. However, homogenous broth is hardly achieved especially in large scale fermenters. Considerable dead zones may exist. This would reduce the effective fermentation volume and thus lower the overall efficiency of fermentation.

Higher molecular weight (MW) pullulan is more desirable for commercial use (Gibson and Coughlin, 2002). Higher MW stands for higher quality in some of its applications. In fact, the low MW of pullulan produced was one of the reasons why its applications have been limited (Lee et al., 2001). Unfortunately, pullulan is subjected to enzyme hydrolysis, known as pullulanolysis, in the later stage of fermentation. Due to this effect, the MW of pullulan is usually decreasing at the late stage of fermentations. Stopping the fermentation at early stages is clearly not practical because little pullulan would have been produced by then. The MW of pullulan is also influenced by fermentation conditions such as the concentration of K_2HPO_4 in the medium and the initial pH. However, the pullulan yield is lower when higher MW pullulan is produced (Sugimoto, 1978).

There are two major contributing factors that would influence the viscosity of the fermentation broth. One is the concentration of pullulan; the other one is its MW (Leduy et al., 1974). When high concentration of high MW pullulan is produced, the fermentation broth will be inevitably highly viscous. Providing adequate mixing to this medium remains an engineering challenge that is encountered in many scientific and industrial disciplines (Patel, 2008).

Microbial fermentation is recognized as a complex multiphase, multi-component process. Both cell growth and product formation are influenced by a larger number of factors, such as the medium composition, pH, temperature, agitation, aeration, and age of inoculum. The approach to investigate one factor at a time has been proved to be inefficient. Design of experiments has to be used when there are factor interactions. This is usually the case in a complex system like microbial fermentation. However, nowadays, there exist numerous experimental designs that can be selected. The challenge is to choose

the most appropriate design that would provide the desired information while keeping the number of experiments and, as a result, the cost of performing experiments to a minimum. And thus, comparison of different experimental designs is an important topic on its own.

1.1 Objectives

If the production cost of pullulan can be lowered, the price of pullulan should follow. This would enhance the use of pullulan for a larger number of potential applications. So the overall objective of this research project was to improve the mass production of high MW pullulan efficiently and economically. In order to achieve this overall objective, the following actions were taken:

(1) Perform a comprehensive review of pullulan production methods and identify possible factors for improvement.

(2) Conduct experiments in Erlenmeyer flasks to screen out the important factors among many potential factors that may influence the pullulan production.

(3) Investigate the efficiency of popular experimental designs using artificial neural networks in an attempt to find the most appropriate combination of experimental design and method of analysis in the case where only small experimental data sets can be obtained.

(4) Design and build a new mixing mechanism, the radial reciprocating plate impeller (RRPI), based on an axial reciprocating plate impeller (ARPI) in order to handle more effectively viscous non-Newtonian fermentation broths.

(5) Determine the power requirement and mass transfer characteristics of the RRPI and compare its performance to those of standard Rushton turbines and the ARPI.

(6) Model the RRPI using computational fluid dynamics (CFD) software Fluent® to gain more insight into its mixing performances.

(7) Optimize the fermentation conditions for the production of high MW pullulan using the RRPI in a laboratory scale bioreactor using experimental designs.

1.2 Structure of thesis

This thesis consists of three papers that have already been published (Chapters 2-4). Three more papers will be submitted shortly (Chapters 5-7). All papers are presented using the format of journal articles.

Chapter 2 is dedicated to the review of pullulan microbial production methods. It is published as a chapter in the book of Encyclopedia of Industrial Biotechnology: Bioprocess, Bioseparation, and Cell Technology (2010). It focuses mainly on the industrial methods: the commercial production procedures, and the requirements for technology improvement. In Chapter 3, six factors were investigated for their effects on the production of pullulan by fermentation using the microorganism *Aureobasidium pullulans* in Erlenmeyer flasks using 2-level fractional factorial design. Influential factors were revealed together with recommended directions to follow for further investigation in bioreactors. This paper is published in Process Biochemistry (2007). Chapter 4 presents the comparison of several popular 3-level experimental designs and uniform designs coupled with modeling using artificial neural networks. This paper is published in The Canadian Journal of Chemical Engineering (2009). Chapter 5 reports on a new mixing mechanism, the RRPI, that was designed based on the ARPI with the intention to make it more compatible with existing industrial equipments that are designed to handle rotating mixing devices. Its power requirement and mass transfer characteristics were compared to those of the ARPI and a triple Rushton impeller (TRI) in model fluids with different viscosities. Chapter 6 examines the uniformity of mixing when different impellers are used. In order to assess the uniformity of mixing, three volume-averaged distributions were determined: the liquid velocity, the shear rate and the viscosity. This information, which is not easily measured experimentally, was obtained using CFD. Chapter 7 presents the optimization of operating conditions when the RRPI is used in a laboratory scale bioreactor by using a 6-run uniform design in the screening stage and a D-optimal design in the optimization stage. Finally, a summary of the conclusions drawn from this research together with a few recommendations are presented in Chapter 8.

1.3 References

Bauer, R. (1938). Physiology of *Dematium pullulans* de Bary. Zentralbl Bacteriol Parasitenkd Infektionskr Hyg Abt2, 98, 133-167.

Bender, H., Lehmann, J., and Wallenfels, K. (1959). Pullulan, an extracellular glucan from Pullularia pullulans. Biochimica et Biophysica Acta, 36(2), 309-316.

Bender, H., and Wallenfels, K. (1961). Investigation on pullulan. II. Specific degradation by means of a bacterial enzyme. Biochemische Zeischrift, 334, 79-95.

Bernier, B. (1958). The production of polysaccharides by fungi active in the decomposition of wood and forest litter. Canadian Journal of Microbiology, 4(3), 195-204.

Gibson, L. H. and Coughlin, R. W. (2002). Optimization of high molecular weight pullulan production by *Aureobasidium pullulans* in batch fermentations. Biotechnology Progress, 18(3), 675-678.

Leathers, T. D. (2003). Biotechnological production and applications of pullulan. Applied Microbiology and Biotechnology, 62(5-6), 468-473.

Leduy, A., Marsan, A. A., and Coupal, B. (1974). Study of rheological properties of a non-Newtonian fermentation broth. Biotechnology and Bioengineering, 16(1), 61-76.

Lee, J. H., Kim, J. H., Zhu, I. H., Zhan, X. B., Lee, J. W., Shin, D. H., and Kim, S. K. (2001). Optimization of conditions for the production of pullulan and high molecular weight pullulan by *Aureobasidium pullulans*. Biotechnology Letters, 23(10), 817-820.

Patel, N. (2008). Influence of process parameters on the morphology and enzyme production of *Trichoderma reesei*. Ph.D. Thesis, University of Ottawa, Ottawa, Canada

Sugimoto, K. (1978). Pullulan: production and applications. Fermentation and Industry. 36(2), 98-108.

Thibault, J. and LeDuy, A. (1999). Pullulan, microbial production methods. in Encyclopedia of Bioprocess Technology: Fermentation, Biocatalysis, and Bioseparation. M. C. Flickinger and S. W. Drew, Eds., John Wiley & Sons, New York, pp. 2232-2247.

Tsujisaka, Y., and Mitsuhashai, M. (1993). Pullulan. in Industrial gums, polysaccharides and their derivatives, R. L. Whistler and J. N. BeMiller, Eds., Academic Press, San Diego, CA, pp. 447-460.

CHAPTER 2

PULLULAN - MICROBIAL PRODUCTION METHODS

Yun Lin[1], Jules Thibault[1], and Anh LeDuy[2]

[1]University of Ottawa, Ottawa, Canada

[2]Laval University, Québec, Canada

Keywords: *Aureobasidium pullulans*, Experimental design, Fermentation, Hyperbaric, Microbial polysaccharide, Mixing, Oxygen transfer, Pigmentation, Pullulan, Pullulanolysis, Reciprocating plate bioreactor, Rheology.

2.1 INTRODUCTION

Pullulan is a water-soluble extracellular polysaccharide, that is exopolysaccharide (EPS), synthesized by the yeast-like fungus *Aureobasidium pullulans* (formerly named *Pullularia pullulans*) from a variety of mono- and disaccharides (1). It is generally accepted that pullulan is a neutral glucan that consists of a linear chain of D-glucopyranosyl units that alternate regularly between one (1→6)-α-D and two (1→4)-α-D linkages. Because it is almost quantitatively converted to maltotriose by pullulanase, pullulan is usually described as a linear polymer of maltotriose connected by (1→6)-α-D linkages (Figure 2.1). Among the reported minor structure abnormalities (2), only the presence of random maltotetraose subunits is widely accepted (3,4). On the basis of the proposed pullulan biosynthesis mechanism by Catley and McDowell (5), pullulan is actually a polymer of panose or isopanose subunits, and the minor maltotetraose structure is the result of occasional direct linkage of panosyl and isopanosyl moieties.

Although several strains other than *A. pullulans*, such as *Tremella mesenterica* (6,7), *Cyttaria harioti* (8), and *Cryphonectria parasitica* (9), are able to produce pullulan under certain conditions, *A. pullulans* remains the strain used to produce pullulan in both industry and academia (2). However, the pullulan content in the product synthesized by *A. pullulans* varies from 18% to 100% depending on the strain and fermentation conditions (10-12). The Hayashibara Co. Ltd. claims that their commercial product contains more than 90% pullulan. In fact, a group of strains of *A. pullulans* produce both pullulan and aubasidan. Owing to their distinction of taxonomic entities, it is proposed to classify them as *Aureobasidium pullulans* var. *aubasidani* (13). When some unusual carbon or nitrogen source is supplied to *A. pullulans*, some pullulan-like structures of EPS have been produced (14-18). Since these EPS have high content of mannose instead of glucose, they are less susceptible to pullulanolysis, and thus, the molecular weight (MW) of this EPS is much higher than that of pullulan. In addition, *Teloschistes flavicans* can produce a different pullulan that have different ratios of (1→4)-α-D to (1→6)-α-D glycosidic linkages (19).

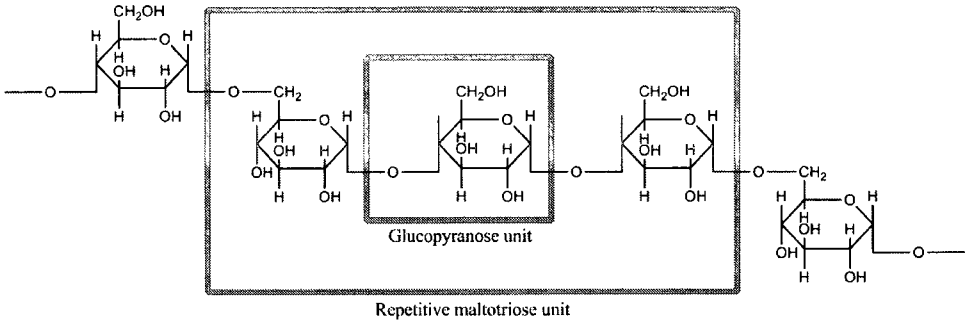

(a)

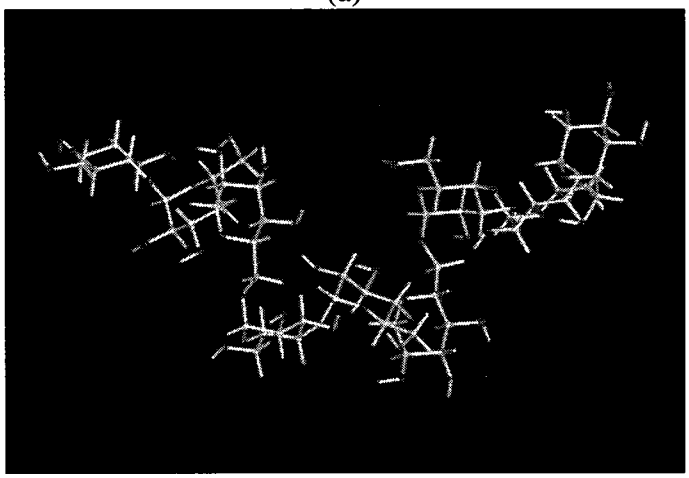

(b)

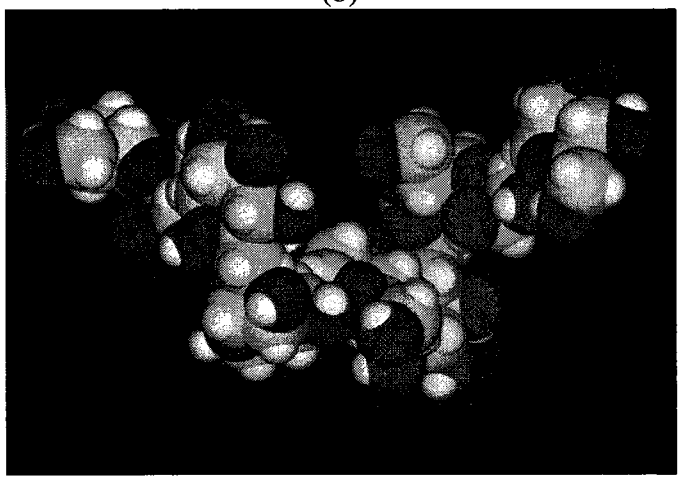

(c)

Figure 2.1 Generally accepted chemical structure of pullulan. (a) chemical formula; (b) ball-and-stick model for one hypothetical conformation of three maltotriose units; (c) space-filled model for one hypothetical conformation of three maltotriose units.

***Source*: The ball-and-stick and space-filled models were kindly provided by Professor Josée Brisson from the Chemistry Department, Laval University.**

Freeze-dried pullulan is white in color, tasteless, odorless, nonhygroscopic, nontoxic, biodegradable, and edible. It is insoluble in many solvents including methanol, ethanol, and acetone, but soluble in water to form a transparent, colorless, viscous, and adhesive solution. Since the pullulan produced by *A. pullulans* has a weight-averaged MW on the order of 10^5 Da, pullulan solution starts to show non-Newtonian and pseudoplastic behavior at moderate concentrations, which creates tremendous challenges for its fermentation process. Molded structures as well as very thin pullulan films, as thin as 0.01 mm, can be formed. Thin films of pullulan are colorless, transparent, tasteless, odorless, tenacious, resistant to oil and grease, unaffected by small thermal variations, impermeable to oxygen, nontoxic, biodegradable, and edible (20,21).

2.2 APPLICATIONS

Numerous applications of pullulan are claimed in a large number of patents. Comprehensive reviews of the applications of pullulan in food and drugs, as well as on the potential uses of pullulan in industrial and medical applications, were previously reported (2,21-24). However, the major market for pullulan remains in specialty food applications. This is probably because of the relatively high price of pullulan, which is about 3-5 times the price of other microbial gums such as dextran and xanthan (25).

As a result, recent developments on pullulan are more focused on high value biomedical applications. The use of pullulan for biomedical applications has been recently reviewed (26). Many different drug delivery systems have been developed based on pullulan micro- and nanoparticles. Owing to pullulan's high liver affinity, interferon-β can be delivered to liver more efficiently to treat chronic hepatitis (27-29). pH-sensitive hydrogel nanoparticles are also a promising system to deliver drugs to the acidic sites such as tumor, ischemia, and inflammation (30-32). Thermosensitive hydrogel nanoparticles are constructed to achieve similar goals (33,34). In addition, pullulan was derivatized in a variety of ways in order to stabilize the drug and control the drug release rate (35-37). Heparin-conjugated pullulan promotes the attachment of endothelial cells and inhibits the proliferation of smooth muscle cells (38). A pullulan-based hydrogel behaves in a similar way (39). They both are suitable supports for vascular cell adhesion, which is a

prerequisite for vascular tissue engineering. In fact, a novel 3D scaffold made of a combination of pullulan and polyhydroxyalkanoate (PHA) is under development in order to guide vascularization within a defined environment (40). Pullulan nanogels can assist protein refolding in a manner similar to the mechanism of molecular chaperones. Owing to this chaperone-like activity, several such protein folding aids have been developed using pullulan (41-44).

In addition to these biomedical applications, several new applications have also been reported. Ion-exchange membranes can be made from pullulan/polyelectrolyte blends (45). Amphiphilic pullulans make a promising new class of polymeric surfactants for membrane protein studies (46). Dichromated pullulan can be used as a novel photosensitive holographic material (47).

2.3 PROCESS TECHNOLOGY FOR THE PRODUCTION OF PULLULAN

The general process flowchart presented in Figure 2.2 illustrates the five main steps in the production of pullulan by fermentation: culture medium preparation, inoculum preparation, fermentation, product separation and purification, and product modification. This five-step general process flowchart for the production of pullulan by fermentation applies for small-scale laboratory experiments as well as for large-scale commercial production of pullulan.

Step A. During the culture medium preparation step, appropriate quantities of raw materials to be used as culture medium ingredients are formulated, weighed, and dissolved in water. The ingredients are chosen and formulated in such a way to provide the amounts of carbon, nitrogen, and mineral salts required for cell growth and pullulan synthesis during the fermentation step. The pH of the solution is adjusted to the desired value; the medium is then sterilized, either directly in a fermenter or in a separate feed tank.

Step B. The inoculum preparation step consists of producing a sufficient quantity of microorganism to seed or to inoculate the sterilized culture medium obtained at the end of step A in order to start the fermentation (step C). The appropriate microbial

strain of microorganism is selected, and then propagated by successive fermentations from a small volume of a pure culture to obtain a large volume of microbial cell suspension required for inoculum purposes. In the industrial production of pullulan, the amount of inoculum required to seed the production fermenter may vary from hundreds to thousands of liters of microbial cell suspension. The inoculum culture-to-medium ratio used may also vary from 0.1% v/v to 10% v/v. Usually, larger inoculum ratios are used for laboratory-scale fermentations, and smaller ratios are more practical for industrial-scale productions.

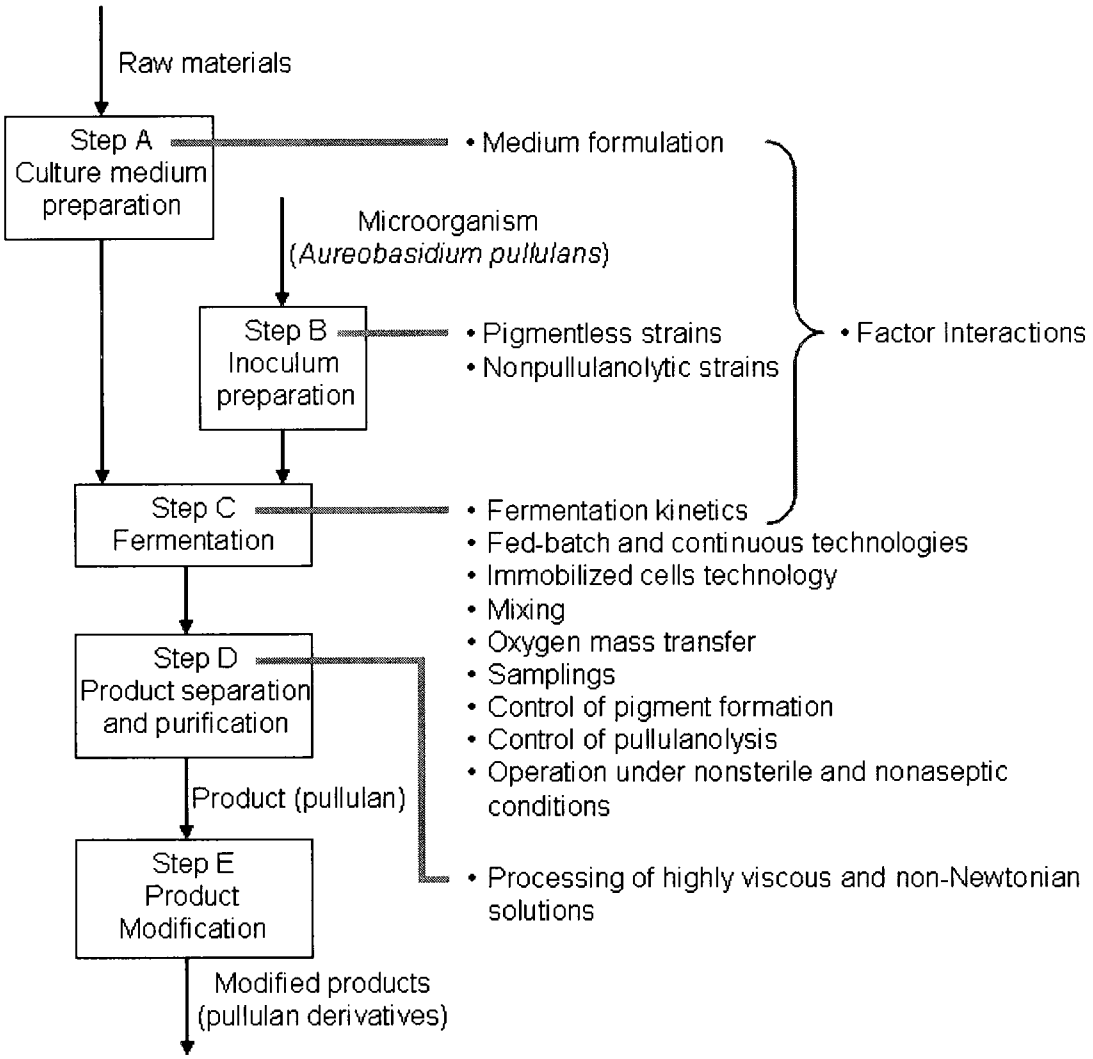

Figure 2.2 Five-step general process flowchart for the production of pullulan by fermentation. Research and development requirements for technology improvement are indicated for each step.

Step C. The fermentation step is the biosynthesis of pullulan from a carbon source by living and growing microbial cells in the fermenter under sterile and aseptic conditions. The fermentation technology for pullulan production may be batch mode, fed-batch mode, or continuous mode, using either free or immobilized cells. Batch fermentation using free cells of *A. pullulans* is still the most popular technology used in pullulan production in small as well as in large scales. The duration and the yield of the fermentation step are determined by the kinetic behavior of the combined system of microorganism-medium-fermentation conditions. This implies that each specific strain of microorganism, in a specific culture medium (ingredients and composition), and under a specific set of fermentation conditions will respond with a specific fermentation kinetic behavior. Therefore, knowledge of fermentation kinetics is important for choosing the best fermentation technology and conditions for each specific strain of microorganism in a specific culture medium. During the fermentation step, operating conditions such as pH, temperature, oxygenation (by aeration), and mixing (by agitation) are either artificially controlled by maintaining each one at a certain value for a specific time period, or simply uncontrolled. Although no particular design is required for the fermenter, special considerations on the capacity of the agitator is necessary to ensure adequate aeration and agitation of the highly viscous culture (48).

Step D. When fermentation is completed, the resulting fermented broth is a mixture of solids in suspension (which consists of microbial cells and cellular debris) together with dissolved solids in the aqueous solution (which comprise water-soluble pullulan synthesized during the fermentation, residual ingredients from the culture medium, and extracellular metabolites produced and excreted during the fermentation). During the subsequent steps (separation and purification), solids in suspension are first separated from the culture medium by centrifugation or filtration. The resulting liquid phase containing soluble pullulan is then decolorized using activated carbon to remove the black pigmentation that is produced by *A. pullulans* during fermentation. The decolorized liquid phase is further purified to remove small molecular compounds (residual ingredients, extracellular metabolites), then dewatered and dried to obtain pullulan as a final product in solid form. The dewatering operation usually

consists of the precipitation of pullulan from the aqueous solution using acetone, methanol, or ethanol as a solvent (Figure 2.3).

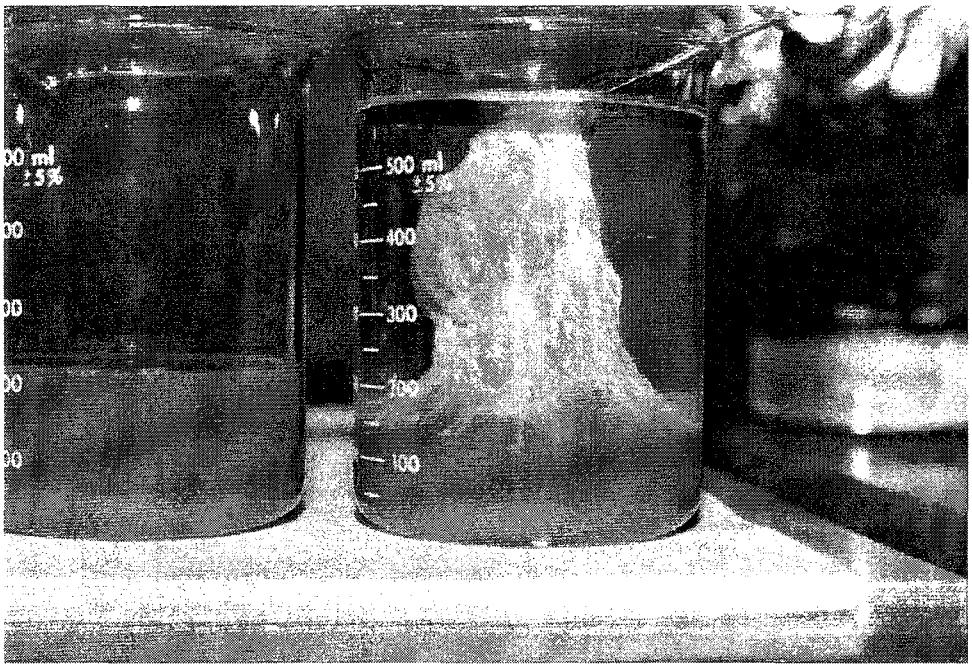

Figure 2.3 Solvent precipitation of pullulan: Pullulan, which is soluble in the fermentation broth (yellow solution), becomes insoluble in methanol (clear liquid). The fibrous texture appearance of the precipitated pullulan indicates that this polysaccharide has very high molecular weight.

Step E. The product modification step is necessary only when modified pullulan or pullulan derivatives are desired as final products. Technologies are available to chemically modify pullulan in order to improve its existing properties and/or to impart newly desired properties to pullulan. Examples of such pullulan derivatives are presented in Table 2.1 (21,49-57).

Table 2.1 Pullulan Derivatives

Modified pullulan	Imported properties	References
Esterified pullulan	Various degrees of water insolubility	21
Etherified pullulan	Various degrees of water insolubility	21
Pullulan sulfate and its salts	Anti-peptidic ulcer; low blood anticoagulation	49
Carboxylated pullulan	High solubility in cold water	50
Cross-linked pullulan	Hydrophilic gel; various degrees of water absorbability	51
Dialdehyde pullulan	Water resistance	52
Pullulan aminoalkyl ether	Cationic polymer	53
Ionic pullulan gel	Charged gel	54
Cyanoethylated pullulan	High heat resistance; insolubility in water; high dielectric constant	55
Hydrogenated pullulan	High heat resistance	56
Cyanoethyldihydroxylakylated pullulan	High dielectric constant	57

2.4 COMMERCIAL PRODUCTION OF PULLULAN

At the present time, the only known commercial producer of pullulan through a fermentation process is the Hayashibara Co., Ltd. in Japan. Figure 2.4 shows the flowchart for the commercial production of pullulan used by this particular company (58). Note that it matches very well the five-step general process flowchart for the production of pullulan by fermentation shown in Figure 2.2. In fact, the pullulan production, recovery and purification operations remain almost identical to those that prevailed 30 years ago (48).

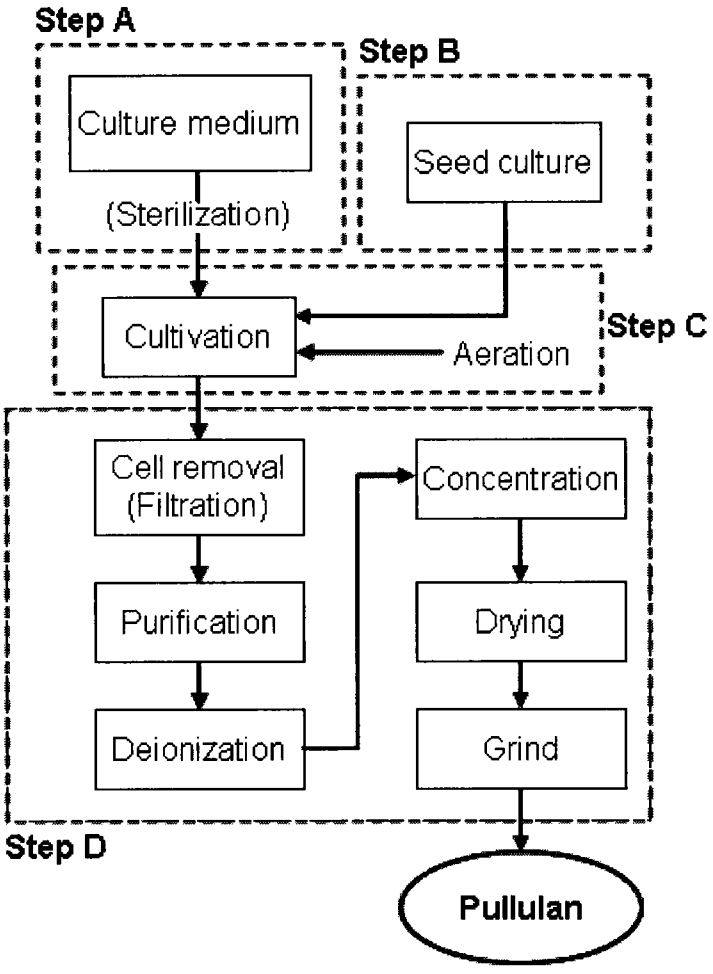

Figure 2.4 Process flowchart for the commercial production of pullulan by Hayashibara Co., Ltd. *Source*: Adapted from Ref. 58, reproduced with permission.

The culture medium used consists of a carbon source (partial starch hydrolyzate with dextrose equivalent [DE] around 50% at a concentration from 10 to 20%), a nitrogen source (formulated from corn gluten, soybean protein, peptone, nitrate salts, and ammonium salts), and other mineral salts. The initial pH is between 5 and 6.8 (48).

The inoculum is prepared from mutated strains. *A. pullulans* AHU 9553, *Dematium pullulans* IFO 4464, and *Pullularia fermentans* var. *fermentans* IFO 6401 were mutated in order to achieve the lowest level of black pigmentation, the shortest duration of fermentation, and the highest yield of pullulan (48).

The fermentation is carried on in batch mode for approximately 4 days in a conventional fermenter, with special consideration to ensure adequate aeration and agitation of the highly viscous fermentation broth. The temperature is maintained at 30°C and aeration at 0.5 VVM (volume of air per volume of culture medium per minute). The kinetic behavior of commercial pullulan fermentation corresponds very well with some of the results reported in the scientific literature (59-62). Since it is left uncontrolled, the pH of the culture medium decreases sharply during the first day and remains constant at around pH 3.5 to the end of the fermentation. Most cell growth and pullulan synthesis occur during this low and constant pH period. The concentrations of cell mass and pullulan continue to increase in the fermentation broth until the end of the fermentation. However, the MW of pullulan in the fermentation broth increases to a maximum value of around 2,000,000-3,000,000 Da in the early stage of fermentation, then drastically decreases to a relatively low MW toward the end of the fermentation. This decrease is presumably caused by the action of α-amylase on maltotetrase residues (63). Consequently, the apparent viscosity of the fermentation broth, which results from pullulan concentration and pullulan MW, increases rapidly in the early stage of fermentation to over 0.3 Pa·s (300 cP), then reduces to less than 0.1 Pa·s (100 cP) at the end of the fermentation. By controlling the fermentation conditions (phosphate content and initial pH), Hayashibara Co., Ltd. obtains a pullulan product whose MW ranges from 50,000 to 500,000 Da (48).

Initially, Hayashibara Co., Ltd. had three different pullulan grades on the market (48). Currently, only the highly purified pullulan, (PI-20), is available for sale, which is intended to be used as the standard for food, pharmaceutical, biomedical and other industrial applications. The annual production of pullulan by Hayashibara Co., Ltd. is

approximately 800 metric tons and the ex-factory sale price is approximately US $25 per kilogram (58).

2.5 RESEARCH AND DEVELOPMENT REQUIREMENTS FOR TECHNOLOGY IMPROVEMENT

Pullulan fermentation, like numerous other extracellular polysaccharide fermentations, is one of the most challenging bioprocesses for engineers and scientists seeking ways to improve fermentation technology. Five groups of problems associated with pullulan fermentation still require better solutions in order to increase the performance of the fermentation process and lower product recovery costs.

2.5.1 Factor Interactions

Numerous contradictions exist in the literature. The production of pullulan was assumed to be growth associated, nongrowth associated, or partially growth associated based on the cell growth and pullulan production profiles obtained by different research groups (17,64-67). The optimal pH for pullulan production varies in the range between 4.0 and 7.5 (2,64,68). Lee et al. reported that high MW pullulan was produced when initial pH was 6.5 (14). However, Lee and Yoo showed that high MW pullulan is produced when initial pH was 3, while high concentration of pullulan was obtained when initial pH was 6 (69). Although *A. pullulans* ATCC 42023 usually produces melanin under several different conditions (70), pigment-free pullulan is also produced by this strain in two-stage fermentation (71). Since *A. pullulans* are polymorphic, and it is admitted that pullulan elaboration is associated with specific cell morphology, thus, it is desired to retain certain morphology in order to promote high productivity. However, which morphological forms of *A. pullulans* are responsible for pullulan production is still open for debate (13,72-74).

The idea that a certain microorganism-medium-fermentation condition system has a specific fermentation kinetic behavior explains at least some of the discrepancies. This is actually the result of factor interactions, which makes the optimization process even more complex. Much attention must be paid to make sure the majority of the EPS produced

under different conditions is still pullulan. The one factor at a time approach is time-consuming and the results are usually unsatisfactory. The most efficient approach is probably using design of experiments methodology. Using this approach, information on the main effects of each factor and factor interactions can be obtained with a relatively small number of experiments. This method has been used successfully in pullulan fermentation (70,75,76). The results of this methodology may not be applied, however, directly to another strain or for different operating conditions. Thus, it is necessary for scientists and engineers to define their own experimental domain and carry out the investigation using a similar experimental design approach.

2.5.2 Viscosity of the Fermentation Broth

The evolution of rheological properties of the fermentation broth during batch fermentation of *A. pullulans* has been studied in detail (59). In batch fermentation, the culture medium initially exhibits Newtonian behavior, and then the rheology of the broth progressively changes to a highly viscous and non-Newtonian behavior. The apparent viscosity of the fermentation broth, η, is dictated by two parameters: the consistency index, K, and the non-Newtonian flow behavior index, n, according to power-law model:

$$\eta = K\dot{\gamma}^{n-1} \tag{2.1}$$

where $\dot{\gamma}$ is the shear rate. Equation 2.1 shows that, in non-Newtonian fluids, the value of viscosity obtained depends on the rate of shear at which the viscosity is measured. The viscosity of a non-Newtonian fermentation broth is commonly standardized by its field value, which is the value measured at the unit rate of shear. Such values of the field apparent viscosity are independent of either rotational speed or geometrical configuration of the viscometer used.

It would be logical to assume that the viscosity of the fermentation broth increases steadily throughout the fermentation to follow the increase in pullulan concentration. However, in the case of pullulan, the field apparent viscosity of the fermentation broth increases slowly during the initial phase of fermentation, then rises rapidly to its maximum value, and finally decreases toward its initial value. The maximum values of the apparent field viscosity, as well as the time when these maximum values occur, depend on

fermentation conditions such as initial pH of the culture medium and age of inoculum (59). The decrease in the field apparent viscosity during later stages of each fermentation, when the polysaccharide concentration has leveled off, is called *pullulanolysis*, which relates to the depolymerase secreted by *A. pullulans*. The evolution of the field apparent viscosity of the fermentation broth depends also on other factors such as the aeration rate and the level of dissolved oxygen concentration during pullulan fermentation (77).

The flow behavior index characterizes very well the average length of the pullulan chain (78). It is therefore interesting to monitor this rheological parameter during the course of fermentation to observe changes in pullulan average MW. At the beginning of a typical pullulan fermentation, the culture medium is Newtonian (n = 1). The non-Newtonian index of the fermentation broth decreases slowly during the initial phase of fermentation, then drops rapidly to its minimum value, and finally rises toward its initial value. Therefore, throughout the fermentation the broth becomes increasingly pseudoplastic (n <1), then returns toward its initial Newtonian behavior. The minimum values of the non-Newtonian index as well as the time when these minimum values occur also depend on fermentation conditions such as initial pH of the culture medium and the age of inoculum (59). The rheological behavior of such non-Newtonian solutions has a profound impact on the flow characteristics within the fermenter. The apparent viscosity decreases when the fluid is in motion. This reduction in apparent viscosity with the velocity of the fluid is more pronounced as the flow behavior index is reduced.

The observed rheological properties of the fermentation broth result from many factors including the pullulan concentration and the average length of the pullulan chain. Both pullulan concentration and pullulan average chain length in the fermentation broth are continuously changing during batch fermentation. LeDuy *et al.* (59) have recovered pullulan from fermentation broths at 1, 3, 5, and 8 days of batch fermentation, freeze-dried the precipitated pullulan, and then dissolved the recovered pullulan in water to form solutions having a pullulan concentration varying from 0.125 to 2.0 g/L. The field apparent viscosities and the non-Newtonian indices of these solutions were measured and are presented in Figure 2.5. At the same concentration of pullulan, the field apparent viscosity of pullulan solution recovered from the early stage of fermentation is higher than that recovered from the later stage, indicating that the pullulan recovered in the first days

of fermentation has higher MW than in subsequent days. The opposite phenomenon is observed for the non-Newtonian index. At the same concentration of pullulan, the non-Newtonian index of pullulan solution recovered from the early stage of fermentation is lower than that recovered from the later stage, indicating that the pseudoplasticity of pullulan solutions is directly related to the high MW of pullulan. Each set of curves prepared with pullulan recovered after the same fermentation time in Figure 2.5 shows the very important contribution of pullulan concentration on the field apparent viscosity as well as on the non-Newtonian index of the pullulan solution. Higher pullulan concentration leads to higher field apparent viscosity and larger pseudoplasticity.

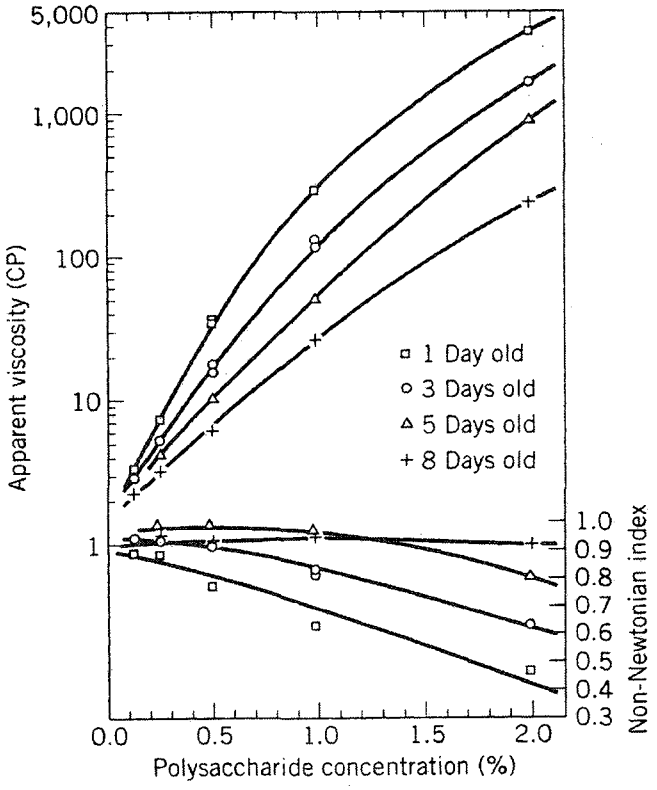

Figure 2.5 Variations of field apparent viscosity and non-Newtonian index as a function of the concentration of pullulan in a solution and the pullulan chain length. Pullulan molecules have longest chain lengths after one day and shortest chain lengths after eight days of batch fermentation. *Source*: From Ref. 59, reproduced with permission.

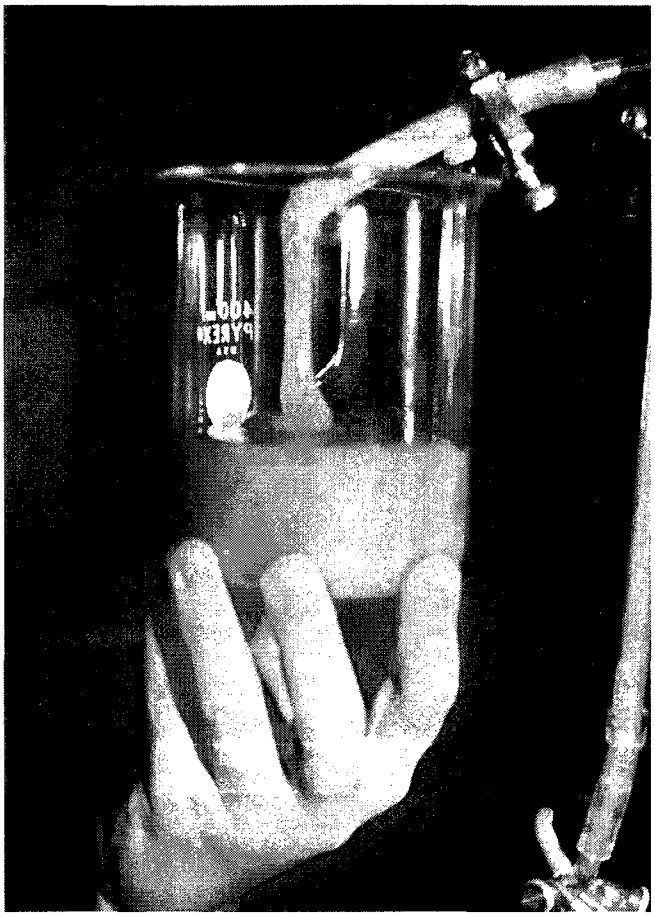

Figure 2.6 Highly viscous fermentation broth of *A. pullulans* in a sucrose medium: the broth slowly flowing out of a fully opened large-size sampling tube under the compressed air inside the fermenter.

Thus, any fermentation process aiming to achieve high yield production of high MW pullulan still provides tremendous engineering challenges in mixing, oxygenation, and sampling during the fermentation, as well as the major challenge of removal of microbial cells from the highly viscous fermentation broth in the product separation and purification step. To clearly illustrate the difficulties involved in dealing with a highly viscous fermentation broth, Figure 2.6 shows a typical fermentation broth flowing out of a fully opened large-size sampling tube under the compression of the aeration gas inside the fermenter. During pullulan fermentation, the nonhomogeneous mixing problem is always observed, even in a laboratory-scale fermenter. The fermentation broth inside the fermenter tank segregates into two regions having different characteristics, with an active core around the impeller where the culture medium is well mixed and properly aerated.

This core is separated from the innermost zone by a fictitious boundary, a stagnant fluid region characterized by a total lack of agitation and aeration (Figure 2.7). Some authors even discuss the formation of three distinct mixing regions: a small central region (often referred to as a *cavern*) in the vicinity of the impellers where the turbulence is important, an annular section characterized by slow fluid motion, and finally, a stagnant outer region where the fluid is motionless and the apparent viscosity is very high (79). The energy imparted to the fluid by the rotating impellers is dissipated in a restricted region of the total volume of the fermentation broth. The high viscosity combined with the non-Newtonian behavior creates major difficulties in sampling, oxygen mass transfer, mixing, and downstream processing. These are briefly analyzed in turn.

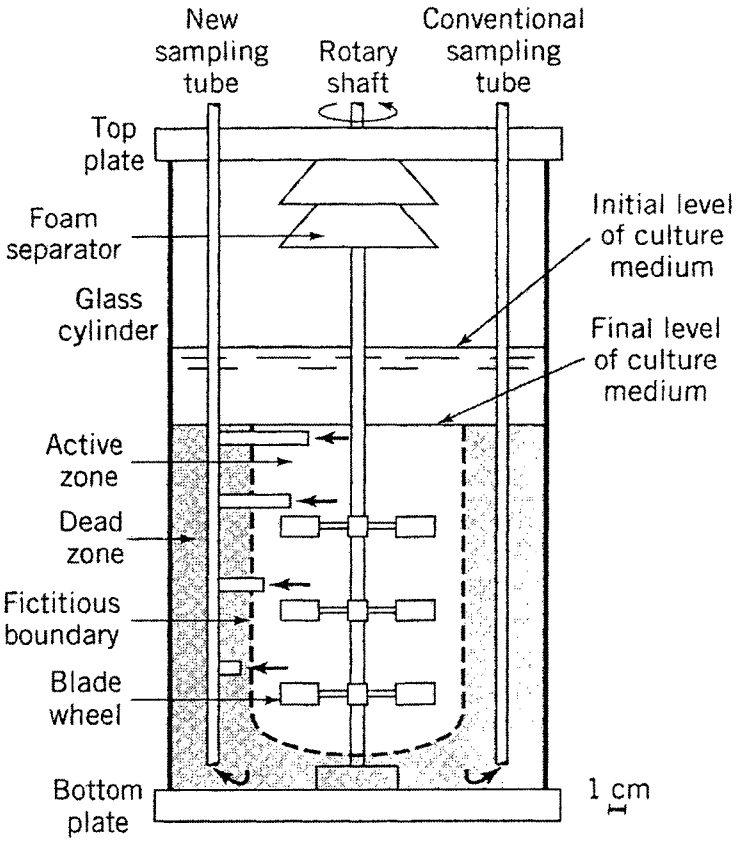

Figure 2.7 Active and stagnant zones of the highly viscous fermentation broth in the fermenter during the pullulan fermentation. Configurations of both conventional and newly improved sampling devices are shown. *Source*: From Ref. 79, reproduced with permission.

Process Monitoring and Sampling. With the absence of homogeneous conditions throughout the fermentation vessel, it is only possible to monitor locally the dissolved oxygen concentration and the pH. This also applies to any novel sensor for monitoring other fermentation process variables such as the *A. pullulans* population (81). These values will therefore depend greatly on the position of the various probes. The same phenomenon applies also to the fermentation broth sampling port. The geometry and the location of the conventional sampling tube, as provided in fermenters by manufacturers (Figure 2.7), shows that the samples are taken very frequently from the stagnant zone, where the data are not representative for the entire culture medium content. A newly improved sampling device was designed and tested in a 7-L fermenter (80) and enables one to obtain a more representative sample because it draws a sample from different locations within the culture vessel (Figure 2.7). Nevertheless, because of the evolving and shear-dependent viscosity, it is not guaranteed that a uniform sampling in all branches of the sampling tube will be achieved. Thus, the sampling of representative samples and process monitoring of highly viscous fermentation broth in larger-scale fermenters having nonhomogeneous mixing remains a challenge that should not be overlooked.

Oxygen Transfer and Mixing. Pullulan synthesis is an aerobic process. It was demonstrated that oxygen is essential for the biosynthesis of pullulan by *A. pullulans*. In a growth medium, pullulan yield and synthesis rates are proportional to the oxygen availability. However, under a controlled oxygen environment in a non-growth (nitrogen-free) medium, pullulan yield and synthesis rates are inversely proportional to the oxygen concentration in the culture medium (82). During the fermentation, air is continuously provided to the culture medium to supply oxygen to the microbial cells. However, oxygen molecules in the air bubbles have to move into the fermentation broth and then diffuse through the liquid phase to reach the microbial cells in order to be used for the growth and biosynthesis of pullulan. With the highly viscous fermentation broth normally encountered in pullulan fermentation, the oxygen mass transfer process is very difficult and remains a major engineering challenge for the future. Indeed, as the fermentation broth becomes increasingly viscous, the gas bubbles in the peripheral stagnant zone of the fermenter remain trapped in the motionless fluid and are progressively depleted from their oxygen content. Figure 2.8 shows a photograph taken during a typical pullulan production where

the fermentation broth and gas bubbles in the outer region remained stagnant for a long period.

Figure 2.8 Mixing and mass transfer challenges in pullulan fermentation. The picture is taken when the agitator equipped with Ruston turbines is rotating at 500 rpm. The layer of fermentation broth adjacent to the fermenter wall remains stagnant with trapped gas bubbles.

The evaluation and comparison of the performance of oxygen mass transfer within a mixing vessel is usually quantified by the volumetric overall oxygen mass transfer coefficient K_La. The overall oxygen transfer rate from air bubbles to the fermentation broth is calculated as the product of the volumetric oxygen transfer coefficient (K_La) and the mean concentration driving force of oxygen in the fermentation broth (C^* - C_L). Throughout the fermentation, the rate of change of the dissolved oxygen concentration (dC_L/dt) is given by the following equation:

$$\frac{dC_L}{dt} = K_L a\left(C^* - C_L\right) - OUR \tag{2.2}$$

where C_L is the dissolved oxygen concentration in the fermentation broth and C^* is the saturated dissolved oxygen concentration in the fermentation broth that corresponds to the solubility of oxygen under the fermentation conditions. OUR is the oxygen utilization rate.

According to Equation 2.2, one possible way to improve the oxygen mass transfer rate is to increase the mean concentration driving force of oxygen in the fermentation broth ($C^* - C_L$) by increasing the solubility of oxygen in the liquid phase. The solubility of oxygen in the fermentation broth, C^*, during the fermentation can be enhanced either by using oxygen enriched gas, up to pure oxygen, in aeration or by pressurizing the fermenter headspace (commonly referred to as *hyperbaric fermentation*). For practical and economic reasons, the use of pure oxygen is not feasible in large-scale fermenters. On the other hand, enriched gas would be used only when air would not suffice to maintain the desired dissolved oxygen concentration within the fermenter. However, higher oxygen concentration in the fermentation broth may enhance the biosynthesis of the black melanin pigment, which is undesirable (82).

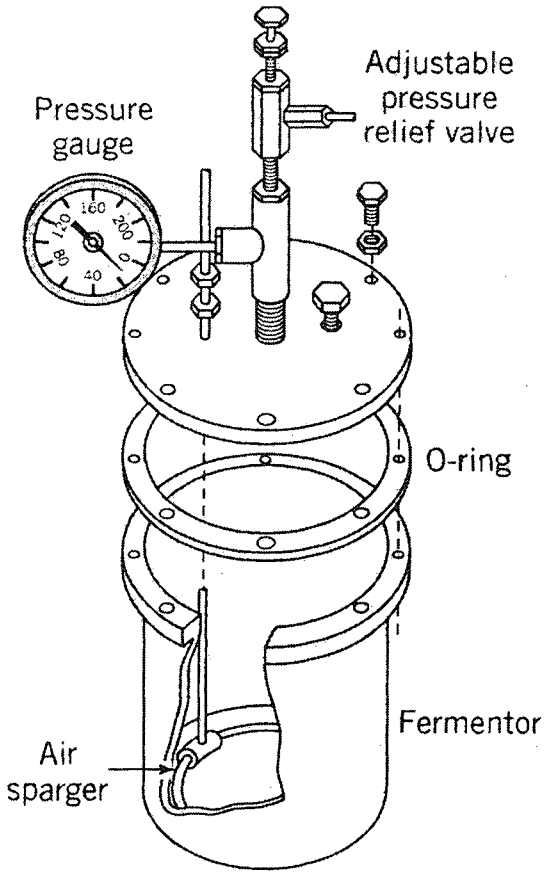

Figure 2.9 The specially designed fermenter for studying pullulan fermentation under hyperbaric conditions. *Source*: From Ref. 83, reproduced with permission.

The effects of pressure on the growth of *A. pullulans* and the synthesis of pullulan have been studied in a specially designed fermenter and fermentation system (Figures 2.9 and 2.10) (83). It is reported that for all volumetric airflow rates in the range of 0.2 to 2.0 VVM, the production of biomass increases with pressure up to a critical value, which ranges from 0.50 to 0.75 MPa, at which point a drastic decrease in biomass production and a change in cellular morphology occur. Above the critical pressure, *A. pullulans* forms aggregates of irregular shape that are fairly uniform in size under each set of fermentation conditions. In general, larger aggregates of approximately 8 mm are associated with a higher pressure level (1.48 MPa) and aeration rate (2 VVM). The details of *A. pullulans* aggregates are shown in the scanning photomicrographs in Figure 2.11. The same pattern is also observed for pullulan synthesis: it increases with pressure up to approximately the same critical pressure, then decreases drastically beyond this value. Further investigation is required to better understand the behavior of hyperbaric pullulan fermentation before reaching a practical and economic solution for this technology.

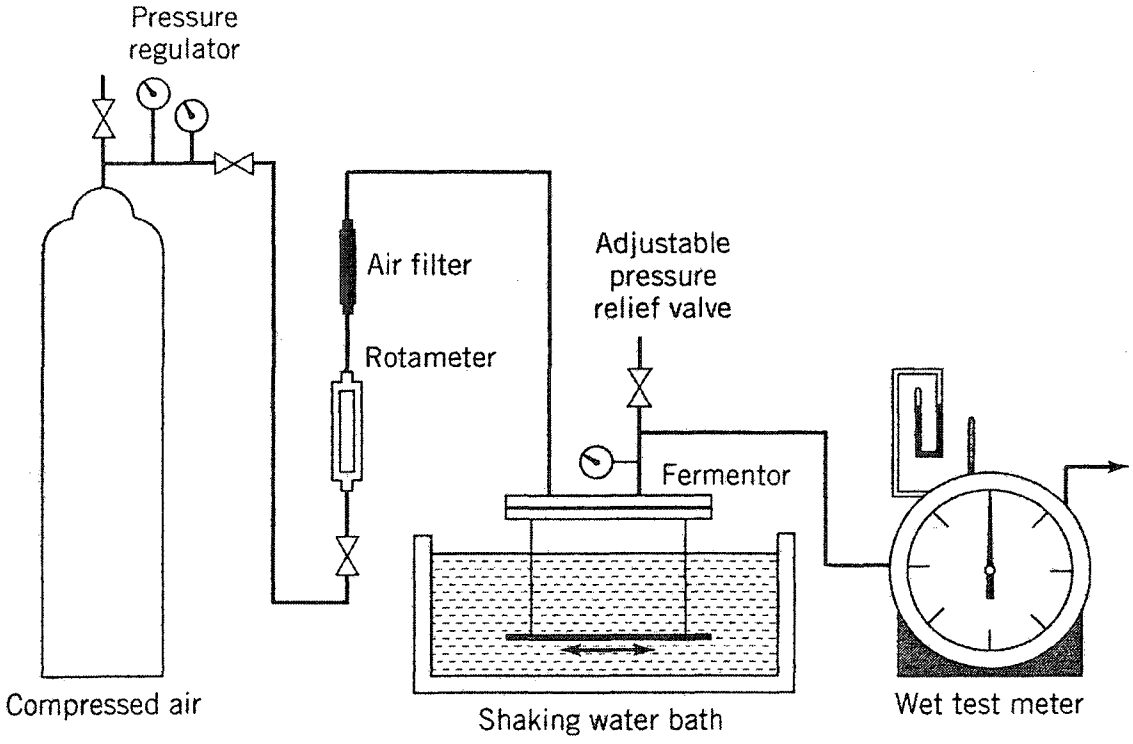

Figure 2.10 The fermentation setup for studying pullulan fermentation under hyperbaric conditions. *Source*: From Ref. 83, reproduced with permission.

A second way to improve the oxygen mass transfer rate is to increase the volumetric oxygen transfer coefficient (K_La) by using better mixing devices. It has been clearly shown that K_La is not uniform throughout most mixing vessels. It is usually large in the vicinity of the mixing element and low further away. It is evident from Figures 2.7 and 2.8 that any mixing device that can reduce or even eliminate the dead zones in the fermenter will have a chance to provide better volumetric oxygen transfer to the pullulan fermentation broth and, in addition, create more homogeneous operating conditions throughout the fermentation vessel. An adequate uniform mixing would also contribute to the maintenance of gas bubbles with high oxygen content and therefore keep the oxygen gradient at a high level. Several unconventional mixing devices have been designed and studied. These are the reciprocating plate mixer, the helical ribbon (HR) mixer, and the HR screw mixer.

Even though the physical properties of the fluid and operating conditions, used by many authors, are hardly comparable over a wide operating range, their results have a common trend of increasing oxygen mass transfer coefficients with increasing agitation and gas flow rate. The efficiency of mixing devices, evaluated in terms of K_La, is usually correlated in terms of the power input per unit volume (P_G/V_L) and the superficial gas velocity (U_G), using the following expression:

$$K_L a = C\left(\frac{P_G}{V_L}\right)^{\alpha} (U_G)^{\beta} \tag{2.3}$$

The correlation coefficients C, α, and β depend on the nature of the fluid, the geometrical configuration of the mixing element, and the hydrodynamic regimes of the fluid (84,85).

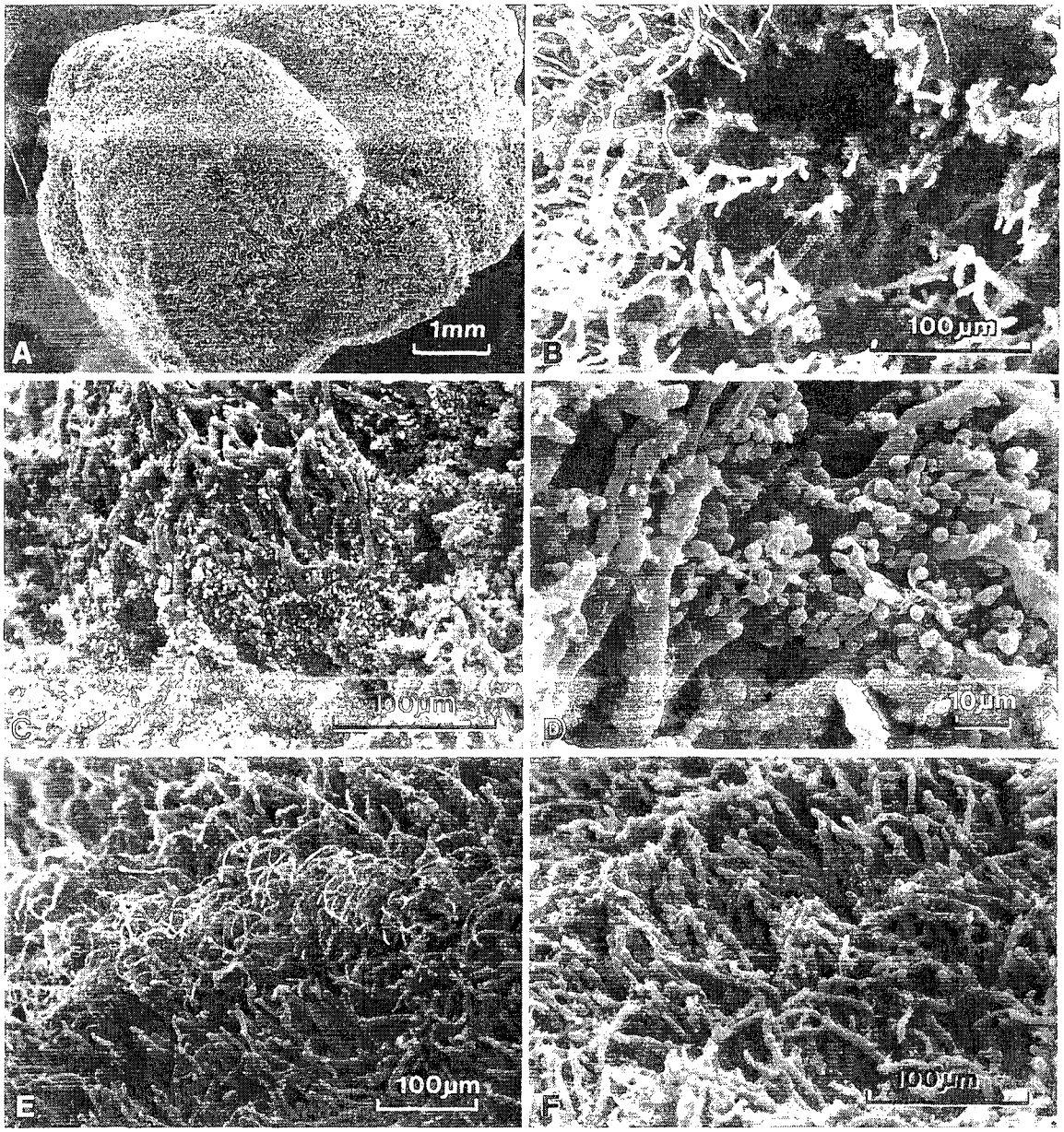

Figure 2.11 Agglomerates of *A. pullulans* in pullulan fermentation under 1.13 MPa and 0.2 VVM: (a) **Global view of agglomerate;** (b) **cavity region;** (c) **and** (d) **regions where yeast cells dominate;** (e) **and** (f) **regions where mycelial cells dominate.** ***Source*: From Ref. 83, reproduced with permission.**

The reciprocating plate bioreactor (RPB), which has been developed in the last two decades in our research group, is particularly well suited for highly viscous fermentation such as for the production of pullulan. The RPB (Figure 2.12a) consists of a stack of

perforated plates that undergoes reciprocating vertical motions inside the fermenter. The RPB, with its particular geometry, possesses the desired attributes to produce efficient mixing, with the result that microorganisms, nutrients, and air bubbles are properly distributed (86). In the RPB, the perforated plates occupy the total cross sectional area of the fermentation vessel such that the upward and downward movements of the plate stack lead to a more uniform mixing. Three different RPBs with aspect ratios (diameter/height), ranging from 0.08 to 0.5, have been characterized with fluid models and pullulan fermentation (77,84,87). Audet *et al.* (85) have performed experiments to evaluate the influence of polysaccharide concentration and MW on oxygen mass transfer in the RPB. They used model fluids consisting of different concentrations of dextran (another water soluble microbial polysaccharide) of different MWs to simulate the pullulan fermentation broth at different stages of fermentation. They correlated their results using Equation 2.3. They reported that the correlation coefficients C, α, and β in this equation also depend on the polysaccharide concentration, the polysaccharide MW, and the hydrodynamic regime of the solution.

The most recently constructed RPB was designed to be identical, except for the mixing mechanism, to a stirred-tank (rotating mixing device) bioreactor that was built simultaneously. The schematic diagram of the experimental setup of the RPB is shown in Figure 2.13. Each bioreactor has a total volume of 22.5 L and a working volume of 18 L. The two bioreactors, using a series of mixing elements, were initially characterized in water for their ability to produce high K_La values. Five different plate stacks, similar to the schematic diagram of Figure 2.12a, were used in the RPB. Another five mixing elements were used with the radial-type bioreactor: assemblies containing one, two, or three identical Rushton turbines (RTs) (Figure 2.12b), and a HR impeller with or without surface baffles (Figure 2.12c). A more detailed description is presented by Gagnon *et al.* (88).

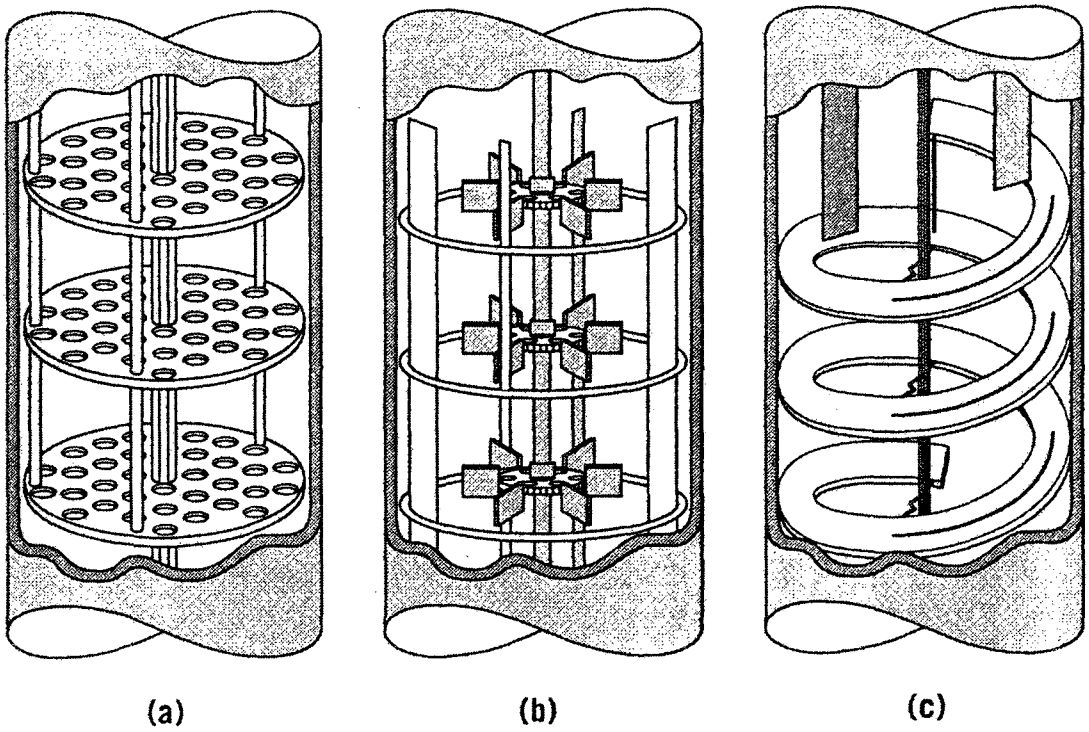

Figure 2.12 Mixers used in pullulan fermentations: (a) the reciprocating plate mixer; (b) the Rushton turbines; (c) the helical ribbon mixer with surface baffles. *Source*: From Ref. 86, reproduced with permission.

These bioreactors were first characterized in terms of oxygen mass transfer (88). The oxygen mass transfer coefficient was measured as a function of the power input per unit volume and the superficial gas velocity for all mixing devices. All mixing devices showed identical patterns. For lower power inputs per unit volume, the oxygen mass transfer, K_La, is constant and varies only with the gas superficial velocity (α value in Equation 2.3 is equal to zero). At a certain power input per unit volume, K_La starts to increase rapidly with the power input per unit volume. Perez and Sandall (89) and Nishikawa *et al.* (90) previously observed these two distinct regimes of operation with RT bioreactors (RTBs).

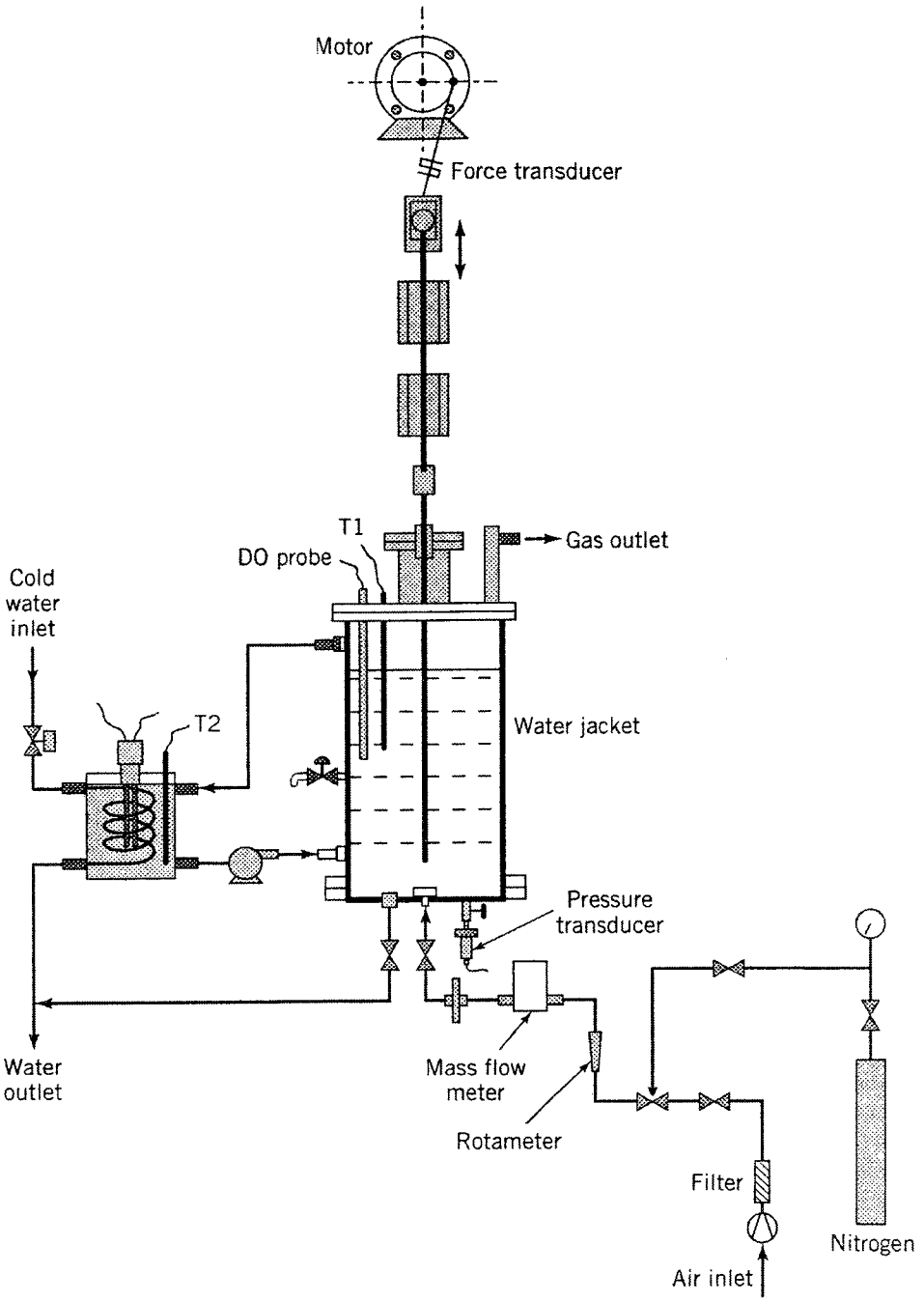

Figure 2.13 Schematic diagram of the experimental system showing the reciprocating plate bioreactor. *Source*: From Ref. 88, reproduced with permission.

The two bioreactors were then used in an investigation undertaken with the objective of comparing experimentally the performance of four different mixing devices for the production of pullulan (86). The four mixing devices include two different reciprocating

plate stacks (RPB1 and RPB2), the assembly of three RTBs, and the HR impeller. These four fermentations were performed with an equal level of power input per unit volume (1000 W/m^3) and gas flow rate (0.5 VVM or 9 L/min) during the entire fermentation. Under identical power inputs per unit volume, better cell growth and pullulan synthesis were obtained with the reciprocating plate mixer that had larger perforations. The HR mixer gave the poorest cell growth and pullulan synthesis. However, pullulan of the highest MW, as indicated by its highest fermentation broth viscosity, was obtained with the HR mixer.

The evolution of dissolved oxygen (Figure 2.14) clearly shows that the RPBs are more efficient at maintaining a high and homogeneous level of dissolved oxygen within the fermentation broth. For the other two mixing devices, it can be stated that the local dissolved oxygen varied greatly and was always very low in the vicinity of the dissolved oxygen probe.

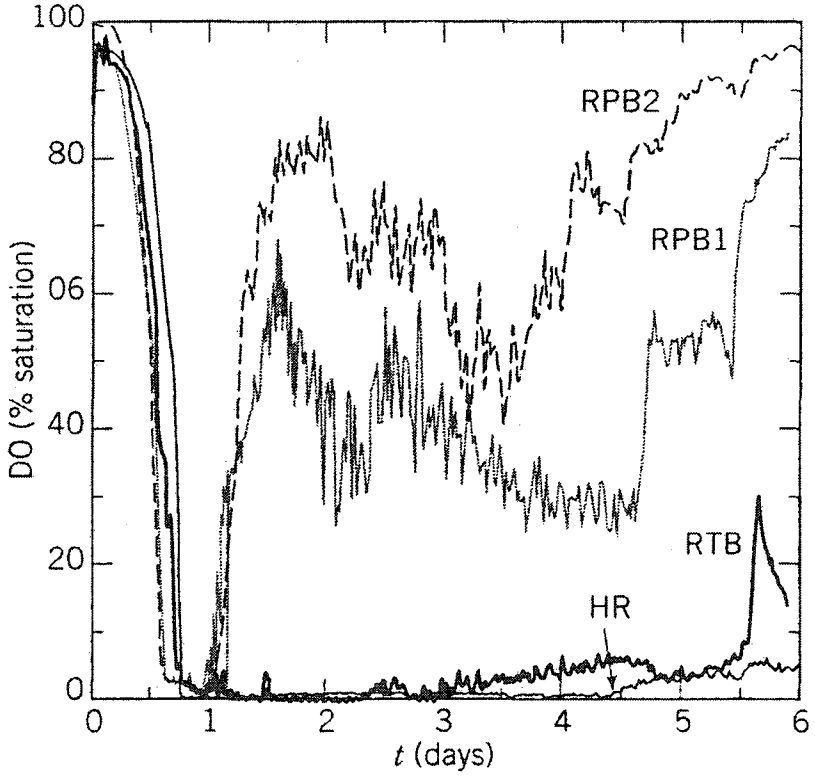

Figure 2.14 Evolution of dissolved oxygen concentration as a function of fermentation time for four mixing devices. *Source*: From Ref. 86, reproduced with permission.

The observed difference may be explained from another point of view. Remote clearance impellers, such as the RT, which is the classic impeller for many bioprocesses, are designed to achieve intensive dispersion. RTs are efficient at breaking large bubbles or maintaining small bubbles that are produced by the gas sparger, and thus providing large interphase surface area for mass transfer, which is the essence of micromixing. Although these types of mixing devices are efficient for fermentation broths of low viscosity, they unfortunately can not handle very well non-Newtonian high viscosity fluid, especially at large scale. On the other hand, close clearance impellers, such as HR impeller, are power efficient in delivering global circulation even at high viscosity. Fluid homogeneity can be achieved with ease, which makes them very useful in polymerization processes. However, the HR impeller is not very good at micromixing and at providing good oxygen mass transfer coefficient.

Polysaccharide productions with their rheologically evolving broth properties present a challenging task that requires both efficient micro- and macromixing. A few alternatives have been investigated to overcome this problem. Guerinik (91) has modified the HR impeller by adding a central screw installed on the rotating shaft to provide an additional pumping action on the fermentation broth in order to enhance its circulation inside the fermenter. He found that pullulan fermentations using the HR screw mixer resulted in a higher concentration of pullulan of higher MW as compared with that obtained using standard RT. Tanguy *et al.* (92) proposed a dual coaxial impeller composed of a RT and a HR impeller, both rotating clockwise but at different speeds. They have shown that the hybrid mixer system outperforms the standard HR impeller when the fluid rheology changes with time. A similar ungassed system was further investigated with different rotational speed ratio of two independently driven impellers, which rotate in opposite directions (93). Three distinct flow patterns were revealed. For high viscosity fluids, a well-distributed flow pattern was achieved when the ratio of the rotation speed of the turbine to that of the HR was 10. For low viscosity fluids, the same ratio of rotation speed eliminates the vortex, which is usually present in unbaffled tanks. Altogether, it seems that these hybrid systems could be used advantageously for rheologically evolving fluid, including pullulan fermentation.

RPB was designed to handle both micro- and macromixing equivalently well. Uniform mixing and thus better oxygen mass transfer can be achieved. This makes monitoring and sampling much easier and the corresponding results can be used with greater confidence since the samples are more representative of the whole broth. Two problems with the RPB are the special gear system to convert the radial motion of a motor into the relatively slow linear reciprocating motion of the shaft and the plate stack, and the motion of a portion of the shaft periodically entering and exiting the bioreactor vessel. The first problem could be problematic for industrial-scale fermentation in addition to necessitate fairly large power consumption. As an alternative, using a close clearance impeller directly with a radial motion, such as the Maxblend system, could be more desirable to achieve uniform mixing (94-96).

Product Separation and Recovery. The separation processes are usually responsible for a large portion of the production costs and, thus, separation is a key aspect of pullulan fermentation. The first operation in the product separation and purification step (Step D in Figures 2.2 and 2.4) is the removal of *A. pullulans* cells from the highly viscous fermentation broth. This is done by either centrifugation or filtration. The fermentation broth has to be diluted many fold to lower its viscosity prior to the centrifugation or filtration operation. The resulting large volume of diluted processing broth leads to higher operating costs in the subsequent steps of pullulan purification. In order to eliminate the presence of cells in the highly viscous fermentation broth, attempts to immobilize *A. pullulans* cells on solid supports and to use immobilized cells in pullulan fermentation has been reported. The utilization of immobilized cells for this purpose is not feasible because considerable numbers of cells leak into the fermentation broth (97). In addition, because pullulan synthesis is partially growth associated, it is inevitable that some cells will be present in the fermentation broth. Filtration is preferred over centrifugation due to lower energy consumption, especially for large scale production. Cross-flow filtration has been used to recover microbial polysaccharides from fermentation broth and showed promising results (98,99). More efficient solvent precipitation methods have also been explored for the recovery pullulan as well as the removal of melanin pigmentation (100).

2.5.3 Melanin Pigmentation

A. pullulans is also known as *black yeast* because of its characteristic black pigmentation associated with mature cells (Figure 2.15). The pigment, melanin, is synthesized from the pentaketide pathway in which 1,8-dihydroxynaphthalene is the direct precursor (101). As a protection strategy in toxic environment (102), melanin, both intracellular and extracellular, is synthesized during the later stage of fermentation where the cell morphology changes from swollen cells to true chlamydospores (103). Thus, melanin production occurs simultaneously with pullulan synthesis, resulting in a dark green to black fermentation broth at the end of the fermentation. This is an undesirable feature for industrial production of pullulan because decolorization (melanin removal) is required during the product separation and purification operations (Step D of Figures 2.2 and 2.4). The synthesis of melanin by *A. pullulans* depends on the culture conditions, such as carbon source and concentration, nitrogen source and concentration, oxygen concentration, and trace minerals (71,82,104) (Figure 2.15). Therefore, such conditions can serve as control variables to minimize melanin synthesis during the pullulan fermentation process. In addition, tricyclazole can be used to repress melanin synthesis, although not completely (102,105). However, the most promising solution to the problem of melanin production during fermentation may be the use of pigment-reduced or nonpigmented strains of *A. pullulans,* which may be obtained by natural isolates or mutation (106). The polysaccharide production capability of the mutant strains seems to be unaffected compared to the parent stains (11,107).

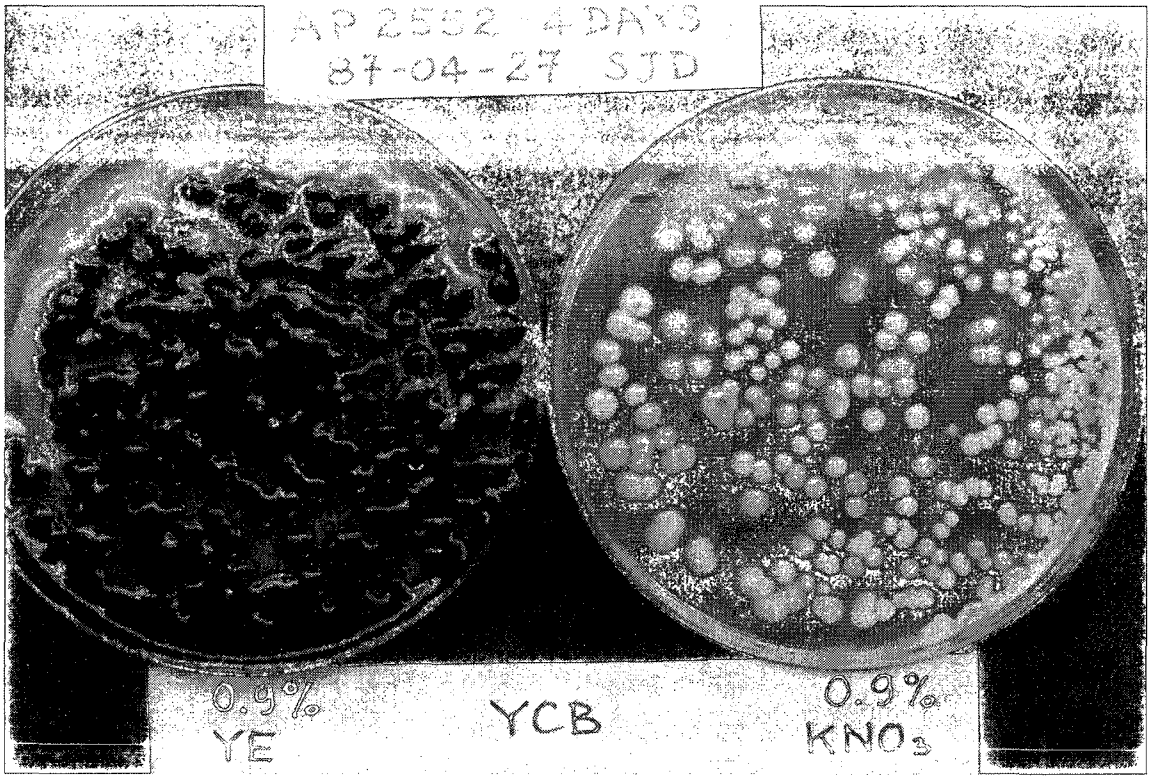

Figure 2.15 Melanin pigment of *A. pullulans* can be controlled by the nitrogen source. Potassium nitrate as nitrogen source instead of yeast extract in a yeast-carbon-base medium greatly reduces the melanin synthesis (*A. pullulans* 2552 after 4 days of incubation).

2.5.4 Pullulanolysis

Pullulanolysis is the breakdown of high MW pullulan in the fermentation broth into lower MW pullulan by the depolymerase activity of *A. pullulans*. The pullulanolysis always occurs during the progress of fermentation and is responsible for the decrease of viscosity of the fermentation broth during the later stage of fermentation. The resulting consequence of pullulanolysis is that only low MW pullulan is obtained at the end of the fermentation. The presence of an extracellular endoamylase, which would cleave pullulan at the maltotetraose units, is suggested as the cause of the observed phenomenon (108). Several amylolytic enzymes, which are capable of extensive starch degradation, have been identified from *A. pullulans* cultures (109). By adding the alpha-amylase inhibitor acarbose into the culture medium, pullulan of slightly higher MW is obtained from late

cultures, which suggests that alpha-amylase is at least partially responsible for the breakdown of pullulan (105). The pullulanolytic breakdown of the pullulan product is worsened when a high-shearing mixing device such as the RT is employed in the fermenter (87,91). Thus, if high MW pullulan is desired as a final product, the fermentation has to be stopped after approximately 24 h, when the MW of pullulan is at its highest value (69,110). This is not, however, an economically feasible solution for industrial practice because the fermentation efficiency (expressed as grams of pullulan produced per 100 g of substrate supplied) is very low after this short fermentation time. A more effective but challenging alternative solution is to acquire more knowledge on the pullulanolysis phenomenon by research, then to develop the technology for the suppression or the inhibition of pullulan-degrading enzyme synthesis by *A. pullulans* during pullulan fermentation.

2.5.5 Sterile and Aseptic Conditions

At the present time, pullulan production by fermentation is carried under sterile and aseptic conditions, which require very high capital and operating costs as in the case of pharmaceutical production. If pullulan is to be produced for use as bulk chemicals and/or bulk commodities, its production costs need to be greatly lowered. A nonsterile and nonaseptic fermentation process would be a possible alternative solution to partially achieve this purpose. A bi-staged pH process has been developed for this purpose (60). In batch fermentation, the pH of the culture medium decreases rapidly from its initial value of 5.0 to the final value of approximately 2.5 within the first 12-36 h and, then, self-stabilizes at this value until the end of the fermentation. It is observed that most of the polysaccharide from the batch fermentation process was synthesized during the self-stabilized acidic phases. Experiments on the effect of the initial pH on the fermentation reveal that at very low initial pH values, such as pH 2, the polysaccharide production is insignificant. However, the biomass concentration obtained under these conditions is very high. This interesting phenomenon served as the basis for the development of the bi-staged pH fermentation process. In this process, the first stage of fermentation is conducted at a very acidic pH for the best production of biomass. When the biomass

concentration reaches its maximum value, the second stage of fermentation is initiated by adjusting the medium pH to a higher value for promoting the synthesis of pullulan. The bi-staged pH process enhances the pullulan concentration in the medium, influences the rheological properties of the fermentation broth, and has the potential to be conducted under nonsterile and nonaseptic conditions. During the first stage of fermentation, the microbial contamination would be negligible due to the very low pH of the medium. During the second stage of fermentation, the contamination could be minimized to an insignificant level due to the high concentration of *A. pullulans* already present in the culture medium. This bi-staged pH process can be used for batch and, possibly, for continuous fermentation processes.

2.6 ACKNOWLEDGEMENTS

The first two co-authors wish to dedicate this work to Professor Anh LeDuy on his recent retirement from Université Laval (Québec, Canada) and to underline his important contributions to biochemical engineering.

2.7 REFERENCES

1. H. Bender, J. Lehmann, and K.Wallenfels, Biochim. Biophys. Acta 36, 309-316 (1959).
2. T.D. Leathers, in E.J. Vandamme, S. De Baets, and A. Steinbuchel eds., *Biopolymers*, vol. 6, Wiley-VCH, Weinheim, 2002, pp. 1-35.
3. R. Taguchi, Y. Kikuchi, Y. Sakano, and T. Kobayashi, Agric. Biol. Chem. 37, 1583-1588 (1973).
4. B.J. Catley and W.J. Whelan, Arch. Biochem. Biophys. 143, 138-142 (1971).
5. B.J. Catley and W. McDowell, Carbohydr. Res. 103, 65-75 (1982).
6. H.J. Jennings and I.C.P. Smith, J. Amer. Chem. Soc. 95, 606-608 (1973).
7. C.G. Fraser and H.J. Jennings, Can. J. Chem. 49, 1804-1807 (1971).
8. N. Waksman, R.M. Delederkremer, and A.S. Cerezo, Carbohydr. Res. 59, 505-515 (1977).
9. A. Forabosco, G. Bruno, L. Sparapano, G. Liut, D. Marino, and F. Delben, Carbohydr. Polym. 63, 535-544 (2006).

10. T. Roukas and G. Serris, Appl. Biochem. Biotechnol. 80, 77-89 (1999).
11. T.P. West and B. Reed-Hamer, FEMS Microbiol. Lett. 113, 345-349 (1993).
12. C.J. Israilides, A. Smith, J.E. Harthill, C. Barnett, G. Bambalov, and B. Scanlon, Appl. Microbiol. Biotechnol. 49, 613-617 (1998).
13. N.A. Yurlova and G.S. de Hoog, Antonie van Leeuwenhoek 72, 141-147 (1997).
14. J.H. Lee, J.H. Kim, I.H. Zhu, X.B. Zhan, J.W. Lee, D.H. Shin, and S.K. Kim, Biotechnol. Lett. 23, 817-820 (2001).
15. J.H. Kim, M.R. Kim, J.H. Lee, J.W. Lee, and S.K. Kim, Biotechnol. Lett. 22, 987-990 (2000).
16. P. Cescutti, R. Pupulin, F. Delben, M. Abbate, M. Dentini, L. Sparapano, R. Rizzo, and V. Crescenzi, Carbohydr. Res. 337, 1203-1209 (2002).
17. H.P. Seo, C.W. Son, C.H. Chung, D.I. Jung, S.K. Kim, R.A. Gross, D.L. Kaplan, and J.W. Lee, Bioresour. Technol. 95, 293-299 (2004).
18. J.W. Lee, W.G. Yeomans, A.L. Allen, F. Deng, R.A. Gross, and D.L. Kaplan, Appl. Environ. Microbiol. 65, 5265-5271 (1999).
19. R.A. Reis, C.A. Tischer, P.A.J. Gorin, and M. Iacomini, FEMS Microbiol. Lett. 210, 1-5 (2002).
20. Ger. Pat. 1,096,850 (January 12, 1961), K. Wallenfels and H. Bender (to Farbwerke Hoechst AG).
21. S. Yuen, Process Biochem. 9, 7-9, 22 (1974).
22. A. LeDuy, L. Choplin, J.E. Zajic, and J.H.T. Luong. in H.F. Mark, N.M. Bikales, C.G. Overberger, and G. Menges eds., Encyclopedia of Polymer Science and Engineering, 2nd ed., vol. 13, Wiley, New York, 1988, pp. 650-660.
23. E. Sachlos and J.T. Czernuszka, Eur. Cell Mater. 5, 29-39 (2003).
24. Y. Tsujisaka and M. Mitsuhashi, in R.L. Whistler and J.N. BeMiller eds., Industrial Gums: Polysaccharides and Their Derivatives, 3rd ed., Academic Press, San Diego, 1993, pp. 447-458.
25. T.D. Leathers, Appl. Microbiol. Biotechnol. 62, 468-473 (2003).
26. M.R. Rekha, and C. P. Sharma, Trends Biomater. Artif. Organs 20, 116-121 (2007).
27. Y. Suginoshita, Y. Tabata, T. Matsumura, Y. Toda, M. Nabeshima, F. Moriyasu, Y. Kada, and T. Chiba, J. Control. Release 83, 75-88 (2002).

28. Y. Suginoshita, Y. Tabata, F. Moriyasu, Y. Ikada, and T. Chiba, J. Pharmacol. Exp. Ther. 298, 805-811 (2001).
29. Y. Tabata, Y. Matsui, K. Uno, Y. Sokawa, and Y. Ikada, J. Interferon Cytokine Res. 19, 287-292 (1999).
30. T. Coviello, P. Matricardi, C. Marianecci, and F. Alhaique, J. Control. Release 119, 5-24 (2007).
31. K. Na and Y.H. Bae, Pharm. Res. 19, 681-688 (2002).
32. K. Na, K.H. Lee, and Y.H. Bae, J. Control. Release 97, 513-525 (2004).
33. K. Akiyoshi, E.C. Kang, S. Kurumada, J. Sunamoto, T. Principi, and F.M. Winnik, Macromolecules 33, 3244-3249 (2000).
34. G. Masci, D. Bontempo, and V. Crescenzi, Polymer 43, 5587-5593 (2002).
35. K. Akiyoshi, S. Kobayashi, S. Shichibe, D. Mix, M. Baudys, S.W. Kim, and J. Sunamoto, J. Control. Release 54, 313-320 (1998).
36. S.W. Jung, Y.I. Jeong, Y.H. Kim, and S.H. Kim, Arch. Pharm. Res. 27, 562-569 (2004).
37. S.W. Jung, Y.I. Jeong, and S.H. Kim, Int. J. Pharm. 254, 109-121 (2003).
38. K. Na, D. Shin, K. Yun, K.H. Park, and K.C. Lee, Biotechnol. Lett. 25, 381-385 (2003).
39. N.B. Thebaud, D. Pierron, R. Bareille, C. Le Visage, D. Letourneur, and L. Bordenave, J. Mater. Sci. Mater. Med. 18, 339-345 (2007).
40. Personal communication with Dr. Charles Doillon, Laval University, Québec, Canada, June 2007
41. Y. Nomura, M. Ikeda, N. Yamaguchi, Y. Aoyama, and K. Akiyoshi, FEBS Lett. 553, 271-276 (2003).
42. T. Hirakura, Y. Nomura, Y. Aoyama, and K. Akiyoshi, Biomacromolecules 5, 1804-1809 (2004).
43. N. Morimoto, T. Endo, M. Ohtomi, Y. Iwasaki, and K. Akiyoshi, Macromol. Biosci. 5, 710-716 (2005).
44. N. Morimoto, T. Endo, Y. Iwasaki, and K. Akiyoshi, Biomacromolecules 6, 1829-1834 (2005).
45. L. Lebrun, J. Blanco, and M. Metayer, Carbohydr. Polym. 61, 1-4 (2005).

46. C. Duval-Terrie, P. Cosette, G. Molle, G. Muller, and E. De, Protein Sci. 12, 681-689 (2003).

47. D. Pantelic, S. Savic, and D. Jakovljevic, Opt. Lett. 23, 807-809 (1998).

48. K. Sugimoto, Ferment. Ind. 36, 98-108 (1978).

49. French Pat. 2,287,911 (May 14, 1976), Anonymous (to Sumitomo Chemical Co., Ltd. and Hayashibara Biochemical Laboratories, Inc.).

50. U.S. Pat. 4,090,016 (May 16, 1978), K. Tsuji, M. Fujimoto, F. Masuko, and T. Nagase (to Sumitomo Chemical Co., Ltd. and Hayashibara Biochemical Laboratories, Inc.).

51. U.S. Pat. 4,152,170 (May 1, 1979), T. Nagase, K. Tsuji, M. Fujimoto, and F.Masuko (to Sumitomo Chemical Co., Ltd. and Hayashibara Biochemical Laboratories, Inc.).

52. U.S. Pat. 4,186,024 (January 29, 1980), M. Fujimoto, K. Fukami, K. Tsuji, and T. Nagase (to Sumitomo Chemical Co., Ltd. and Hayashibara Biochemical Laboratories, Inc.).

53. Can. Pat. 1,078,830 (June 3, 1980), F. Fujita, K. Fukami, and M. Fujimoto (to Sumitomo Chemical Co., Ltd. and Hayashibara Biochemical Laboratories, Inc.).

54. Can. Pat. 1,094,550 (January 27,1981), F. Fujita, K. Fukami, M. Fujimoto, and T. Nagase (to Sumitomo Chemical Co., Ltd.).

55. French Pat. 2,461,718 (February 6, 1981), H. Muto and H. Suzuki (to Shin-Etsu Chemical Co., Ltd.).

56. U.S. Pat. 3,931,146 (January 6, 1976), K. Kato and M. Shiosaka (to Hayashibara Biochemical Laboratories, Inc.).

57. European Pat. 76,698(April 3, 1983), I. Murase, F. Fujita, T. Ohnishi, and T. Tamura (to Sumitomo Chemical Co., Ltd.).

58. Personal communication with Edward Stephenson, Hayashibara Co., Ltd., Colorado, USA, August 2007

59. A. LeDuy, A.A. Marsan, and B. Coupal, Biotechnol. Bioeng. 16, 61-76, (1974).

60. C. Lacroix, A. LeDuy, G. Noel, and L. Choplin, Biotechnol. Bioeng. 27, 202-207 (1985).

61. A. Mulchandani, J.H.T. Luong, and A. LeDuy, Biotechnol. Bioeng. 32, 639-646 (1988).

62. J.M. Boa and A. LeDuy, Biotechnol. Bioeng. 30, 463-470 (1987).

63. B.S. Campbell, B.M. McDougall, and R.J. Seviour, Enzyme Microb. Technol. 33, 104-112 (2003)
64. F. Youssef, T. Roukas, and C.G. Biliaderis, Process Biochem. 34, 355-366 (1999).
65. B.J. Catley, Appl. Microbiol. 22, 650-654 (1971).
66. H.K. Gaidhani, B. McNeil, and X. Ni, Chem. Eng. Res. Des. 83, 640-645 (2005).
67. Z.M. Chi and S.Z. Zhao, Enzyme Microb. Technol. 33, 206-211 (2003).
68. M. Reeslev, T. Strom, B. Jensen, and J. Olsen, Mycol. Res. 101, 650-652 (1997).
69. KY. Lee and Y.J. Yoo, Biotechnol. Lett. 15, 1021-1024 (1993).
70. Y. Lin, Z.S. Zhang, and J. Thibault, Process Biochem. 42, 820-827 (2007).
71. Y. Shabtai and I. Mukmenev, Appl. Microbiol. Biotechnol. 43, 595-603 (1995).
72. B.S. Campbell, A.B.M. Siddique, B.M. McDougall, and R.J. Seviour, FEMS Microbiol. Lett. 232, 225-228 (2004).
73. M. Ronen, H. Guterman, and Y. Shabtai, J. Biochem. Biophys. Methods 51, 243-249 (2002).
74. M.A.J. Finkelman and A. Vardanis, Appl. Environ. Microbiol. 43, 483-485 (1982).
75. Y. Goksungur, S. Dagbagli, A. Ucan, and U. Guvenc, J. Chem. Technol. Biotechnol. 80, 819-827 (2005).
76. L. Tarabasz-Szymanska, E. Galas, and T. Pankiewicz, Enzyme Microb. Technol. 24, 276-282 (1999).
77. J. Audet, M. Lounes, and J. Thibault, Bioprocess Eng. 15, 209-214 (1996).
78. S. Onogi, T. Masuda, and K. Kitagawa, Macromolecules 3, 109-116 (1970).
79. G.B. Tatterson, Fluid Mixing and Gas Dispersion in Agitated Tanks, McGraw-Hill, New York, 1991, pp. 417-528.
80. A. LeDuy and J.E. Zajic, Biotechnol. Bioeng. 15, 579-581 (1973).
81. H. Guterman and Y. Shabtai, Biotechnol. Bioeng. 51, 501-510 (1996).
82. D. Rho, A. Mulchandani, J.H.T. Luong, and A. LeDuy, Appl. Microbiol. Biotechnol. 28, 361-366 (1988).
83. R. Dufresne, J. Thibault, A. LeDuy, and R. Lencki, Appl. Microbial. Biotechnol. 32, 526-532 (1990).
84. M. Lounes, J. Audet, J. Thibault, and A. LeDuy, Bioprocess Eng. 13, 1-11 (1995).
85. J. Audet, J. Thibault, and A. LeDuy, Biotechnol. Bioeng. 52, 507-517 (1996).

86. H. Brauer, Bioprocess Eng. 6, 939-944 (1991).

87. J. Audet, H. Gagnon, M. Lounes, and J. Thibault, Bioprocess Eng. 19, 45-52 (1998).

88. H. Gagnon, M. Lounes, and J. Thibault, Can. J. Chem. Eng. 76, 379-389 (1998).

89. J.F. Perez and O.C. Sandall, AIChE J. 20, 770-775 (1974).

90. M. Nishikawa, M. Nakamura, H. Yagi, and K Hashimoto, J. Chem. Eng. Jpn. 14, 219-226 (1981).

91. K Guerinik, Ph.D. Thesis, Université Laval, Sainte-Foy, Canada, 1989.

92. P.A. Tanguy, F. Thibault, E. Brito-De la Fuente, T. Espinosa-Solares, and A. Tecante, Chern. Eng. Sci. 52, 1733-1741 (1997).

93. T. Espinosa-Solares, E. Brito-De la Fuente, A. Tecante, and P.A. Tanguy, Chem. Eng. Technol. 24, 913-918 (2001).

94. S. Hasegawa, M. Nagatsuru, M. Shibutani, S. Yamamoto, and S. Hasebe, J. Biosci. Bioeng. 88, 68-71 (1999).

95. O. Hiruta, K. Yamamura, H. Takebe, T. Futamura, K. Iinuma, and H. Tanaka, J. Ferment. Bioeng. 83, 79-86 (1997).

96. W.G. Yao, M. Mishima, and K. Takahashi, Chem. Eng. J. 84, 565-571 (2001).

97. A. Mulchandani, J.H.T. Luong, and A. LeDuy, Biotechnol. Bioeng. 33, 306-312 (1989).

98. A. Haarstrick, U. Rau, and F. Wagner, Bioprocess Eng. 6, 179-186 (1991)

99. C. Harscoat, M.Y. Jaffrin, P. Paullier, B. Courtois, and J. Courtois, J. Chem. Technol. Biotechnol. 74, 571-579 (1999)

100. D.K. Kachhawa, P. Bhattacharjee, and R.S. Singhal, Carbohydr. Polym. 52, 25-28 (2003)

101. D.J. Siehr, J. Coatings Technol. 53, 23-25 (1981).

102. R.V. Fogarty and J.M. Tobin, Enzyme Microb. Technol. 19, 311-317 (1996).

103. G.M. Gadd, FEMS Microbiol. Lett. 9, 237-240 (1980).

104. T.P. West and B. Strohfus, World J. Microbiol. Biotechnol. 13, 233-235 (1997).

105. S. Prasongsuk, M.A. Berhow, C.A. Dunlap, D. Weisleder, T.D. Leathers, D.E. Eveleigh, and H. Punnapayak, J. Ind. Microbiol. Biotechnol. 34, 55-61 (2007).

106. T.J. Pollock, L. Thorne, and R.W. Armentrout, Appl. Environ. Microbiol. 58, 877-883 (1992).

107. T.P. West and B. Strohfus, Lett. Appl. Microbiol. 33, 169-172 (2001).

108. B.J. Catley, FEBS Lett. 3, 190-193 (1970).

109. B.C. Saha, R.W. Silman, and R.J. Bothast, Curr. Microbiol. 26, 267-273 (1993).

110. B. McNeil and B. Kristiansen, Biotechnol. Lett. 9, 101-104 (1987).

CHAPTER 3

Aureobasidium pullulans batch cultivations based on a factorial design for improving the production and molecular weight of exopolysaccharides

Yun Lin, Zisheng Zhang, and Jules Thibault *

Department of Chemical Engineering

University of Ottawa

Ottawa, Ontario, K1N 6N5, Canada

* Corresponding author

Email: thibault@genie.uottawa.ca

Tel.: +1-613-5625800 Ext. 6094

Fax: +1-613-5625172

Abstract

Six factors: strain, carbon source, nitrogen source, nitrogen concentration, aeration, and initial pH, were investigated for their effects on exopolysaccharides (EPS) production in Erlenmeyer flasks by *Aureobasidium pullulans* using 2-level fractional factorial design. The concentration and molecular weight (MW) of EPS were optimized simultaneously. The effects of main factors together with possible two-factor interactions were detected, and the levels of the six factors were optimized using empirical models. Analysis of factor effects revealed that strain had the strongest influence on EPS concentration, and nitrogen source on MW of EPS. However, nitrogen concentration did not show significant influence on both parameters. The influences of factors on the production variability were also monitored for quality control purposes. At the optimum levels of control factors investigated, as high as 22.6 g/L EPS with a weight average MW of higher than 2×10^6

was produced. The results of this work indicate that the production kinetics varies for different microorganism-medium-environment systems.

Keywords: *Aureobasidium pullulans*; Pullulan fermentation; Molecular weight; Experimental design; Optimization; Shake flask culture

Nomenclature

A-F	Process variables
ANOVA	Analysis of variance
C	Concentration
d.f.	Degree of freedom
E	Effect of factor
EPS	Exopolysaccharides
F	F ratios
MS	Mean square
MW	Molecular weight
P	Probability
s	Standard deviation
SS	Sum of squares
y_i	Mean of the response of *i*th run

Greek letters

α_i	EPS concentration model coefficient (g/L)
β_i	EPS MW model coefficient

3.1 Introduction

Pullulan is a linear homopolysaccharide of glucose that is produced extracellularly by *Aureobasidium pullulans*. It is usually described as an α-(1→6) linked polymer of maltotriose subunits [1]. The regular alternation of α-(1→4) and α-(1→6) linkages (in the ratio of 2:1) results in some distinctive properties, such as structure flexibility, enhanced water-solubility, and excellent film- and fiber-forming properties [2]. Pullulan is also edible and biodegradable. All these characteristics make it a very useful material. Pullulan is usually used as low-calorie food additives, oxygen-impermeable film for packaging, adhesives, and thickening and extending agents. Pullulan has been in commercial production for about 30 years. It is currently sold at $25/kg. This is still too high for many of its potential applications. Recently, pullulan has been getting renewed attention as an excellent material for pharmaceutical and biomedical applications [1,3].

The high price of pullulan is attributed mainly to the difficulties in its production through fermentation such as high broth viscosity, low product yield, pigmentation, and product degradation [4]. Many factors can influence the pullulan production, including strain [5], temperature [6], pH [7], dissolved oxygen (DO) level (influenced by agitation, aeration) [8], substrate [9,10], trace element [11], fermentation model [12], mixing device [13], and so on. Similar to any other polymer, the molecular weight (MW) of pullulan is a very important parameter, as it determines the polymer characteristics to a large extent. Higher MW pullulan is more desirable for commercial use [5]. Typically, the MW reaches the maximum in the early stage of fermentation and then drastically decreases to a significantly lower level toward the end of fermentation [4,14]. A few factors, such as strain [5], pH [15], substrate [16-18], have been tested for their influence on the MW of pullulan. However, the improvement is so far limited, at the expense of losing productivity in some cases.

Many efforts have been devoted to optimize the fermentation conditions so as to improve the pullulan or crude exopolysaccharides (EPS) production, using the one factor at a time approach [2,6]. However, this approach is not really cost-effective, especially when there might be interactions between some factors. Many results from different studies are not comparable with each other. Sometimes, contradictions are found, such as

the optimal pH for pullulan production [12]. The observed variation in optimal pH was attributed to the different microorganisms, substrate compositions, and fermentation conditions used. This conclusion further implies that specific microorganism-medium-environment systems have specific production kinetics [4]. It is therefore important to optimize the fermentation conditions in different systems.

Statistical methods have proved to be efficient to resolve similar problems in a large number of scientific disciplines. However, to our knowledge, only a few have been used to improve pullulan production. Tarabasz-Szymanska et al. improved pullulan productivity by determining the optimal fermentation medium components and the initial pH using multivariable linear regression analysis [19]. Goksungur et al. investigated sugar concentration, agitation, and aeration at three different levels using response surface methodology [20]. Compared to the 2-level factorial design method, both techniques require to conduct a significantly larger number of experiments yet cannot lead to the identification of easily understood interaction effects [21].

In this investigation, a 2-level fractional factorial design was used to reveal the effects of six physical, chemical and biological factors and their interactions on the fermentation of exopolysaccharides by *A. pullulans*, in order to produce high MW pullulan in large quantities.

3.2 Materials and methods

3.2.1 Microorganisms and culture conditions

Two strains of *A. pullulans*, ATCC 42023 and ATCC 62921, purchased from ATCC, were revived from freeze-dried cultures following the accompanying instructions. They were maintained on their recommended medium, malt extract agar (Blakeslee's formula) and yeast malt agar, respectively, at 4°C, and then subcultured every three weeks. The inoculums for the experimental design were prepared in 300 mL Erlenmeyer flasks containing 100 mL medium. The inoculum medium had the same composition as the culture maintenance medium except that agar was not added. The inoculums were incubated at 28°C and 200 rpm for 36 h. The resulting cultures were used to inoculate the production medium at a level of 5% (v/v). The production medium used had the following

composition (g/L): yeast extract 2.5, K_2HPO_4 5.0, $MgSO_4 \cdot 7H_2O$ 0.2, NaCl 1.0. In addition, as shown in Table 3.1, 50 g/L glucose or sucrose (Lantic granulated table sugar from supermarkets) was used as carbon and energy source. $(NH_4)_2SO_4$ or $NaNO_3$ containing 0.005 M or 0.009 M element nitrogen was used as nitrogen source. Initial pH was adjusted to 5.5 or 6.5 before autoclaving. Two medium volumes (100 mL or 150 mL in 500 mL Erlenmeyer flasks) were used to mimic two aeration conditions. All the flasks were incubated in an orbital incubator-shaker (LAB-LINE, Model 3525CC) operating at 28-30°C and 250 rpm for 7 days. All chemicals were purchased from Sigma-Aldrich Ltd. unless specified otherwise.

3.2.2 Analytical techniques

Samples (6 mL) were taken from each flask every 24 h. The first samples (day 0) were taken from inoculum flasks. The resulting data divided by the dilution rate (i.e. 21) gave the starting point data. Two thirds of each sample (i.e., 4 mL) was diluted with 1 volume of distilled deionized (DD) water before centrifugation at 15 000 rpm (22 000 g) for 15 min. The supernatants were conserved. The cell pellets were washed with 2 mL DD water, and centrifuged again. The second supernatants were combined with the first ones for EPS precipitation by adding 2 volumes of anhydrous ethanol (Commercial Alcohols Inc.). The cells were then suspended and transferred to pre-dried and pre-weighed aluminum dishes, and dried in an oven (Fisher, Model 281) at 105°C overnight before weighing again. The precipitated EPS together with the mother liquor were kept in a refrigerator (Wood's, Model R05NAB) at 4°C for 24 h before filtration through pre-dried and pre-weighed 1 μm membrane filter (Gelman type A/E). The EPS were dried at 105°C for 24 h and then weighed.

The remaining portions of the samples (about 2 mL each) were stored in the refrigerator at -20°C initially for subsequent analysis by gel permeation chromatography (GPC). The EPS were precipitated and washed with ethanol, and then dissolved to give a concentration of 2 g EPS/L in 50 mM $NaNO_3$. All samples were filtered through 0.45 μm membrane filter (Millipore) before injection. The GPC system consists of a Waters 501 HPLC pump, a Waters R401 differential refractometer, and a Shodex OHpak SB-806M HQ column together with its guard column (SB-G). Mobile phase, 50 mM $NaNO_3$, was

running at 1 mL/min. The injection volume was 20 μL for each sample. Narrow pullulan standards (American Polymer Standards Corporation), with molecular weights ranging from 70 to 825 kDa, were used to construct the calibration curve. The signal was collected by a LabView® program and analyzed with Microsoft Excel®.

Two additional replicates of this experimental design were carried out following the identical procedure except that the samples were taken only on day 5 and day 7.

3.2.3 Experimental design

The six factors were examined at two levels as listed in Table 3.1. The levels of the factors were chosen based on information from literature and preliminary experiments. The experiment was carried out using a 16-run (2^4) orthogonal array which is derived from the four-factor full factorial design. The factors were assigned into the columns as shown in Table 3.1.

3.3 Results and discussion

3.3.1 Growth, production and MW curves

Effects of selected factors on cell growth and EPS production, which are the difference between the two levels of each factor, are depicted in Figures 3.1 and 3.2, respectively. The data are from the first set of experiments.

The cell growth curves of the 16 individual runs showed only small differences (data not shown). As a result, the influence of all the six factors are very small as represented by Factors A and B in Figure 3.1. This indicates that cell growth is nearly independent of the fermentation conditions investigated.

On the contrary, the EPS production showed relatively large variation under different conditions. For example, by comparing factor A (Figure 3.2a), it is clear that the EPS concentration reached a plateau on day 5 when using ATCC 42023 (level -1), whereas using ATCC 62921 (level 1), the plateau occurred as early as day 3. The difference of the average EPS concentration of the two strains was even more apparent. And generally, the influences of factors were greater at the later stage of fermentation. However, opposite to

the results in the literature [6, 22, 23], the observed influence of nitrogen concentrations (factor *D*) was insignificant under the conditions examined (Figure 3.2b). All of these observations indicate that the production kinetics is significantly different for different microorganism-medium systems.

Given the dynamic behavior of the cell growth and product formation, day 5 was chosen as the end point of fermentation for the purpose of analysis. And the corresponding data were analyzed to estimate the effect of different factors and their interactions. The small decrease in product concentration from day 5 to day 7, observed in about 50% of the experimental runs (data not shown), is most likely caused by enzymatic degradation [22].

The MW results showed very strong dependence on the strain. First, the day 1 MW results of all the 8 runs using the same strain were located in a narrow region. That range was 1.88-6.08 $\times$ 10^5 for ATCC 42023, and 2.58-6.15 $\times$ 10^4 for ATCC 62921. This indicates that the initial MW was different when different strain was used. Subsequently, the MW differences between runs were widening as the fermentation progressed. The difference between the two strains was diminishing towards the end of fermentation (data not shown). This is probably because one day is not enough to show a significant difference even under very different conditions when the same inoculum is used. However, it may also be hypothesized that, during the lag phase, when the microorganisms were all adapting to the new medium, their behavior for the production of EPS was very similar regardless of different conditions. In addition, most of the runs using ATCC 42023 followed a decreasing trend from day 1 to day 7 as represented by runs 2 and 8 (Figure 3.3a), which is in agreement with most results in the literature [4,14,18]. On the other hand, most of the runs using ATCC 62921 followed a different trend showing a large decrease on day 3 as represented by runs 12 and 15 (Figure 3.3b). However, there were some cases in which the MW values followed very different routes in reaching a plateau, such as in runs 6 and 10 (Figure 3.3). Therefore, it seems possible and quite promising to produce high MW products by manipulating the fermentation conditions.

Table 3.1 Design of experiments: the matrix of 2^4 full design, the factor assignment, and the triplicate results of concentration and MW of EPS on day 5

Run	Main Factors				Interactions											Results *	
	A	*B*	*C*	*D*	*AB*	*AC*	*AD*	*BC*	*BD*	*CD*	*ABC*	*ABD*	*ACD*	*BCD*	*ABCD*	EPS Concentration g/L	Log (MW)
	1	2	3	4	5	6	7	8	9	10	11	12	13	14	15		
1	-1	-1	-1	-1	1	1	1	1	1	1	-1	-1	-1	-1	1	19.31 ± 2.76	5.06 ± 0.74
2	-1	-1	-1	1	1	1	-1	1	-1	-1	-1	1	1	1	-1	19.24 ± 1.09	5.02 ± 0.25
3	-1	-1	1	-1	1	-1	1	-1	1	-1	1	-1	1	1	-1	12.79 ± 2.27	5.32 ± 0.63
4	-1	-1	1	1	1	-1	-1	-1	-1	1	1	1	-1	-1	1	13.14 ± 5.25	5.57 ± 0.48
5	-1	1	-1	-1	-1	1	1	-1	-1	1	1	1	-1	1	-1	16.69 ± 3.96	5.35 ± 0.44
6	-1	1	-1	1	-1	1	-1	-1	1	-1	1	-1	1	-1	1	15.23 ± 1.52	6.55 ± 0.02
7	-1	1	1	-1	-1	-1	1	1	-1	-1	-1	1	1	-1	1	19.91 ± 1.59	4.96 ± 0.59
8	-1	1	1	1	-1	-1	-1	1	1	1	-1	-1	-1	1	-1	20.59 ± 1.15	4.98 ± 0.52
9	1	-1	-1	-1	-1	-1	-1	1	1	1	1	1	1	-1	-1	7.76 ± 3.84	4.79 ± 0.69
10	1	-1	-1	1	-1	-1	1	1	-1	-1	1	-1	-1	1	1	3.43 ± 0.81	6.26 ± 0.06
11	1	-1	1	-1	-1	1	-1	-1	1	-1	-1	1	-1	1	1	7.21 ± 4.58	4.73 ± 0.51
12	1	-1	1	1	-1	1	1	-1	-1	1	-1	-1	1	-1	-1	10.28 ± 3.15	4.51 ± 0.41
13	1	1	-1	-1	1	-1	-1	-1	-1	1	-1	-1	1	1	1	7.01 ± 1.70	5.69 ± 0.15
14	1	1	-1	1	1	-1	1	-1	1	-1	-1	1	-1	-1	-1	9.01 ± 2.20	4.99 ± 0.56
15	1	1	1	-1	1	1	-1	1	-1	-1	1	-1	-1	-1	-1	14.21 ± 0.29	4.00 ± 0.23
16	1	1	1	1	1	1	1	1	1	1	1	1	1	1	1	10.75 ± 0.84	4.11 ± 0.19

A: Strain, ATCC42023 (level -1) & ATCC62921 (level 1)
B: Carbon Source, Glucose (level -1) & Sucrose (level 1)
C: Nitrogen Source, NH_4^+ (level -1) & NO_3^- (level 1)
D: Nitrogen Concentration, 0.005 mol/L (level -1) & 0.009 mol/L (level 1)
E: Aeration (Medium Volume) (assigned to column 11), 100 mL (level -1) & 150 mL (level 1)
F: initial pH (assigned to column 12), 5.5 (level -1) & 6.5 (level 1)
* Results are reported as mean ± S.D.

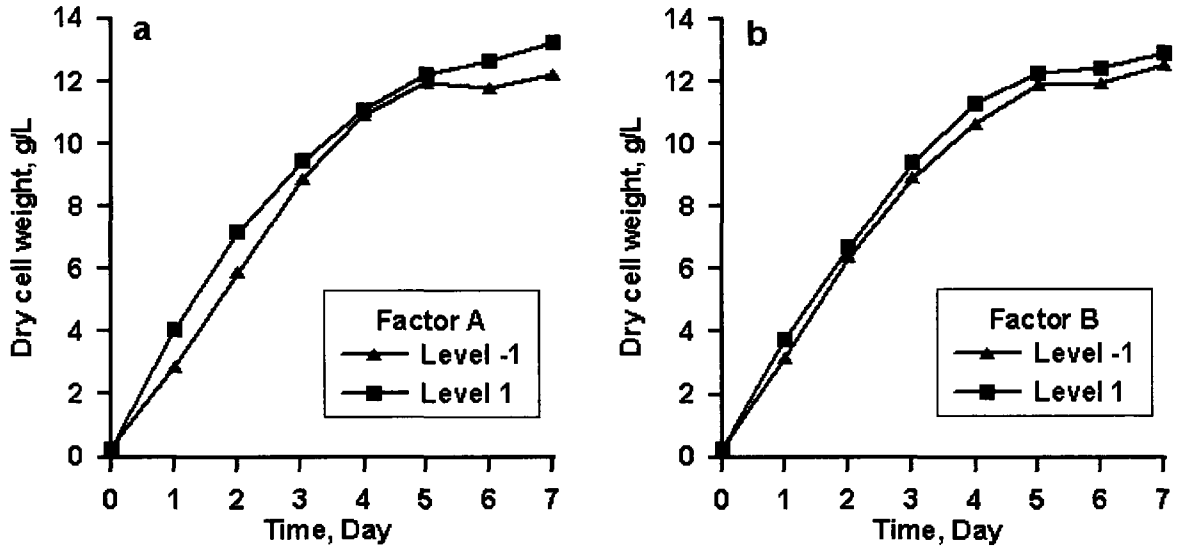

Figure 3.1 Effects of representative factors on cell growth, illustrated by the profile of average dry cell weight at each factor level. a: **Factor A,** b: **Factor B.**

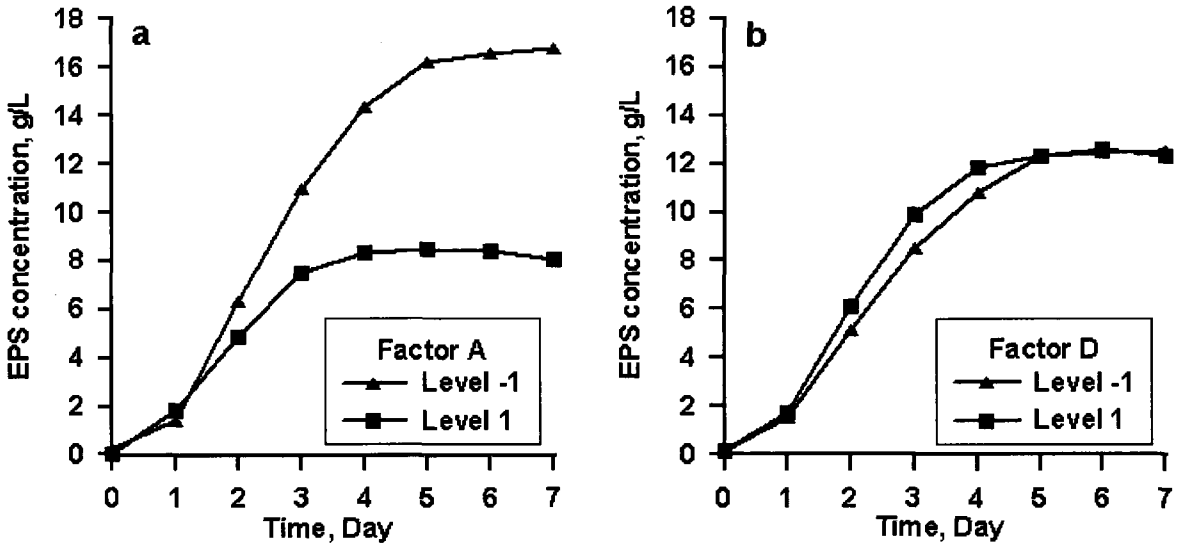

Figure 3.2 Effects of representative factors on EPS production, illustrated by the profile of average EPS concentration at each factor level. a: **Factor A,** b: **Factor D.**

3.3.2 Data Analysis

The triplicate data obtained from day 5 samples are tabulated in Table 3.1. Four parameters were monitored: EPS concentration, MW (in the log form) and their corresponding variability (in the form of log(standard deviation)). It is believed that, if the variability is decreased, the process stability and the product quality will improve. The analysis of EPS concentration is explained below and will serve to illustrate the procedure.

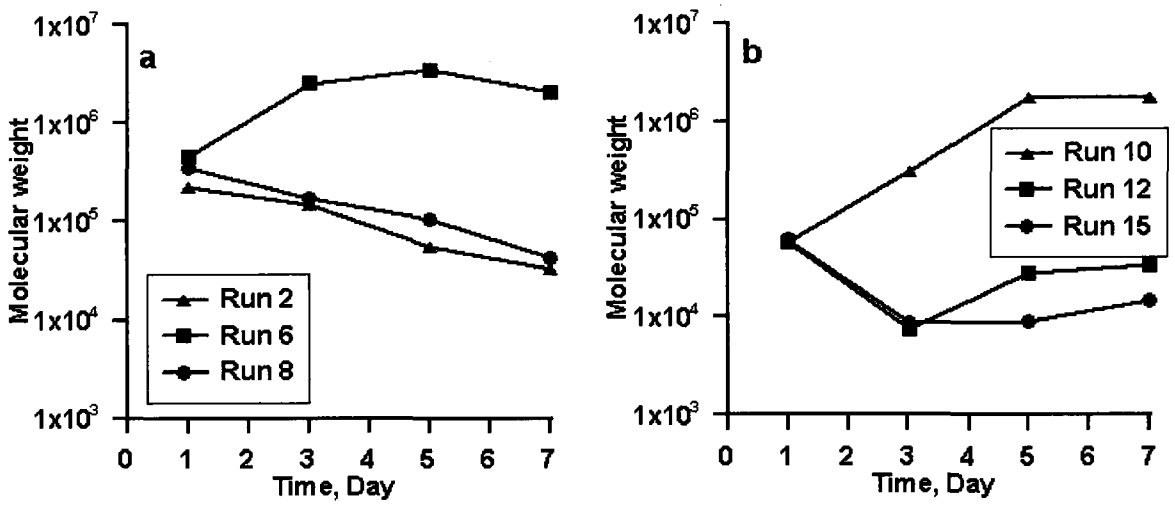

Figure 3.3 Representative molecular weight profiles of each strain. a: **ATCC 42023,** b: **ATCC 62921.**

Although relatively large variations among the triplicates were observed under a few conditions, a two-way analysis of variance (ANOVA) proved that the block effect among the triplicates was not significant at 10% level as shown in Table 3.2. However, the runs showed very significant difference (0.5% level). Therefore, the triplicates were considered as coming from the same statistical distribution in the subsequent analysis, and the block effect was included into the error term.

Table 3.2 Block effect test on EPS concentration (ANOVA)

Source	d.f.	SS	MS	*F*
Run	15	1262.70	84.18	11.88
Block	2	23.63	11.81	1.67
Error	30	212.49	7.08	
Total	47	1498.82		

Notes: $F_{0.10,\,2,\,30} = 2.49$; $F_{0.005,\,15,\,30} = 3.01$

The estimated effect of a factor is calculated by evaluating the average value for the response variable at the high level of the factor, as well as at the low level of the factor, and then taking the arithmetic difference between these two average values [21]. For example: effect of A = (average at level 1 of A)-(average at level -1 of A)

$$E(A) = \frac{\sum_{i=9}^{16} y_i}{8} - \frac{\sum_{i=1}^{8} y_i}{8} \quad (3.1)$$

A positive effect means that the average response at level 1 is higher than that at level -1 for the given factor, and vice versa.

The values of factor effects on all four parameters to be optimized are presented in Table 3.3. By assigning factors *E* and *F* into columns 11 and 12, respectively, the estimated effect calculated from each column has the form as shown in Table 3.3. In this design, the two-factor interactions are always confounding with at least another two-factor interaction. For example, *AC* interaction is confounding with *BE* interaction according to column 6.

Since only rarely will significant three- and four-factor interactions be observed [21], the higher rank interactions were used as noise reference, in this case, columns 13 and 14. The effects calculated from columns 1, 2, 3, 6, 8, 11, and 15 are higher than the noise effects. Since the effect of column 3 is very close to the noise level, only columns 1, 2, 6, 8, 11, and 15, corresponding to Factors *A*, *B*, *AC* or *BE*, *BC* or *AE*, *E*, and *CF* or *DE*, appear to have a significant influence on the EPS concentration. This agrees with the results of the ANOVA analysis, as shown in Table 3.4.

Because of the confounding effects of this design, it is not clear which interaction is responsible for the effect shown. Further test should be performed to differentiate the confounding effects. However, experience has shown that real interaction effects are not likely to occur unless at least one of the factors involved in the interaction has a significant main effect [21]. Therefore, those interactions, of which both component factors do not have significant main effects, are eliminated. For example, "*CF*" interaction was not likely to be a real effect, because both *C* and *F* did not show significant main effects on EPS concentration. If there are still some confounding effects left, any of the confounding effects can be used to represent the effects detected. The relationship between the EPS concentration and the statistically significant factors was established by regression method (Table 3.5). The regression model for EPS concentration is shown below:

$$C(EPS) = \alpha_0 + \alpha_1 A + \alpha_2 B + \alpha_6 AC/BE + \alpha_8 AE/BC + \alpha_{11} E + \alpha_{15} DE$$
$$= 12.91 - 4.20A + 1.26B + 1.20 \times AC/BE + 1.49 \times AE/BC - 1.16E - 0.91 \times DE \quad (3.2)$$

With a coefficient of determination R^2 of 0.95 and where all factors are defined as -1 or 1 as presented in Table 3.1.

The same method was applied to the analysis of the "log(*s*)" values of EPS concentration in order to decrease the variability with the exception that "pooled out" ANOVA was used for the log(*s*) analysis. Since the errors had to be pooled from columns 13 and 14, only two degrees of freedom remained. Thus, any effect had to have a very large *F* value in order to show statistical significance. Since this was not the case, there was no need to derive a mathematical model.

The MW data were analyzed using the same technique. The only difference is that the block effect among triplicates was identified to be significant at 1% level. However, it was still treated as an error term in the ANOVA, because this effect was not controllable.

Table 3.5 also shows that the regression model between log(MW) and the statistically significant factors is:

$$\log(MW) = \beta_0 + \beta_1 A + \beta_3 C + \beta_5 AB/CE/DF + \beta_6 AC + \beta_8 BC/AE + \beta_{12} F + \beta_{15} CF$$
$$= 5.12 - 0.23A - 0.35C - 0.15 \times AB/CE/DF - 0.20 \times AC - 0.22 \times BC/AE - 0.18F + 0.25 \times CF \quad (3.3)$$

With a coefficient of determination R^2 of 0.87.

All the optimized levels of factors, which are indicated by the ANOVA and factor effect analysis, are summarized in Table 3.6. For EPS concentration and log(MW), the optimized levels are listed when their significance levels are higher than 5%. For the log(s) analysis of log(MW), no factor is significant even at the 10% level. However, the five most influential ones are listed for further consideration.

Table 3.3 Effects of the different factors and their interactions

Factor	A	B	C	D	AB CE DF	AC BE	AD BF	BC AE	BD AF	CD EF	E	F	*	*	CF DE
Column	1	2	3	4	5	6	7	8	9	10	11	12	13	14	15
EPS Concentration, g/L	-8.41	2.53	1.40	-0.40	0.54	2.41	-0.28	2.98	-0.16	0.56	-2.32	0.11	-0.08	-1.39	-1.82
log(s)	-0.12	-0.28	-0.05	-0.11	-0.15	-0.08	0.04	-0.37	0.11	0.24	-0.09	0.24	-0.02	-0.08	0.04
log(MW)	-0.46	-0.08	-0.69	0.26	-0.30	-0.40	-0.10	-0.44	-0.10	-0.22	0.25	-0.36	0.00	0.13	0.49
log(s)	-0.1	-0.2	0.27	-0.33	0.11	-0.15	0.15	0.03	0.12	0.24	-0.29	0.3	-0.15	-0.1	-0.32

* indicates noise effect

Table 3.4 ANOVA performed on EPS concentration

Source	d.f.	SS	MS	*F*	
1: *A*	1	847.77	847.77	114.89	***
2: *B*	1	76.70	76.70	10.39	***
3: *C*	1	23.56	23.56	3.19	
4: *D*	1	1.93	1.93	0.26	
5: *AB=CE=DF*	1	3.56	3.56	0.48	
6: *AC=BE*	1	69.66	69.66	9.44	***
7: *AD=BF*	1	0.91	0.91	0.12	
8: *BC=AE*	1	106.58	106.58	14.44	***
9: *BD=AF*	1	0.30	0.30	0.04	
10: *CD=EF*	1	3.81	3.81	0.52	
11: *E*	1	64.58	64.58	8.75	***
12: *F*	1	0.14	0.14	0.02	
13: Noise	1	0.07	0.07	0.01	
14: Noise	1	23.21	23.21	3.14	
15: *CF=DE*	1	39.92	39.92	5.41	**
Error	32	236.12	7.38		
Total	47	1498.821			

Notes: $F_{0.05,1,32} = 4.15$, $F_{0.01,1,32} = 7.51$;
** indicates that the effect is statistically significant at the 5% significance level
*** indicates that the effect is statistically significant at the 1% significance level

Table 3.5 Estimated regression coefficients for EPS concentration and MW of EPS

EPS Concentration				Log(MW) of EPS			
Term	Estimate	*t* Ratio	P > |*t*|	Term	Estimate	*t* Ratio	P > |*t*|
Constant	12.91	35.4	<0.0001	Constant	5.12	61.18	<0.0001
1	-4.2	-11.52	<0.0001	1	-0.23	-2.78	0.0239
2	1.26	3.47	0.0071	3	-0.35	-4.14	0.0032
6	1.21	3.31	0.0092	5	-0.15	-1.78	0.1129
8	1.49	4.08	0.0027	6	-0.2	-2.4	0.043
11	-1.15	-3.18	0.0112	8	-0.22	-2.63	0.0301
15	-0.91	-2.5	0.0338	12	-0.18	-2.13	0.0654
				15	0.25	2.97	0.018

3.3.3 Discussion

3.3.3.1 Biological effect on EPS production

Strain (factor *A*) showed the strongest influence on the EPS production. The average EPS concentration of all runs using ATCC 42023, was 8.41 g/L higher than that of all runs using ATCC 62921 (Table 3.3). The average molecular weight of the EPS produced by

ATCC 42023 strain was also significantly higher than that produced by ATCC 62921 (Table 3.6). This clearly shows that the production kinetics is different for different microorganism-medium-environment systems with respect to the microorganism.

However, strain ATCC 42023 usually produces some pigments in the fermentation broth, depending on the operating conditions, whereas ATCC 62921 is almost pigment-free. If ATCC 42023 is used for production, one additional purification step, the adsorption of melanin with activated carbon, is required to remove the melanin.

Table 3.6 Summary of analyses of factor effects (based on ANOVA)

Column	Factor	Level which will optimize			
		EPS Concentration		Log(MW)	
		Mean	log *s*	Mean	log *s*
1	***A*: Strain**	-1 ***		-1 ***	
2	***B*: Carbon**	1 ***	1 **		
3	***C*: Nitrogen**			-1 ***	-1
4	***D*: N Concentration**				1
5	***AB=CE=DF***			-1 **	
6	***AC=BE***	1 ***		-1 ***	
7	***AD=BF***				
8	***BC=AE***	1 ***	1 **	-1 ***	
9	***BD=AF***				
10	***CD=EF***		-1 *		
11	***E*: Aeration**	-1 ***			1
12	***F*: pH**		-1 *	-1 **	-1
15	***CF=DE***	-1 **		1 ***	1

* indicates that the effect is statistically significant at the 10% significance level
** indicates that the effect is statistically significant at the 5% significance level
*** indicates that the effect is statistically significant at the 1% significance level

3.3.3.2 Physical effect on EPS production

Aeration effect was mimicked using different volumes of medium in the flasks as used by Rho et al. [24]. More medium in the flask gives lower headspace and gas-liquid interfacial surface area and therefore lower available oxygen per unit volume of medium. It was not possible to measure the dissolved oxygen with 16 shake flasks running simultaneously. From Table 3.6, we can see that level -1, which corresponds to a lower medium volume and higher aeration, was better than level 1, indicating that more aeration will increase the EPS production. This result agrees with the findings of many other groups [24-26]. However, it was reported that very high DO level was not conducive to

better EPS production [8], and high level of DO promoted melanin production [24]. Also, high aeration rate was detrimental to achieving high MW [5]. However, our results for the conditions tested in this investigation do not support this previous observation on MW (Table 3.6). A possible explanation for the disagreement is that increasing aeration rate in a fermenter is inevitably accompanied by higher shear stress, under which long molecular chains are subjected to physical degradation. In the current investigation, change in the aeration rate by changing the medium volume did not produce a change in shear stress, and thus had no significant effect on the MW.

3.3.3.3 Chemical effects on EPS production

Four chemical factors were investigated: carbon source, nitrogen source, nitrogen concentration, and pH. As a carbon source, sucrose was found to be better than glucose in enhancing EPS production and in lowering production variability. Nitrogen source had the most significant influence on MW of the products. For the production of high MW product, NH_4^+ was found to be better than NO_3^-. However, nitrogen concentration did not show any significant influence on the "Mean" and "log(*s*)" of both the concentration and MW of the product. This result is probably caused by the yeast extract used in the fermentation medium. Compared to the concentration of yeast extract, the inorganic nitrogen concentration was relatively low. The effect of nitrogen concentration, even if present, may have been masked by the element present in the yeast extract. When the initial pH assumed the lower level, 5.5, measured MW of the EPS was higher and the variability of both EPS concentration and MW were lower. However, pH seemed to have very little influence on EPS concentration.

3.3.3.4 Interaction effects and optimization of fermentation conditions

Sometimes the factors influence each other. Their effects cannot be treated as being additive. It is easier to understand the interactions using the mathematical models. For example, if only factors *A*, *C* and their interaction *AC* in the MW model (-0.23*A*-0.35*C*-0.20*AC*) are considered, it can be observed that when *C* is set to level -1, the influence of *A* is counteracted by *AC* interaction. Indeed, the difference between the two levels of *A* is only 0.06. However, when *C* is set to level 1, the influence of *A* is amplified by *AC* interaction, the difference between two levels of *A* become 0.86. The effect of factor interactions can be greater than those of individual factors. As indicated in Table 3.3, the

effect of *BC* or *AE* interaction on EPS concentration is greater than the main effect of many factors.

Due to the existence of confounding interaction effects in Equations 3.2 and 3.3, two unique sets of optimal parameters cannot be obtained directly from this work. We have identified several possibilities for the optimal conditions that would lead to high EPS concentration or high MW EPS using the model, as shown in Table 3.7. There are four possible combinations of the interaction terms in Equation 3.2, including, *AE* and *AC*, *AE* and *BE*, *BC* and *AC*, as well as *BC* and *BE*. Similarly six possible combinations of the interaction terms were identified from Equation 3.3, and they are *AE* and *AB*, *AE* and *CE*, *AE* and *DF*, *BC* and *AB*, *BC* and *CE* as well as *BC* and *DF*. Based on the results in Table 3.7, the optimal levels of factors *A*, *B*, and *F* should be -1, 1, and -1, respectively, which is also the requirement to reduce process variability (Table 3.6). The combinations of the other factors can be narrowed down to four possibilities, as shown in Table 3.8. And the predictions are calculated by applying all the four EPS concentration models and six MW models to the possible optimal conditions.

Table 3.7 Predicted possible optimal conditions for EPS concentration and MW

Interaction combinations	Factors and optimal levels						Model predictions
	A	*B*	*C*	*D*	*E*	*F*	
EPS Concentration							**g/L**
AE and *AC*	-1	1	-1	1	-1	*	23.13
AE and *BE*	-1	1	*	1	-1	*	20.73
BC and *AC*	-1	1	1	1	-1	*	20.73
BC and *BE*	-1	1	1	-1	1	*	20.81
EPS Molecular Weight							**log(MW)**
AE and *AB*	-1	1	-1	*	1	-1	6.3
AE and *CE*	-1	*	-1	*	1	-1	6.3
AE and *DF*	-1	*	-1	1	1	-1	6.3
BC and *AB*	-1	1	-1	*	*	-1	6.3
BC and *CE*	-1	1	-1	*	1	-1	6.3
BC and *DF*	-1	1	-1	1	*	-1	6.3

* the level 1 or level -1.

Based on the predictions, it is obvious that only the first set of fermentation conditions listed in Table 3.8 is promising for the production of high MW EPS at large quantities. A four-replicate confirmation test was carried out under such condition: *A* = -1,

$B = 1$, $C = -1$, $D = 1$, $E = -1$ and $F = -1$. The EPS concentration on day 5 was found to be 22.6 ± 0.7 g/L. This agrees very well with the prediction of 20.44 ± 2.21 g/L. The corresponding weight average MW values were always higher than 2×10^6 [log(MW) = 6.41 ± 0.09], which is slightly higher than the predicted value of 5.98 ± 0.29. According to our knowledge, this is so far the best results produced by ATCC 42023. The production of EPS is 51% higher than that obtained by Lee et al., with comparable MW [2].

Table 3.8 Predictions of the EPS concentration and the logarithm of its MW for the four possible optimal conditions

	Factor Levels *			Predictions **	
	C	*D*	*E*	EPS Concentration, g/L	Log(MW)
High EPS Concentration	-1	1	-1	20.44 ± 2.21	5.98 ± 0.29
	1	1	-1	20.73 ± 0	5.06 ± 0
	1	-1	1	18.12 ± 2.21	5.08 ± 0.29
High MW	-1	1	1	16.01 ± 0	6.30 ± 0

* Factors *A*, *B*, and *F* are at level -1, 1 and -1, respectively.

** Prediction values are reported as mean ± S.D. of the different model predictions.

3.4 Conclusions

The cell growth of *A. pullulans* followed almost the same trend within the scope of our experiment, while EPS production showed various responses to different conditions. The decrease trend of MW values was quite clear in some cases. However, the increase of MW was also observed under certain conditions. The analysis of factor effects revealed that strain had the strongest influence on EPS concentration, and nitrogen source on MW of EPS, while nitrogen concentration did not show significant influence on both concentration and MW of EPS. The optimal conditions were determined from the regression models and confirmed by the additional runs. All these results imply that the EPS production kinetics by *A. pullulans* is dependent on the specific microorganism-medium-environment systems.

3.5 Acknowledgements

The authors wish to acknowledge the financial support of the Natural Sciences and Engineering Research Council of Canada.

3.6 References

[1] Leathers TD. Biotechnological production and applications of pullulan. Applied Microbiology and Biotechnology 2003; 62:468-473.

[2] Lee JH, Kim JH, Zhu IH, Zhan XB, Lee JW, Shin DH, Kim SK. Optimization of conditions for the production of pullulan and high molecular weight pullulan by *Aureobasidium pullulans*. Biotechnology Letters 2001; 23:817-820.

[3] Shingel KI. Current knowledge on biosynthesis, biological activity, and chemical modification of the exopolysaccharide, pullulan. Carbohydrate Research 2004; 339:447-460.

[4] Thibault J, LeDuy A. Pullulan, microbial production methods. In: Flickinger MC, Drew SW editors. Encyclopedia of Bioprocess Technology: Fermentation, Biocatalysis, and Bioseparation. New York: John Wiley & Sons; 1999. p. 2232-2247.

[5] Gibson LH, Coughlin RW. Optimization of high molecular weight pullulan production by *Aureobasidium pullulans* in batch fermentations. Biotechnology Progress 2002; 18:675-678.

[6] Chi ZM, Zhao SZ. Optimization of medium and cultivation conditions for pullulan production by a new pullulan-producing yeast strain. Enzyme and Microbial Technology 2003; 33:206-211.

[7] Lacroix C, Leduy A, Noel G, Choplin L. Effect of pH on the Batch Fermentation of Pullulan from Sucrose Medium. Biotechnology and Bioengineering 1985; 27:202-207.

[8] Gibbs PA, Seviour RJ. Does the agitation rate and/or oxygen saturation influence exopolysaccharide production by *Aureobasidium pullulans* in batch culture? Applied Microbiology and Biotechnology 1996; 46:503-510.

[9] Barnett C, Smith A, Scanlon B, Israilides CJ. Pullulan production by *Aureobasidium pullulans* growing on hydrolysed potato starch waste. Carbohydrate Polymers 1999; 38:203-209.

[10] Goksungur Y, Ucan A, Guvenc U. Production of pullulan from beet molasses and synthetic medium by *Aureobasidium pullulans*. Turk J Biol 2003; 28:23-30

[11] West TP, Strohfus B. Effect of manganese on polysaccharide production and cellular pigmentation in the fungus *Aureobasidium pullulans*. World Journal of Microbiology & Biotechnology 1997; 13:233-235.

[12] Youssef F, Roukas T, Biliaderis CG. Pullulan production by a non-pigmented strain of *Aureobasidium pullulans* using batch and fed-batch culture. Process Biochemistry 1999; 34:355-366.

[13] Audet J, Gagnon H, Lounes M, Thibault J. Polysaccharide production: Experimental comparison of the performance of four mixing devices. Bioprocess Engineering 1998; 19:45-52.

[14] Lee JW, Yeomans WG, Allen AL, Deng F, Gross RA, Kaplan DL. Biosynthesis of novel exopolymers by *Aureobasidium pullulans*. Applied and Environmental Microbiology 1999; 65:5265-5271.

[15] Lee KY, Yoo YJ. Optimization of pH for High Molecular Weight Pullulan. Biotechnology Letters 1993; 15:1021-1024.

[16] Kim JH, Kim MR, Lee JH, Lee JW, Kim SK. Production of high molecular weight pullulan by *Aureobasidium pullulans* using glucosamine. Biotechnology Letters 2000; 22:987-990.

[17] Seo HP, Son CW, Chung CH, Jung DI, Kim SK, Gross RA, Kaplan DL, Lee JW. Production of high molecular weight pullulan by *Aureobasidium pullulans* HP-2001 with soybean pomace as a nitrogen source. Bioresource Technology 2004; 95:293-299.

[18] Israilides C, Scanlon B, Smith A, Harding SE, Jumel K. Characterization of Pullulans Produced from Agroindustrial Wastes. Carbohydrate Polymers 1994; 25:203-209.

[19] Tarabasz-Szymanska L, Galas E, Pankiewicz T. Optimization of productivity of pullulan by means of multivariable linear regression analysis. Enzyme and Microbial Technology 1999; 24:276-282.

[20] Goksungur Y, Dagbagli S, Ucan A, Guvenc U. Optimization of pullulan production from synthetic medium by *Aureobsidium pullulans* in a stirred tank reactor by response surface methodology. Journal of Chemical Technology and Biotechnology 2005; 80:819-827.

[21] Lochner RH, Matar JE. Designing for quality: an introduction to the best of Taguchi and western methods of statistical experimental design. New York: Quality Resources; 1990. p. 29, 80, 164.

[22] Campbell BS, McDougall BM, Seviour RJ. Why do exopolysaccharide yields from the fungus *Aureobasidium pullulans* fall during batch culture fermentation? Enzyme and Microbial Technology 2003; 33:104-112.

[23] Bulmer MA, Catley BJ, Kelly PJ. The Effect of Ammonium-Ions and pH on the Elaboration of the Fungal Extracellular Polysaccharide, Pullulan, by *Aureobasidium Pullulans*. Applied Microbiology and Biotechnology 1987; 25:362-365.

[24] Rho D, Mulchandani A, Luong JHT, Leduy A. Oxygen Requirement in Pullulan Fermentation. Applied Microbiology and Biotechnology 1988; 28:361-366.

[25] McNeil B, Kristiansen B. Influence of Impeller Speed Upon the Pullulan Fermentation. Biotechnology Letters 1987; 9:101-104.

[26] Lazaridou A, Roukas T, Biliaderis CG, Vaikousi H. Characterization of pullulan produced from beet molasses by *Aureobasidium pullulans* in a stirred tank reactor under varying agitation. Enzyme and Microbial Technology 2002; 31:122-132.

CHAPTER 4

Comparison of experimental designs using neural networks

Yun Lin, Zisheng Zhang and Jules Thibault*
Department of Chemical and Biological Engineering
University of Ottawa
Ottawa, Ontario, K1N 6N5, Canada

*Corresponding author.
Email: Jules.Thibault@uottawa.ca
Tel.: +1-613-5625800 Ext. 6094; Fax: +1-613-5625172

Abstract

Experimental designs were compared using stacked-layer feed-forward neural networks. Several traditional 3-level designs and uniform designs were investigated using 3-factor linear and non-linear models. The prediction error was found to be inversely proportional to the number of experiments. Uniform designs displayed better performance than traditional 3-level designs for the same number of experiments. The sum of squares of prediction errors was generally smaller for uniform designs. The performance difference between 3-level designs and uniform designs was attributed to the number of factor levels. This was confirmed by further investigation on random designs with more factor levels.

Keywords: neural networks, design of experiments, uniform design, prediction, modeling

4.1 INTRODUCTION

One factor at a time approach has been proved inefficient in many optimization processes, and experimental designs are getting increasingly popular in both industry and academia. In industry, the most frequently used designs are the highly fractional factorial design and Plackett-Burman design due to the small number of experiments needed. These two-level designs can estimate the main effect of factors with a small number of experiments in the screening phase, and then they can be folded over in the optimization phase, in order to estimate the 2-factor interactions (Nelson et al., 2000). In academic research, more comprehensive and accurate models are usually required. However, nowadays, there are numerous experimental designs that can be chosen from, such as Box-Behnken design, central composite design (CCD), and Taguchi design. These designs vary significantly in their complexity, the number of experiments required and, more importantly, the amount and accuracy of the information that can be gathered. The challenge is to choose the most appropriate design methodology that would provide the desired information while keeping the number of experiments and, as a result, the cost of performing experiments to a minimum.

Many studies have been performed to compare some of the designs and strategies. Monness et al. (2007) have revealed how efficient Plackett–Burman design and fractional factorial design are compared to the full design. Hurrion and Birgil (1999) have compared the full designs to some random designs of similar size. Jensen and Ramirez (1996a, b) analyzed several designs using complexity as a criterion as well as A- and D-optimality. Nelson et al. (2000) explored several design augmentation strategies.

In this investigation, several traditional and newer experimental designs were compared to each other. Due to its global approximation capability, neural networks were chosen to extract and encapsulate the information from each design set in order to rebuild the underlying model. The prediction errors of a large set of random points within the experimental domain were used to assess the fitness of the models obtained from different experimental designs. The efficiency of different designs was revealed and discussed as well as possible reasons to explain the observed differences between them.

4.2 METHODOLOGY

4.2.1 Experimental Designs

Since the introduction of Plackett-Burman design in 1946, a large number of experimental designs have been proposed. Detailed description of many of these designs can be found on-line (NIST/SEMATECH, 2008). Some of the most popular designs, as listed below, were considered and compared in this work. All these designs were used to deal with two model problems, both of which involve 3 factors. Most of these designs investigate only 3 levels for each factor so as to minimize the requirement on the number of experiments.

9-run Taguchi Design L_9 (3^4)

A typical Taguchi design includes both inner and outer arrays. However, only the inner array is considered here. Taguchi L_9 design is an orthogonal design capable of examining up to four factors, each at three levels.

11-run D-optimal Design

Optimal designs have several variants. D-optimal design is more popular than the others. It is generated by seeking the maximum of the determinant of the information matrix of the design, based on a predetermined model and the researcher's requirement on the number of experiments. Optimal designs are flexible in terms of the number of experiments. The incorporation of a model prior to the experiments is very effective in reducing the number of experiments. However, it could also lead to biased results if the model is not a sufficiently good representation of the process being studied.

For a 3-factor problem, the minimal number of experiments to estimate all first- and second-order effects (X_1, X_2, X_3, X_1X_1, X_1X_2, X_1X_3, X_2X_2, X_2X_3, X_3X_3) is 10. Together with a center point (no replicate), the total number of experiments for the D-Optimal design is 11.

13-run Box-Behnken Design

For a 3-level 3-factor problem, Box-Behnken design consists of 12 peripheral design points together with some, usually 3, center points to estimate the variance.

However, for this investigation, only 1 center point is included. This leads to the 13-run Box-Behnken design.

15-run Central Composite Design (face centered, $\alpha = 1$)

Central composite design (CCD), also known as Box-Wilson central composite design, has three variants: circumscribed, inscribed, and face centered CCD. Since only 3 levels per factor are to be investigated, the only candidate is the face centered CCD. Again, only one center point is considered in this design.

27-run Full Design

Full design covers all possible combinations of factors and levels, and thus provides more complex and detailed information. A 2-level full design is capable of differentiating all the main effects and factor interactions. However, it is rarely carried out in practice due to the large number of runs required, especially when there are a large number of factors and levels. The full design for a 3-level 3-factor problem requires 27 (3^3) experiments.

In addition to the designs listed above, two more designs are included to more adequately cover the wide gap between the 15-run CCD and the 27-run full design.

19-run D-Optimal Design

For this 19-run D-Optimal design, the same priori model is assumed in order to estimate all first- and second-order effects just as what was done for the 11-run D-Optimal design. The center point happens to be already included.

23-run 3-level Random Design.

Since there is no suitable experimental design that performs 23 runs to deal with 3 factors each at 3 levels, 4 points are randomly removed from the full design to produce a 3-level random design.

Uniform Designs

In addition to the traditional designs, uniform design is also getting the attention of many research groups since its introduction (Fang, 1980; Wang and Fang, 1981; Zhang et al., 1993, 1998; Liang et al., 2001). Uniform designs make no assumption about the underlying function. They are based on the assumption that the more uniform the design points are spread within the domain, the better the model will represent the underlying function (Fang et al., 2000). In uniform designs, the objective is to allocate experimental

points uniformly scattered in the experimental domain. Uniform designs based on centered L_2 discrepancy ($U_n(n^s)$) have a unique property in that it can estimate n levels of up to n-1 factors with just n runs. This reduces dramatically the required number of experiments, especially when a large number of levels have to be investigated. In addition, similar to optimal designs, the number of experiments is flexible for a specific problem. As tabulated on a website dedicated to this type of design, for a 3-factor problem, the number of runs as well as levels for each factor can be any integer between 4 and 30 (Anonymous, 2008).

Uniform designs with the same number of experiments as the other designs mentioned above are investigated so that these two fairly different categories of experimental designs can be compared to each other. Since all the other designs investigate only 3 levels for each factor, they will be collectively referred to as "3-level designs".

23-run 7-level and True Random Designs

In order to confirm the possible reasons for the difference in performance between 3-level designs and uniform designs, a 23-run 7-level random design and a true random design are also investigated. In the 7-level random design, each factor can assume any of the 7 equally spaced levels randomly. In the true random design, each experiment is chosen in a completely random fashion within the domain of experimentation.

4.2.2 Models

In order to properly evaluate the efficiency of the different designs, multi-dimensional theoretical models, whose solutions are known, were used as the true underlying functions. Two such models are selected. The first one is a linear model with respect to parameters. This model represents processes that can be tackled using response surface methodology. The second one is a non-linear model. It represents any problem with independent variables that have wider range of interest, and thus invariably making the dependent variable non-linear.

4.2.2.1 Pullulan production model

Although pullulan has been produced commercially since 1978, the production mechanism on the genetic level is still far from being fully understood. As a result, only empirical models can be built to optimize pullulan production. One of these models was derived from an experimental central composite design (Goksungur et al., 2005):

$$Y = -29.851 + 1.189X_1 + 0.057X_2 + 5.086X_3 - 0.011X_1^2 - 0.0000607X_2^2 - 1.3633X_3^2 - 0.000296X_1X_2 + 0.0263X_1X_3 \quad (4.1)$$

This model predicts the final concentration of pullulan (g/L) as a function of the initial substrate concentration (X_1), the speed of agitation (X_2), and the air flow rate (X_3). The ranges of variation of the independent variables are X_1: 30-70 g/L, X_2: 200-600 rpm, and X_3: 1.0-3.0 vvm. The range of variation of the dependent variable Y is [4.96, 17.00].

4.2.2.2 Non-linear model

The non-linear model is an equation selected for its very different topology and nonlinearity compared to the first model. The equation for the nonlinear model is:

$$Y = \frac{\ln(X_1)(\sin X_2 + 4)}{e^{X_3}} + \ln(X_1)e^{X_3} \quad (4.2)$$

where the ranges of variation of the independent variables are X_1: [0.1, 10], X_2: [$-\pi/2$, $\pi/2$], and X_3: [0, 1] leading to a variation of the dependent variable Y in the range of [-13.82, 13.82].

For both models, all the input variables were scaled in the range [-1, 1] before being used as training data in the neural networks. Except for the true random designs, the levels investigated are always equally spaced between -1 and 1. For example, -1, 0, and 1 are used for all 3-level designs, while 0, ±0.2, ±0.4, ±0.6, ±0.8 and ±1 are used for the 11-run uniform design.

4.2.3 Neural Networks

Artificial neural networks have been used for numerous applications in many disciplines (Metting and Coenegrache, 1996; Lanouette et al., 1999; Nagata and Chu, 2003). It can also be used for data analysis of experimental designs (Hurrion and Birgil, 1999). It is usually found to have equivalent or superior performance than traditional

analysis methods for experimental designs, that is, analysis of variance and/or regression method. However, it is important to stress that traditional analysis method can retrieve some important information such as: the main effect and interaction effect in terms of their coefficients, the alias structures and thus the confounding effects, the steepest ascent direction. This kind of information is not obvious to obtain, if it is actually possible, using neural networks (Nagata and Chu, 2003).

Neural Networks were chosen to develop the model relating the dependent variable to the independent variables for all experimental designs because they possess universal approximation capability (Cybenko, 1989; Bishop, 1994). This property makes it possible to represent any continuous function with the required accuracy. The only difficulty is to find an optimal structure that is determined by the number of hidden layer neurons and the activation functions used for both hidden and output layers, for a specific problem. Typical activation functions for standard three-layer feed-forward neural networks (FFNNs) include linear, threshold, and sigmoid functions (Bishop, 1994).

In addition to standard three-layer FFNNs, stacked neural networks showed very promising properties when dealing with small training data set samples (Lanouette et al., 1999). Since most of the experimental designs are characterized by a limited number of experiments, stacked neural networks will be used throughout the analysis procedure. To develop stacked neural network models that best represent the data, the set of experimental or simulated data was divided into two subsets: a validation data subset composed of a few data points that were selected randomly, and a training data subset that contains the remaining of the data points. The sum of the squares of prediction errors (SSE) for the validation subset was used as an indication of the fitness of the corresponding FFNN model. Several methods can be used to combine a series of FFNN models, having an identical structure, to produce a final stacked neural networks model.

4.2.4 Noise

Values calculated directly from both models, that is, without noise, are used first. It is hypothesized that in the absence of noise, neural networks will be able to capture the underlying trend to the most possible extent, and the influence of any factor would be

more clearly shown. The influence of normally-distributed random noise affecting the training data set were then investigated in order to simulate more realistic situations.

4.2.5 Platform

All computations were performed on IBM PC model 8811-E4U. The software used to code and implement the neural networks and comparison and elimination algorithm is Compaq Visual Fortran Standard Edition 6.1.0. All the 3-level designs were generated using JMPIN 4.0.4 Academic Edition, except for the 23-run random designs. Uniform designs were obtained from the website as tabulated (Anonymous, 2008).

4.2.6 Procedure

Many factors can influence the procedure and, thus, the results of the analysis. These factors include the underlying model, the experimental design, the structure of the standard FFNN (activation function, number of hidden neurons), the number of points that are selected prior to training to form the validation data subset and later used for stack combination, the algorithm used to combine the standard FFNN together, the level of noise, and many others. Based on the conclusion and recommendations from a previous study (Lanouette et al., 1999), some of the choices were made arbitrarily by the authors in order to reduce the dimensionality of the analysis, while other factors were investigated.

Since both models involve 3 input variables and 1 response, the structure of the NN only relies on the number of hidden layer neurons and the activation function used for both hidden and output layers. As recommended in a previous study (Lanouette et al., 1999), a sigmoid activation function was used for the neurons in the hidden layer, while a linear activation function was used for the neuron of the output layer in this investigation. In a practical situation, the problem of choosing the appropriate number of hidden neurons to model the response needs to be resolved strictly on the experimental data set. In this investigation, it was desired to use the same NN structure for the same underlying function, regardless of the experimental design. So an optimal number of hidden neurons was determined by training the neural networks with 1000 random points within the experimental domain, whose response is known from the underlying function, while

increasing the number of hidden neurons until the underlying function was represented adequately. For the pullulan production model, the number of hidden neurons was found to be 4 whereas it was 5 for the non-linear model.

For each design, two data points were randomly removed from the design set of points to be used as validation data set for the construction of the stacked FFNN, the remaining points were used as the actual training data set for a normal FFNN. A total of 1000 FFNNs were generated using different initial weights and validation data set. Because of the nonlinear nature of neural network models, a proportion of the generated 1000 models lead to poorer predictions. Ideally, these models should be eliminated from the set of models. These models can be eliminated based on two types of predictions: (1) unreasonable extreme predictions, and (2) identical predictions for numerous points in the data set. A fixed set of 1000 random points within the 3-dimensional experimental domain was used as the test data set. The responses on this test data set were calculated together with the experimental design points for each of the 1000 neural networks that were obtained. These responses were used to find and eliminate the models that show any of these two unrealistic patterns.

After the first round of elimination, the predictions at every point for all the remaining standard FFNN models are further compared to each other in order to identify and get rid of possible outlier models that give predictions too much different from those depicted by most of the models. The algorithm employed to achieve this goal is to compare every FFNN model to 10 other models at all of the 1000 points on the test data set. If the difference between the predictions of two FFNN models at 4 or more points exceeds a certain threshold, they are deemed to be different from each other at that level. When a given FFNN model is different from the others for at least eight occurrences out of a total 10 counts, it is considered as an outlier model and eliminated from the pool of candidate models. By gradually lowering the threshold, models are removed until 35% of the FFNN models have been eliminated.

Among the remaining models, n (up to 60) of them are randomly selected and combined to produce the final n-level stacked neural network model. A weighted sum method, based on the prediction errors of the validation data subset, was used to produce the final stacked neural networks model. The weighing factors are the inverse of the

contribution of each FFNN model to the total SSE on the validation data subset. Since only a few data points are randomly selected as validation data subset from the entire data set, it is possible that the prediction errors of these few data points may be very small. As a result, the weighting factor of that particular FFNN would be very high and would dominate the overall prediction. To avoid this situation to occur, the prediction errors of the validation subset were adjusted to a minimum threshold value if it was smaller than that value. Considering the typical error level of the predicted dependent variable, this value was chosen to be "1" in the present investigation.

To properly evaluate the accuracy of the resulting model over the whole domain of solution, the test data set of 1000 random points were used to validate the final stacked neural networks. A total of 100 such stacked neural network models were obtained in the same way in order to estimate the performance of the final model. This performance was evaluated in terms of the average of the SSE on the test data set and the corresponding standard deviation (SD).

4.3 RESULTS AND DISCUSSION

4.3.1 Results obtained using noise-free data

4.3.1.1 Influence of stack levels

Five different stacked FFNN configurations, 5-, 10-, 15-, 20-, and 60-level, were first investigated and compared on all 3-level designs for the pullulan production model. Selected designs are shown in Table 4.1. When the training data set is relatively small, such as in the case of 9-run Taguchi design, the results are similar to those obtained by Lanouette et al. (1999). In this case, a 10-level stacked FFNN is adequate to model the underlying function. Further increase in the number of stack levels only increases the level of confidence as indicated by the decrease in SD. However, when more data points are used, both SSE and SD are decreasing gradually although their rates of decrease are declining. A 20-level stacked FFNN was used for the rest of the comparisons. Table 4.2 presents all the results that were obtained for all experimental designs using a 20-level

stacked FFNN. Different aspects of these results will be discussed in the following sections.

Table 4.1 The influence of stack levels on selected 3-level designs of the pullulan production model.

	9-run Taguchi		15-run CCD		27-run Full Design	
Stack Levels	SSE	SD	SSE	SD	SSE	SD
5	8017	3639	169	213	80	63
10	6764	2311	112	99	41	25
15	6819	1907	88	73	29	17
20	6714	1646	79	60	24	14
60	6612	785	49	18	12	5

Table 4.2 Prediction errors for various designs obtained from noise-free data.

Number of Experiments	Pullulan Production Model				Non-linear Model			
	3-level Designs		Uniform Designs		3-level Designs		Uniform Designs	
	SSE	SD	SSE	SD	SSE	SD	SSE	SD
9	6714	1646	6780	377	5221	479	2746	627
11	2402	2528	3681	569	6946	878	1450	557
13	1291	1386	1107	291	5505	926	1186	409
15	79	60	783	271	5551	617	1268	195
19	49	22	295	87	3958	273	1103	270
23	42	26	0.042	0.010	4145	342	310	90
27	24	14	0.013	0.002	3927	853	255	69

4.3.1.2 Influence of the number of experiments

The qualitative influence of the number of design points is intuitive: the greater the number of experiments, the more accurate the resulting model should be. However, it is not trivial to determine which design is the most cost effective. Despite a few irregular points, the SSE and SD are generally decreasing as the number of experiments increases

for all 4 series presented in Table 4.2. The first two series of Table 4.2 are illustrated in Figure 4.1. The SSE decreases quite rapidly initially, and then flattens as the number of runs increases, showing a trend that behaves like an inverse function. The effort to get better predictions by conducting more experiments is amply rewarded at the beginning. As the number of runs increases, the improvement in prediction accuracy, indicated by the slope of the plot, is diminishing significantly. A judicious compromise between accuracy and the number of experimental runs would undoubtedly lead to choosing a design located in the middle of this trend.

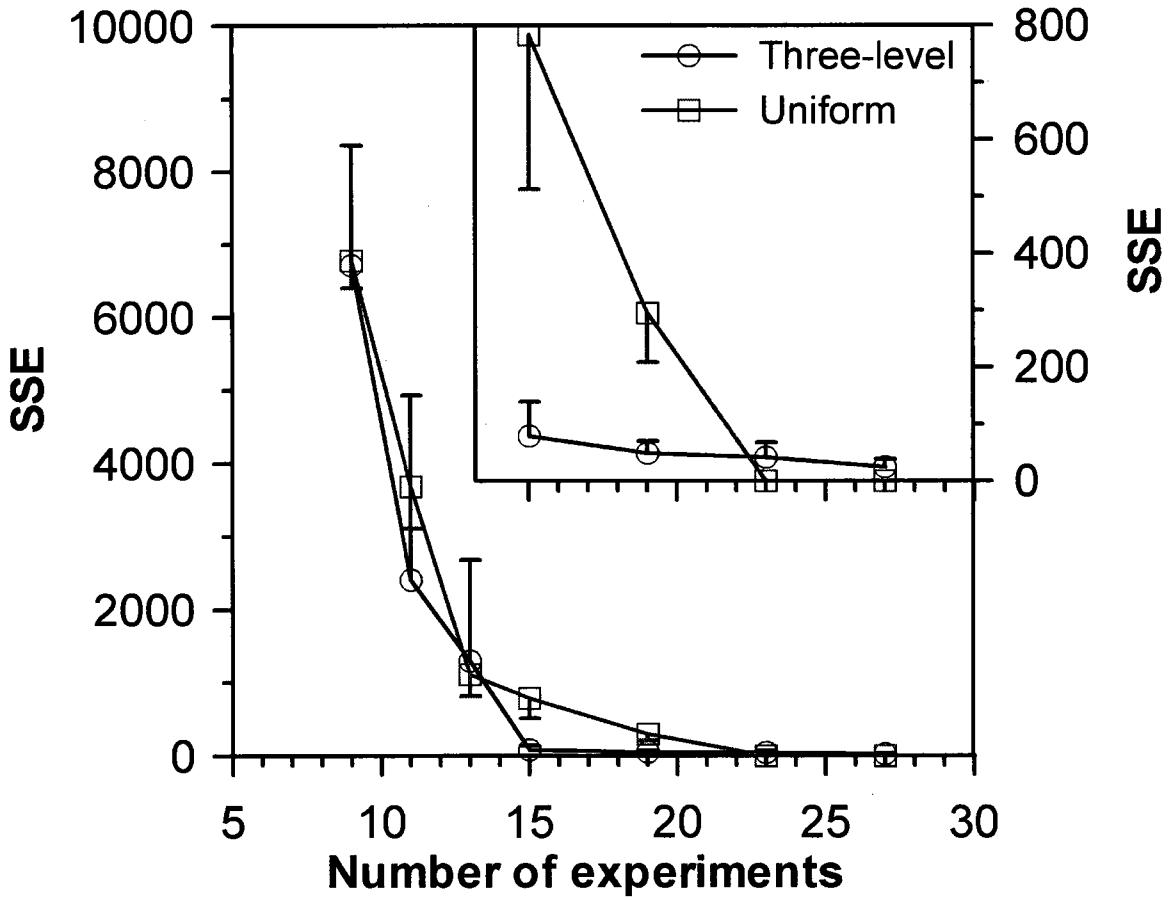

Figure 4.1 Comparison of the 3-level designs and uniform designs for the linear pullulan production model. The insert represents the SSE in the range of 15-27 experiments. The one-sided error bars indicate 1 SD.

4.3.1.3 Uniform versus 3-level designs

Zhang et al. (1998) compared uniform design to CCD and orthogonal array design using neural networks. In their study, the performance of UD was not found to be substantially better than traditional designs. In the present investigation, similar results are obtained for the pullulan production model (Figure 4.1). In fact, for a certain number of design points, UD gave slightly worse predictions than the equivalent 3-level design. This is probably because the underlying function is deduced from a CCD results. Thus, all the 3-level designs gain a substantial benefit of assuming a priori model that is very close to the underlying function. However, even though the SSE is not always better with uniform design, the SD of the uniform designs is generally smaller than that of the 3-level designs for the same number of runs. This is another form of improvement, since higher level of confidence is achieved. It can be concluded that both categories of designs produce comparable results for the pullulan production problem.

However, for the nonlinear problem, results clearly show that the performance of uniform designs is much better than those of 3-level designs (Figure 4.2). The 9-run uniform design gave lower prediction errors than the traditional 27-run full design. Such a difference is most likely because 3-level designs can only investigate few nonboundary points when the total number of experiments is limited. In the case of 3 factors at 3 levels, even if a full design is used, 26 of the design points are located on the boundaries of the experimental domain, and only the center point lies inside the domain. Thus, there is very little information available to reveal the landscape of the underlying function inside the 3-dimensional cube. As a result, the model developed from a 3-level design could therefore assume a greater variety of shapes. Some of the candidate neural networks combined to form the stacked FFNN could fail drastically to capture the real underlying function, and thus, giving quite large SSE and/or SD eventually. On the other hand, uniform design can adopt more than 3 levels for each factor. Because the design points are uniformly distributed within the experimental domain, uniform design provides balanced information from all regions and thus reduces the possibility to get FFNN models that have good predictions only around the design points. This subsequently reduces the deviation of the final stacked neural network model from the underlying function in the whole experimental domain.

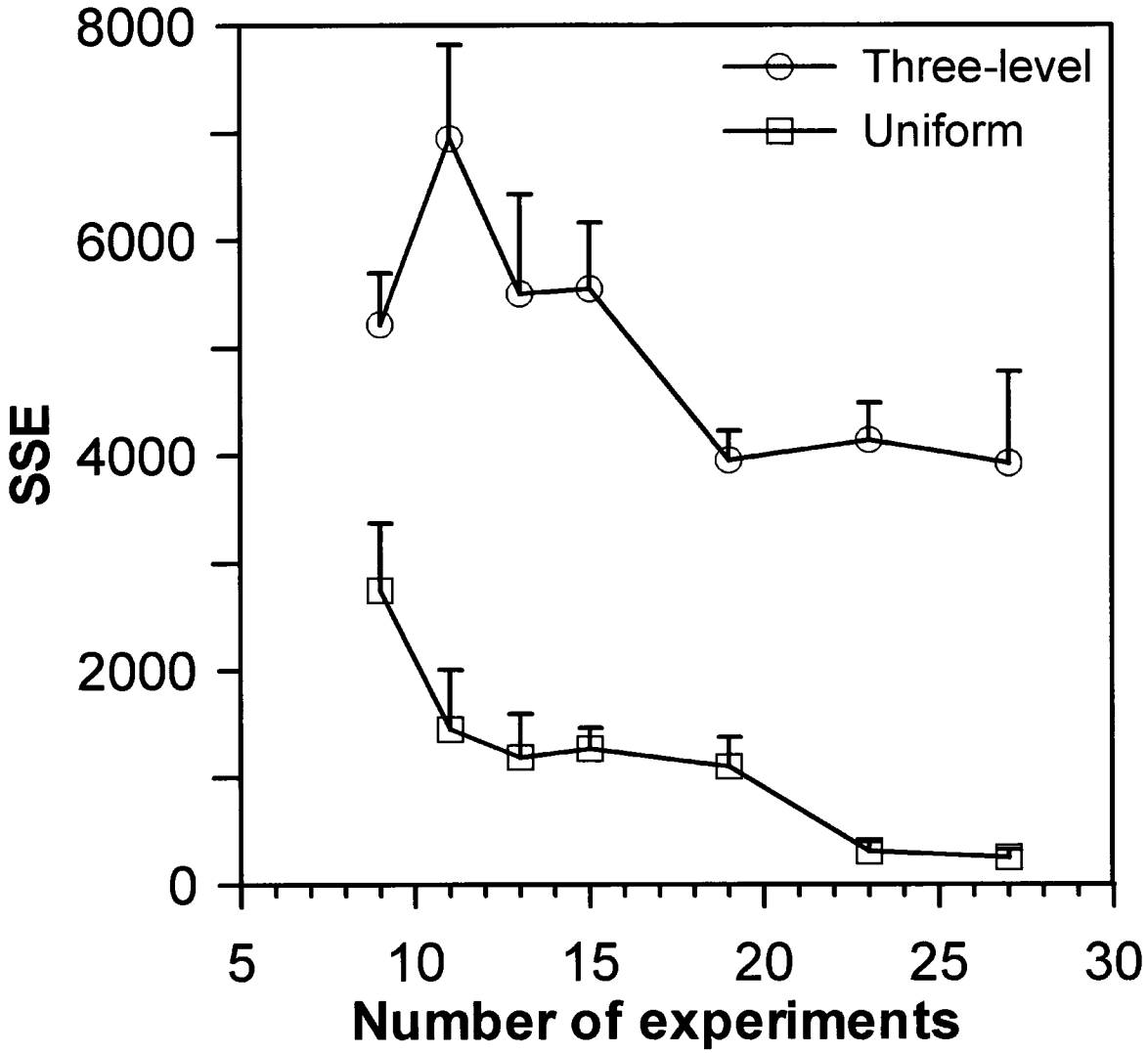

Figure 4.2 Comparison of the 3-level designs and uniform designs for the nonlinear model.

4.3.1.4 Pullulan production model versus nonlinear model

The difference in the underlying function has also influenced the behavior of experimental designs. For the pullulan production model, adding more runs to 3-level designs is very effective. With only 15 experiments, the model can capture the function to the extent that the difference between predicted and real values is already negligible (Figure 4.1). However, it is completely the opposite for the nonlinear model. Adding more runs does not improve the prediction much, and the prediction error is always higher than 4000, which means on average, the prediction for each point has an error of more than 2,

which is 7.2% of the total range of the variation of the dependent variable, even with 27-run full design (Figure 4.2). This may be resolved by using more levels at the expense of requiring significantly more experiments. On the other hand, the predictions obtained from UD are gradually improving when more runs are added for both cases (Figure 4.2).

This phenomenon may be partially explained with what has been pointed out by Duineveld et al. (1993): the specific situation encountered in a problem is probably the reason why it is so difficult to draw a general and definite conclusion when comparing different experimental designs. However, in the case of UD, the addition of more runs implies a better coverage within the experimental domain, whereas, for the 3-level designs, additional runs simply place a greater emphasis on the actual boundary of the experimental domain.

4.3.1.5 Random designs

Hurrion and Birgil (1999) concluded that random designs outperform full designs based on their comparison between 5-level random designs and 2-, 3-level full designs for one problem, and between 7-level random designs and 2-, 3-, 4-level full designs for another problem. However, they did not suggest a reason for the observed difference, and the performance of their 7-level random design is not noticeably better than that of the 4-level full design.

The 3-level random design used in this investigation had 3 levels for each factor akin to all the other traditional designs. It was shown that this design followed quite well the trend set by the traditional 3-level designs (Table 4.2). Although it is referred to as a random design, this 3-level design is actually a reduced full design, since its randomness has been tightly restricted due to the use of 3 levels per factor and the large number of runs used.

From another point of view, most experimental designs can be viewed as random design with different restriction on the factor levels, the number of experiments, and the method used to select the design points. The 27-run 3-level full design is a random design with extreme restrictions. For such a small number of factor levels, an extremely large number of experiments are used so that all possible factor level combinations have been included. On the other extreme, a true random design can be viewed as having an infinite

number of levels for each factor, however, only a small fraction of all possible combinations is selected randomly to fulfill the requirement on the number of experiments.

Table 4.3 Comparison of 23-run design results

23-run Designs	Pullulan Model		Non-linear Model	
	SSE	SD	SSE	SD
3-level Random	42	26	4145	342
True Random	24	19	601	247
7-level Random	16	14	568	119
Uniform	0.042	0.010	310	90

In this work, a true random design and a 7-level random design are further investigated, both with 23 runs. Despite their nonuniform and nonorthogonal properties, the prediction results obtained from both random designs are better than those of the 3-level random designs, especially for the nonlinear model problem (Table 4.3). This is additional evidence for the explanation deduced in previous sections: the points located inside the experimental domain undoubtedly provide more appropriate constraint for fitting the model, and thus resulting in better predictions.

The difference in performance between the 7-level random design and the true random design was subtle. Furthermore, the uniform design showed substantial improvement over the true random design. Both improvements indicate that restriction on the allocation of experimental points in a reasonable way can be beneficial to the performance of experimental designs.

4.3.2 Noise effect

In practice, experimental data are inevitably corrupted with noise. The accuracy of models derived from such data will obviously be influenced. Two different levels of Gaussian random noise, having a SD of 2.5% and 5% respectively, were added to the noise-free model data in order to simulate more realistic situations. The prediction results

from stacked neural network models were obtained in the same way as those of the noise-free data.

Compared to the results obtained with the noise-free data, the presence of noise having a SD of 2.5% does not significantly affect the prediction of the stacked NN, although the prediction errors are generally higher (data not shown). Taking into account the fact that 99.7% of a Gaussian random noise lies within three times of the SD, our results are in good agreement with those of Lanouette et al. (1999).

Predictions obtained for data corrupted with 5% noise are affected to different extent (Table 4.4). Although more irregular points exist, especially in the region of large experiment number, the decreasing trend of the prediction errors is still quite clear for each series when the number of experiments increases. However, the most affected series is the uniform design for the pullulan production model. This is probably because when the problem is linear, the effect of noise in the data on the prediction will be more pronounced if the distance between two adjacent levels for each factor is small as it is in the case with uniform designs.

Table 4.4 Prediction errors for various designs obtained from data with 5% (SD) noise.

Number of Experiments	Pullulan Production Model				Non-linear model			
	3-level Designs		Uniform Designs		3-level Designs		Uniform Designs	
	SSE	SD	SSE	SD	SSE	SD	SSE	SD
9	6992	1522	3601	421	4627	476	2733	645
11	1827	668	4267	1147	6761	976	2195	1302
13	915	221	2908	539	4807	1211	1778	595
15	335	196	678	95	5678	736	1671	260
19	117	24	1225	197	4646	531	929	197
23	378	101	978	192	3772	671	549	196
27	830	578	499	58	3764	1282	986	288

4.4 CONCLUSION

Several popular experimental designs were compared for two different cases using stacked FFNN to develop the underlying model. Traditional 3-level design and uniform designs were used. The prediction error was found to be inversely proportional to the number of experiments in the designs. Results obtained with uniform designs were generally better than those obtained with 3-level designs if the same number of experiments was used. Indeed, lower prediction error and/or higher confidence in the estimates were achieved using uniform designs. A 3-level random design was compared to two other random designs. The difference in their performance can only be explained by the difference in the number of factor levels, akin to the difference between 3-level designs and uniform designs.

4.5 NOMENCLATURE

L Taguchi orthogonal array design

n number of runs

U uniform design

X independent variable

Y dependent variable

Subscripts

n number of runs

Superscripts

s number of factors

4.6 REFERENCES

Anonymous, "The Uniform Design," http://www.math.hkbu.edu.hk/UniformDesign/ (2008).

Bishop, C. M., "Neural Networks and Their Applications," Review of Scientific Instruments **65**(6), 1803-1832 (1994).

Cybenko, G., "Approximation by superpositions of a sigmoidal function," Math Control Syst. **2**, 303-314 (1989).

Duineveld, C. A. A., A. K. Smilde, and D. A. Doornbos, "Comparison of Experimental-Designs Combining Process and Mixture Variables .1. Design Construction and Theoretical Evaluation," Chemometrics and Intelligent Laboratory Systems **19**(3), 295-308 (1993).

Fang, K. T., "The Uniform Design: Application of Number-Theoretic Methods in Experimental Design," Acta Mathematicae Applicatae Sinica **3**, 363-372 (1980).

Fang, K. T., D. K. J. Lin, P. Winker, and Y. Zhang, "Uniform design: Theory and application," Technometrics **42**(3), 237-248 (2000).

Goksungur, Y., S. Dagbagli, A. Ucan, and U. Guvenc, "Optimization of pullulan production from synthetic medium by Aureobsidium pullulans in a stirred tank reactor by response surface methodology," Journal of Chemical Technology and Biotechnology **80**(7), 819-827 (2005).

Hurrion, R. D. and S. Birgil, "A comparison of factorial and random experimental design methods for the development of regression and neural network simulation metamodels," Journal of the Operational Research Society **50**(10), 1018-1033 (1999).

Jensen, D. R. and D. E. Ramirez, "Complexity in experimental design .1. Relation to efficiency," Journal of Statistical Computation and Simulation **55**(3), 245-250 (1996).

Jensen, D. R. and D. E. Ramirez, "Complexity in experimental design .2. Comparing second-order designs," Journal of Statistical Computation and Simulation **55**(3), 251-257 (1996).

Lanouette, R., J. Thibault, and J. L. Valade, "Process modeling with neural networks using small experimental datasets," Computers & Chemical Engineering **23**(9), 1167-1176 (1999).

Liang, Y. Z., K. T. Fang, and Q. S. Xu, "Uniform design and its applications in chemistry and chemical engineering," Chemometrics and Intelligent Laboratory Systems **58**(1), 43-57 (2001).

Metting, H. J. and P. M. J. Coenegracht, "Neural networks in high-performance liquid chromatography optimization: Response surface modeling," Journal of Chromatography A **728**(1-2), 47-53 (1996).

Monness, E., M. J. Linsley, and I. E. Garzon, "Comparing different fractions of a factorial design: A metal cutting case study," Applied Stochastic Models in Business and Industry **23**(2), 117-128 (2007).

Nagata, Y. and K. H. Chu, "Optimization of a fermentation medium using neural networks and genetic algorithms," Biotechnology Letters **25**(21), 1837-1842 (2003).

Nelson, B. J., D. C. Montgomery, R. J. Elias, and E. Maass, "A comparison of several design augmentation strategies," Quality and Reliability Engineering International **16**(5), 435-449 (2000).

NIST/SEMATECH. "e-Handbook of Statistical Methods," http://www.itl.nist.gov/div898/handbook/ (2008).

Plackett, R. L. and J. P. Burman, "The design of optimum multifactorial experiments," Biometrika **33**(4), 305-325 (1946).

Wang, Y. and K. T. Fang, "A note on uniform distribution and experimental design," KeXue TongBao (Chinese Science Bulletin), **26**, 485-489 (1981).

Zhang, L., Y. Z. Liang, J. H. Jiang, R. Q. Yu, and K. T. Fang, "Uniform design applied to nonlinear multivariate calibration by ANN," Analytica Chimica Acta **370**(1), 65-77 (1998).

Zhang, W., X. J. Yu, and Q. Yuan, "Uniform Design: A New Approach of Designing Fermentation Media," Biotechnology Techniques **7**(5), 379-384 (1993).

CHAPTER 5

A new impeller for viscous fermentation: power input and mass transfer coefficient correlations

Yun Lin, Zisheng Zhang, and Jules Thibault
Department of Chemical and Biological Engineering
University of Ottawa
Ottawa, Ontario, K1N 6N5, Canada

Abstract

To mix viscous fermentation broths more efficiently, a new close-clearance impeller, the radial reciprocating plate impeller (RRPI), was designed to partly mimic the axial reciprocating plate impeller (ARPI). Akin to the axial movement of a reciprocating plate impeller, this new RRPI rotates back and forth driven by a three-arm linkage system. Its power consumption and overall mass transfer coefficient (K_La) were determined in a 22 L laboratory scale bioreactor using model fluids of different viscosities. Results obtained with this new impeller were compared to those of a triple Rushton impeller (TRI) and an ARPI. In water, results were the same as those of the TRI. However, the ARPI gave significantly lower K_La than the other two impellers for the same power input per unit volume. In highly viscous non-Newtonian carboxymethyl cellulose (CMC) solutions, the new impeller showed similar performance as the ARPI, whereas the TRI was not able to provide acceptable mixing due to the presence of stagnant zones. Therefore, this new impeller proves to be a better alternative to existing impellers for use in fermentations having rheologically-evolving broth.

Keywords

Reciprocating plate impeller, mass transfer, mixing power, viscous fermentation, design

List of symbols

A_c	cross section area, m^2
A	amplitude of rotation speed, rpm
C	Cross model time constant, s
C_L	dissolved oxygen concentration in medium, % saturation
C_L^*	saturated dissolved oxygen concentration, 100%
C_P	dissolved oxygen concentration in probe, % saturation
k	angular frequency, radian/s
K_La	overall oxygen mass transfer coefficient, s^{-1}
m	Cross model rate constant
N	rotation speed, revolution/s
P	power, W
	pressure, Pa
ΔP_f	frictional pressure drop, kPa
t	time, s
V	velocity, m/s

Greek letters

α, β, γ	constants in Equation 5.11
η	viscosity, Pa·s
η_0	zero shear viscosity, Pa·s
η_∞	infinite shear viscosity, Pa·s
ε	gas holdup
$\dot{\gamma}$	shear rate, s^{-1}
ω	angular velocity, rpm or Hz
τ	torque, N·m
τ_P	dissolved oxygen probe time constant, s
θ	phase, radian

Subscripts

0	initial (phase)
	empty bioreactor
L	liquid phase
P	plate

5.1 Introduction

Rushton turbine is the most frequently used impeller for mixing in aerobic fermentation processes. This is mainly because, at a given power input per unit volume, it can create high shear stress necessary to break air bubbles into small ones, and thus increase the mass transfer rate. However, when the viscosity of the broth is high, Rushton turbines cannot operate as effectively as in a water-like medium where the viscosity is relatively low. In some extreme cases where high viscosity broths prevail, stagnant zones of significant magnitude may exist. As a result, the overall fermentation efficiency is reduced.

Several approaches have been proposed to solve this problem. Probably the simplest one is to use multiple impellers on the same shaft, so that a higher fraction of the liquid broth can be agitated and the power given to the fluid is more evenly distributed. The impellers can be of the same type, such as using three Rushton turbines together (Audet et al., 1998), or a combination of different impellers (Dohi et al., 2004). Another method is to use different impellers on two or more shafts that rotate at different speeds. In a previous study, one Rushton turbine rotated at high speed in the center of the mixing tank, while a helical impeller close to the bioreactor wall rotated at a slower speed to homogenize the fermentation broth (Espinosa-Solares et al., 2001, 2002a and 2002b). Although a helical impeller does not normally create sufficient shear stress to significantly break up the bubbles, it provides a global circulation of the broth with relatively little energy consumption. A third way is to use a close-clearance impeller, whose diameter is almost as large as the bioreactor diameter, such as the Maxblend impeller (Dohi et al., 2004, 2006).

Among the family of close-clearance impellers, the axial reciprocating plate impeller (ARPI) has a unique characteristic: the oscillatory axial movement of a stack of perforated plates. This type of impeller is used in Karr columns (Karr, 1959) which are found in numerous applications in the pharmaceutical, hydrometallurgical, chemical, petrochemical, and environmental industries (Aravamudan and Baird, 1999). This impeller has demonstrated some benefits in bioreactors, such as a more uniform distribution of the local mixing energy (Lounes et al., 1995). Promising results were obtained in several viscous fermentations which were carried out using this impeller (Audet et al., 1996a, 1998). However, since the impeller shaft moves in and out of the bioreactor, a special design of the bioreactor headspace is needed to meet the sterilization requirement. In addition, its axial movement would make it more difficult to be adapted in an industrial context, since most of the existing industrial equipments are designed to handle rotating mixing devices.

In this work, a new rotating close-clearance impeller was designed based on the ARPI, in the hope that it would overcome some of the shortcomings caused by the axial movement and still keep the benefit of uniform mixing over a larger fluid volume. The more uniform mixing can be obtained by reciprocating perforated plates to span the whole cross-sectional area of the bioreactor resulting in the elimination of stagnant zones. This impeller is referred to as the radial reciprocating plate impeller (RRPI). In this investigation, the relationship between the power input per unit volume and K_La for this new impeller was determined, and its performance was compared to those of a triple Rushton impeller (TRI) and an ARPI, using model fluids with different viscosities.

5.2 Materials and Methods

5.2.1 Bioreactors

The two bioreactors used in this investigation were designed and constructed in our laboratory. They have identical dimensions: a height of 55 cm and an internal diameter of 22.8 cm, giving a total volume of 22 L. In this investigation, the working volume used in all experiments was 12 L. One bioreactor was equipped with the ARPI whereas the

other bioreactor was used for evaluating the performance of the two rotating mixing devices: the TRI and the new RRPI. When the TRI is used, four equally-spaced baffles were also used, each having a length of 23 cm and a width of 2.5 cm.

During each experiment, the tested medium was maintained at 28°C using a water bath that circulates water through the annular jacket on the outside of the bioreactor. At the bottom of the bioreactor, a plate perforated with 100 small 1-mm diameter orifices is used as the air sparger. The perforations are evenly allocated along three concentric rings, which contain 16, 32 and 52 holes, respectively. The diameters of these rings are 7.6, 13.25 and 18.75 cm, respectively. Three aeration rates were investigated: 0.5, 0.75 and 1 volume of gas per volume of liquid per minute (vvm), which correspond to a superficial gas velocity of 0.25, 0.37 and 0.49 cm/s, respectively.

5.2.2 Impellers

5.2.2.1 Triple Rushton impeller (TRI)

Three standard Rushton turbines were mounted on the same shaft and used together in order to better handle viscous medium. The diameter of the impeller shaft is 1 cm. The impeller diameter is 10 cm. The locations of the Rushton turbines, measured from the bottom of the bioreactor, were 4.9, 14.7 and 24.5 cm, respectively. A toothed belt gear system was used to connect the impeller shaft and the motor shaft. The speed of the impeller shaft was controlled between 50 to 400 rpm in step sizes of 50 rpm.

5.2.2.2 Axial reciprocating plate impeller (ARPI)

The ARPI consists of a stack of four perforated plates. The diameter of the plates is 22 cm. The distance between adjacent plates is 5 cm. The diameter of the holes is 2 cm. The center of the holes is placed in a square pattern: 2.7 cm between adjacent holes in one direction and 4.4 cm in the other direction. The axial movement of the plate stack is achieved with the mechanism illustrated in Figure 5.1. The amplitude of the axial movement (r) is 5 cm, and the connecting rod has a length (l) of 19.5 cm. The frequency of the oscillatory movement is controlled between 0.125 and 1.5 Hz in step sizes of 0.125 Hz or 0.25 Hz when it is higher than 0.75 Hz.

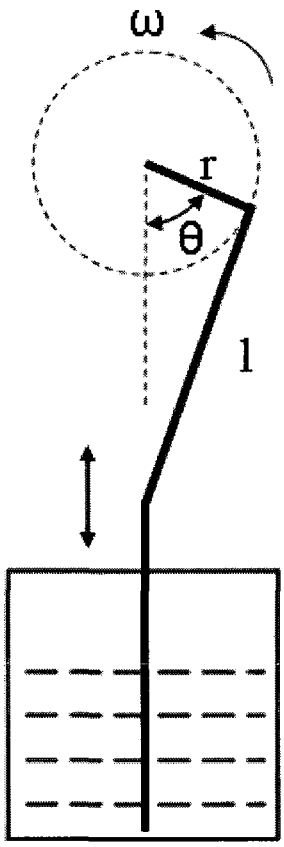

Figure 5.1 Schematic diagram of the ARPI drive mechanism (not to scale).

5.2.2.3 Radial reciprocating plate impeller (RRPI)

For practical reasons, a rotational movement of mixing devices is preferred over an axial movement. The RRPI was designed to benefit from the advantages of the reciprocating perforated plates of the ARPI and the rotational motion of the TRI by adopting a back and forth partial rotation spanning a portion of the cylindrical tank. The design of this mixer was inspired by the oscillatory movement of a clothes washing machine. The oscillatory motion of the RRPI is achieved using a simple three-arm linkage system (Figure 5.2). One arm is fastened to the bioreactor shaft and another to the motor shaft. The third arm connects the first two arms together. The effective length of the first (R), second (r), and third arm (L) are 10.4, 2.5 and 13.2 cm, respectively. The distance between the two shafts (l) is 14 cm. While the motor shaft rotates at a constant speed in one direction, the bioreactor shaft rotates back and forth such that each impeller blade

covers a region of the mixing tank that spans an angle of approximately 46°. The angular speed of the RRPI can be approximated by a basic sine wave (Equation 5.1).

$$\omega(t) = A\sin(kt + \theta_0) \tag{5.1}$$

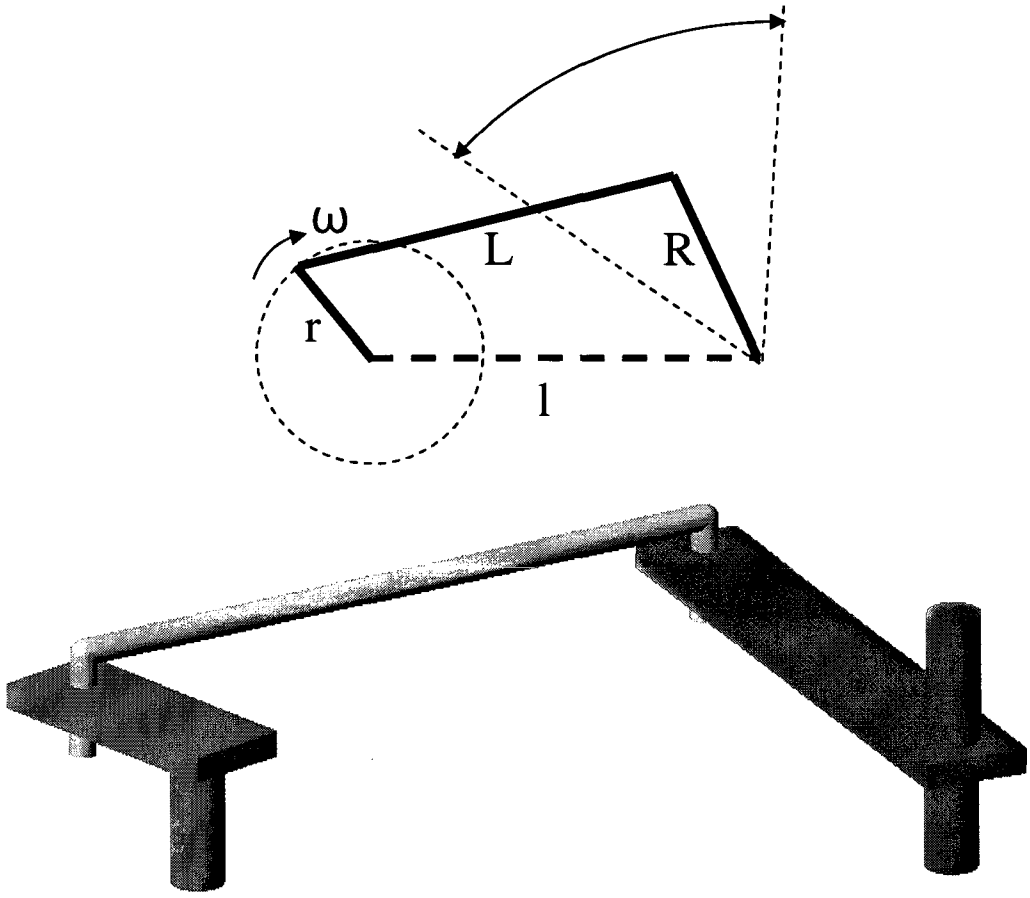

Figure 5.2 2D and 3D schematic diagrams of the RRPI drive mechanism.

As depicted in Figure 5.3, the structure of the RRPI, consisting of two hubs, is very similar to a typical Rushton turbine impeller. Six equally spaced blades are mounted on each hub. The blades are however much larger and each blade is perforated with 2-cm diameter holes arranged in an equilateral triangle pattern. The distance between the centers of each adjacent hole is 3 cm. Each blade is a rectangular plate having a width of 9 cm and a height of 12 cm. The two hubs of the mixing assembly are positioned with a 30° angle relative to each other (Figure 5.3). The diameter of the impeller assembly is 21.5 cm which leaves 0.65 cm spacing between the tips of the blades and the internal wall of the mixing tank. Two of the blades on the upper hub are cut at appropriate locations to

accommodate the fermentation probes. The various speeds of reciprocation that were tested to evaluate the mixing assembly are 0.5, 1, 1.5, 2, 2.33, 2.67 and 3 Hz which correspond to motor speeds of 30, 60, 90, 120, 140, 160 and 180 rpm, respectively.

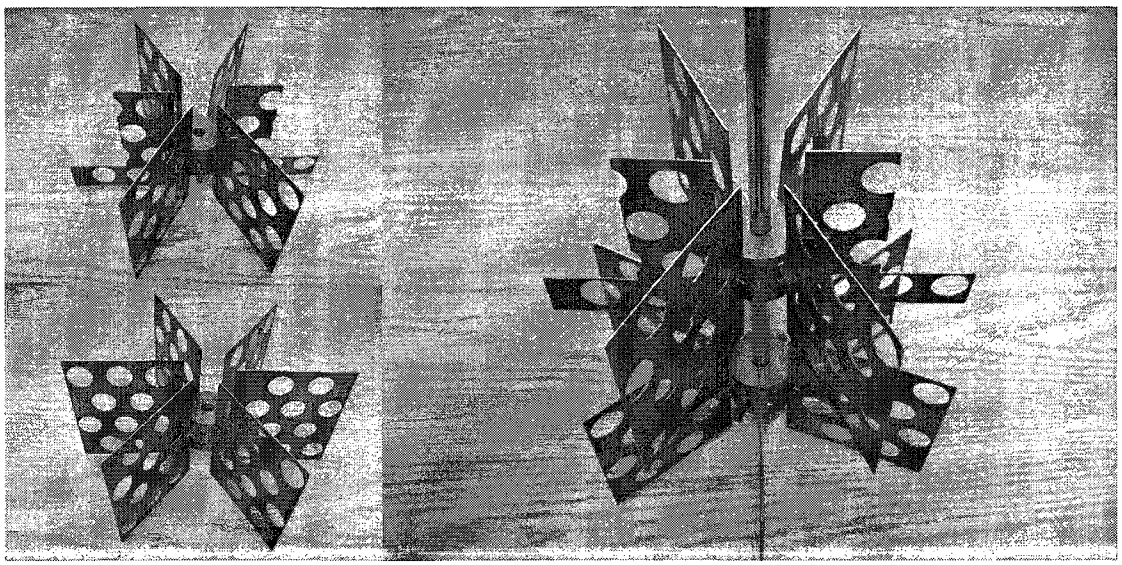

Figure 5.3 The top hub (top left), bottom hub (bottom left) and the assembly (right) of the RRPI.

5.2.3 Model fluids

5.2.3.1 Distilled de-ionized water

As the initial viscosity of a typical fermentation broth is usually very close to that of water, distilled de-ionized water was therefore used as the model fluid to represent the liquid medium at the onset of fermentation. The viscosity of distilled de-ionized water was determined to be 0.00089 Pa·s at 28°C using the Anton Paar's Physica M301 rheometer with a double gap concentric cylinder measuring system (DG42).

5.2.3.2 Carboxymethyl cellulose

Carboxymethyl cellulose (CMC) type 7H3SXF was obtained from Hercules. Three concentrations of aqueous CMC solutions (1, 5 and 10 g/L) were used to represent the different stages of a rheologically evolving fermentation broth. However, most of the efforts have been focused on the 10 g/L CMC solution, because it represents the biggest challenge from a mixing point of view. The viscosity of CMC solutions all showed non-

Newtonian behavior. In the shear rate range of 0.1 to 1000 s^{-1}, CMC solutions can be represented quite well by the Cross rheological model (Equation 5.2). For all the three CMC solution tested, the model coefficients of determination (R^2) are higher than 0.99. The model parameters were determined at 28°C and are presented in Table 5.1.

$$\eta = \frac{\eta_0 - \eta_\infty}{1 + (C\dot{\gamma})^m} + \eta_\infty \tag{5.2}$$

Table 5.1 Cross model parameters of the CMC solutions.

	1 g/L CMC	5 g/L CMC	10 g/L CMC
η_0, Pa·s	0.0129	0.1149	0.6913
η^∞, Pa·s	0.0028	0.0082	0.0116
C, s	0.0038	0.0125	0.0456
m	0.816	0.705	0.658

5.2.4 K_La determination

K_La was determined using the gassing-out method. The dissolved oxygen (DO) probe used was a 12-mm diameter OxyProbe with a length of 420 mm (Broadley-James, Irvine, USA). The medium was first purged using nitrogen until the DO signal read 0%. Air was then supplied and the DO signal was recorded until saturation (100%) was reached. The DO signal from each experiment was fitted to a theoretical signal that considers the dead time, the probe time constant and oxygenation dynamics of a well mixed liquid medium. The theoretical signal was obtained by solving simultaneously, using finite differences, the differential equations that govern the probe dynamics (Equation 5.3) and the well mixed liquid vessel model (Equation 5.4).

$$\tau_P \frac{dC_P}{dt} = C_L - C_P \tag{5.3}$$

$$\frac{dC_L}{dt} = \frac{K_L a}{1-\varepsilon}\left(C_L^* - C_L\right) \tag{5.4}$$

Since the gas holdup under most conditions was small and could not easily be measured accurately, it was decided to define, as in most previous studies reported in the literature, the specific volumetric area a using the initial liquid volume instead of the aerated liquid dispersion volume. Equation 5.5 was therefore used instead of Equation 5.4.

$$\frac{dC_L}{dt} = K_L a\left(C_L^* - C_L\right) \tag{5.5}$$

The DO probe time constant was determined by performing a series of independent experiments using the following procedure. The probe was initially maintained in a nitrogen saturated water solution, and then it was transferred rapidly to an air saturated water solution. To determine the time constant, the signal of the DO probe is compared to the first-order model given in Equation 5.6. Usually, the DO probe time constant was found to be between 12 to 20 s.

$$\tau_P \frac{dC_P}{dt} = C_L^* - C_P \tag{5.6}$$

5.2.5 Power input measurement

5.2.5.1 Triple Rushton and radial reciprocating plate impellers

The motor that was used to drive the TRI and the RRPI is a 140 W variable speed motor (Heidolph's RZR 2102 control, Schwabach, Germany). The portion of the power given to the fluid for mixing is calculated using Equation 5.7. The power consumed by the mixing mechanism in an empty bioreactor ($2\pi N\tau_0$) is subtracted from the total consumed power. Since the speed and torque data reported by the motor are values measured at the motor shaft, the efficiency of both the toothed belt gear system and the three-arm linkage system were assumed to be 100%. In reality, the efficiency of a toothed belt, which is used for the TRI system, is very high, typically over 97% (Anonymous, 2009). However, as estimated by comparing the experimental data to a CFD simulation, the efficiency of the three-arm linkage system for the RRPI is approximately 80% or less (Lin, 2010). One would need to measure the torque directly on the shaft of the bioreactor to have a more accurate appreciation of the actual power input consumed for mixing in this system. However, if it is technically impossible to achieve higher efficiency with this three-arm linkage system, the power input results obtained using the motor values is still more useful for practical purposes.

$$\overline{P} = 2\pi N\left(\tau - \tau_0\right) \tag{5.7}$$

5.2.5.2 Axial reciprocating plate impeller

The instantaneous effective power given by the ARPI to the fluid for mixing can be calculated using the force necessary to reciprocate the plate stack or the variation of pressure at the bottom of the bioreactor (Lounes and Thibault, 1993). In this investigation, the power was obtained through the pressure variation at the bottom of the bioreactor (Equation 5.8) using a pressure sensor (Cole-Parmer model H-68845-52). The velocity of the impeller was calculated from the sinusoidal pressure data using Equation 5.9, assuming that there is always a phase difference of 180° between the pressure and velocity data. The average power input was obtained by integrating the instantaneous power over four cycles of the impeller movement (Equation 5.10).

$$P = A_c \left| \Delta P_f V_P \right| \tag{5.8}$$

$$V_P = \frac{\omega r \sin\theta \left(1 + \frac{r}{l}\cos\theta\right)}{\sqrt{1 - \left(\frac{r}{l}\sin\theta\right)^2}} \tag{5.9}$$

where all the parameters are illustrated as in Figure 5.1

$$\bar{P} = \frac{1}{4T}\int_0^{4T} P dt \tag{5.10}$$

5.3 Results and Discussion

The variability of both the power input per unit liquid volume and K_La data was estimated for a few selected operating conditions by repeating the same experiment at a different time. One such result is shown in Table 5.2. The percentage error is calculated by dividing the standard deviation of the duplicate data by the average value of the data. In most cases, the percentage error is well within 10%. Because of the low value of the power input per unit liquid volume at the lowest speed of reciprocation, the error is larger. However, the error is very small for all the other speeds of reciprocation.

Correlations relating the power input per unit volume with K_La usually show two distinct regimes of operation (Perez and Sandall, 1974; Lounes et al., 1995; Audet et al., 1996b). In the first regime at low power input, where the energy imparted to the gas-liquid

mixture is not sufficient to break the gas bubbles, K_La remains almost constant for a given gas flow rate. In the second regime, where vivid mixing imparts sufficient shear to break bubbles, K_La increases proportionally to the increase in power input. It will be shown shortly that results obtained in this investigation also follow this trend.

Table 5.2 Duplicate data of RRPI in water at 1 vvm aeration rate.

	Series 1		Series 2		Percentage error	
Motor speed (rpm)	P/V_L, (W/m^3)	K_La (s^{-1})	P/V_L (W/m^3)	K_La (s^{-1})	P/V_L	K_La
30	3.8	0.00475	7.1	0.0052	42.6	6.4
60	30.4	0.00525	32.5	0.0064	4.7	14.0
90	114	0.0067	105	0.0062	5.8	5.5
120	284	0.0115	278	0.013	1.7	8.7
140	497	0.019	489	0.020	1.1	3.6
160	778	0.030	772	0.028	0.6	4.9

5.3.1 Influence of viscosity

Figure 5.4 presents the overall oxygen mass transfer coefficient as a function of the power input per unit liquid volume obtained with the RRPI for water and the aqueous CMC solutions at three different concentrations. As expected, Figure 5.4 shows that K_La decreases significantly for a given power input per unit volume when the viscosity of the medium increases. Similar results were obtained for the ARPI system (data not shown). Multiple factors that lead to this phenomenon have been pointed out by Schugerl (1981).

One interesting observation is that, only for the medium with the highest viscosity, a noticeable increase in power input occurred under the same reciprocation speed. In the other media, although the viscosity is different, the power input is nearly the same for a given speed of reciprocation.

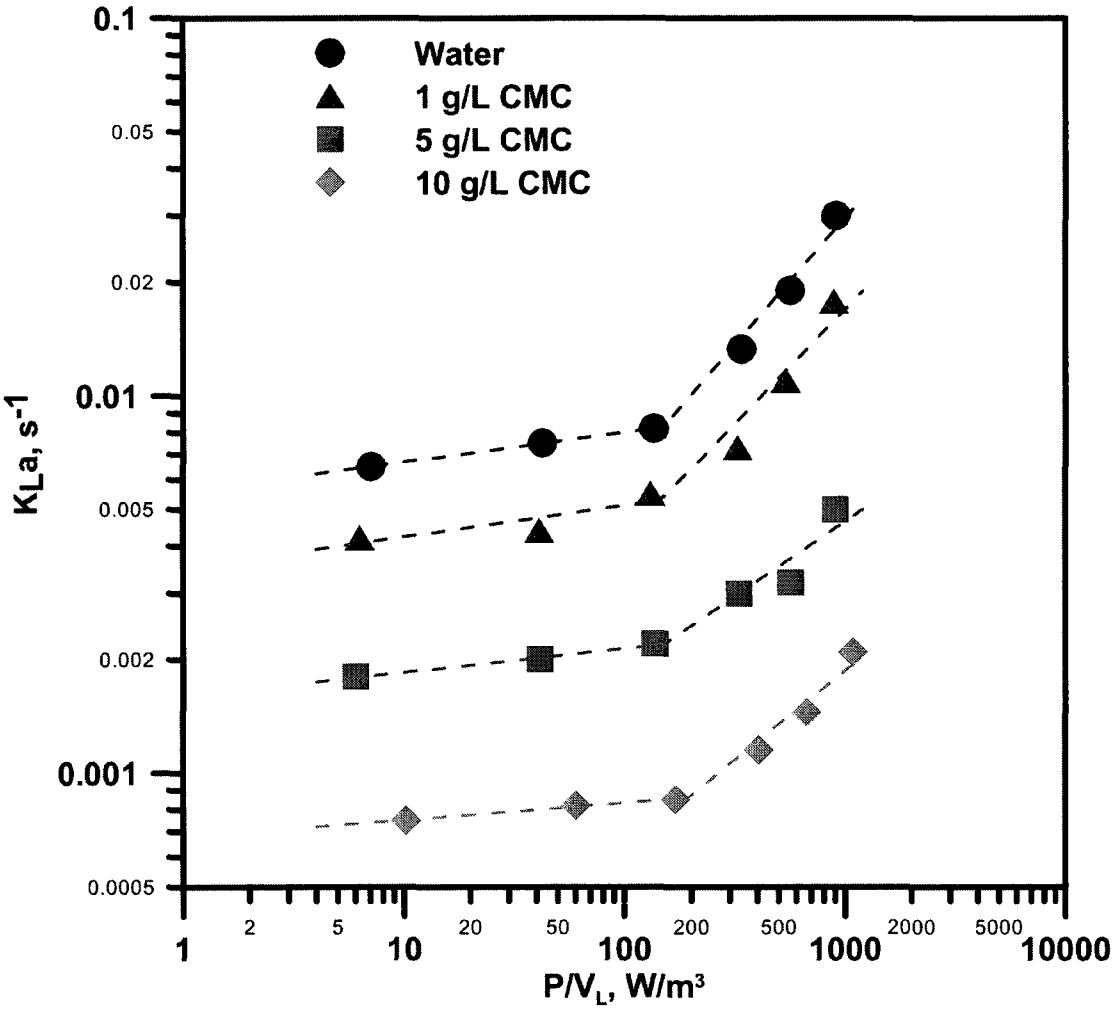

Figure 5.4 Influence of fluid viscosity on the power input per unit volume and K_La data for the RRPI at 0.75 vvm aeration rate.

5.3.2 Influence of the aeration rate

A series of oxygen mass transfer experiments were performed in water (Figure 5.5) and in a 10 g/L aqueous CMC solution (Figure 5.6) under different aeration rates using the RRPI. Under otherwise identical conditions, aeration rate has very little effect on the power input per unit volume, whereas it has a significant effect on the value of K_La. In general, a higher value of K_La is observed for a higher aeration rate at a given reciprocation speed, while the power input per unit volume remains almost the same.

In order to compare the performance of a given mixing device with other mixing devices under different operating conditions, K_La is usually correlated with the power input per unit volume P/V_L, and the superficial gas velocity U_G using Equation 5.11, one correlation for each regime. The parameters of the correlations for the two model fluids were found by minimizing the sum of squares of the differences between the predicted and experimental values of K_La. The parameters of Equation 5.11 for water and 10 g/L CMC solution for the two regimes of operation are listed in Table 5.3. In the first regime, these parameters show that for both fluids the power input per unit volume has a very small effect on the oxygen mass transfer coefficient. On the other hand, the influence of the aeration rate is relatively important. The increase of K_La with the aeration rate is much more important for the 10 g/L CMC solution than for water. For both model fluids, when the power input per unit volume reaches approximately 150 W/m^3, a sharp increase of K_La with the power input per unit volume is observed. In this second regime of operation, the rate of increase of K_La with the power input in the case of water is much greater than for the CMC solution. On the other hand, the rate of increase of K_La with the aeration rate is much greater for the CMC solution than water.

$$K_L a = \gamma \left(\frac{P}{V_L} \right)^{\alpha} (U_G)^{\beta} \tag{5.11}$$

Table 5.3 K_La correlation parameters for the two regimes with the RRPI.

Fluid	First Regime (P/V_L < 150 W/m^3)			Second Regime (P/V_L > 150 W/m^3)		
	γ	α	β	γ	α	β
Water	0.0143	0.0457	0.203	0.000419	0.897	0.329
10 g/L CMC	0.0252	0.0381	0.592	0.00457	0.413	0.629

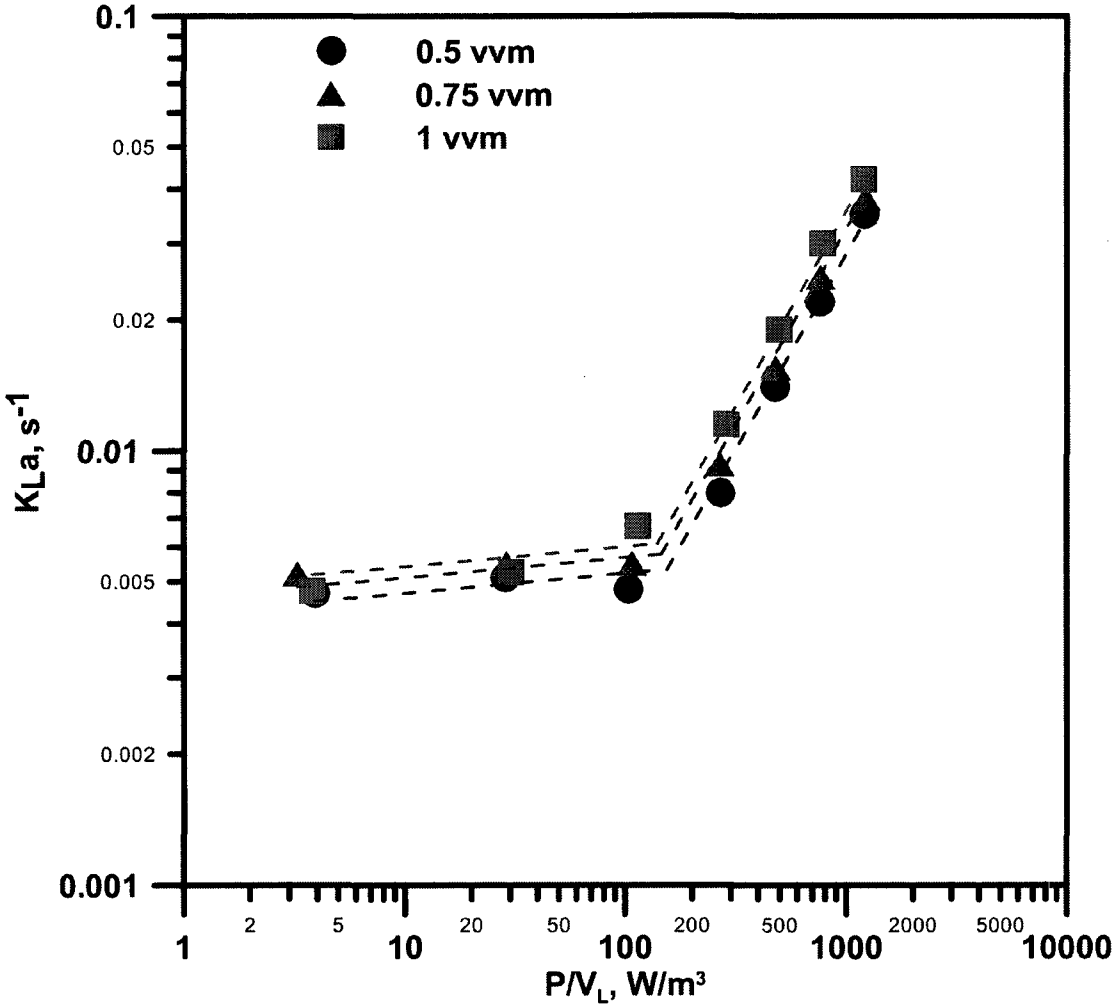

Figure 5.5 K_La versus the power input per unit volume for 3 aeration rates with the RRPI in water. Trend lines are generated using Equation 5.11 and parameters of Table 5.3.

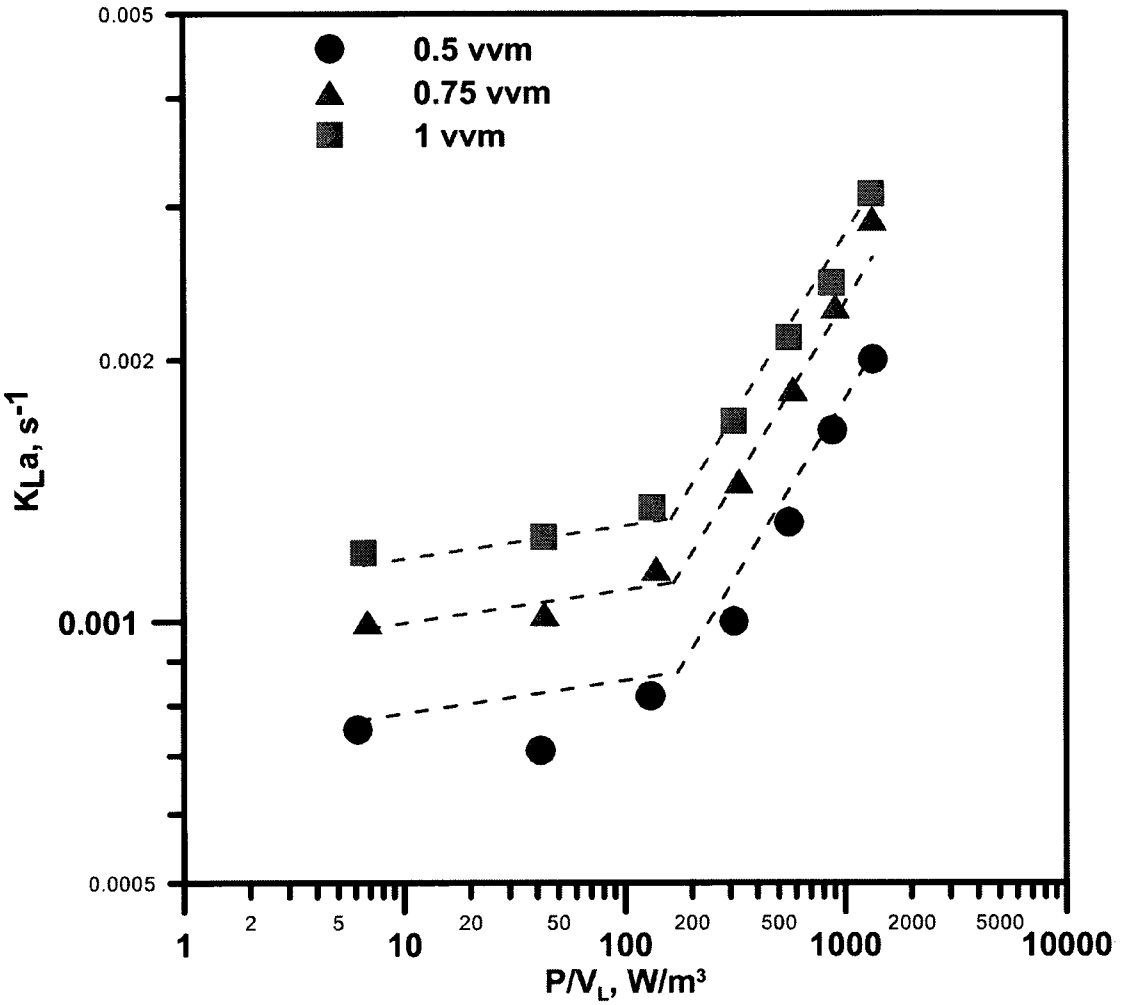

Figure 5.6 K_La versus the power input per unit volume for 3 aeration rates with the RRPI in a 10g/L CMC solution. Trend lines are generated using Equation 5.11 and parameters of Table 5.3.

5.3.3 Influence of the type of impellers

The performance of the RRPI for its ability to provide high oxygen mass transfer coefficient was compared to that of the TRI and the ARPI. The results obtained for the water system are presented in Figure 5.7. The RRPI and the TRI showed similar performance. The reported values for the latter two impellers are conservative because an efficiency of 100% of the drive mechanism between the motor and the mixing devices was assumed. Considering that the three-arm linkage system of the RRPI has a much lower

efficiency than the toothed belt gear system used for the TRI, the performance of the RRPI would actually be better than that of the TRI, if the efficiency of the linkage system can be improved. The ARPI showed much smaller values of K_La under the same power input per unit volume when compared to the other two impellers. Based on the visual observations that gas bubbles seem to be larger in the ARPI system, it is suspected that higher rate of coalescence happened because gas tends to accumulate and coalesce underneath the perforated plates during the upward movement of the plates, and then the gas bubbles pass rapidly through the large perforations without breaking up into small bubbles in the downward movement of the plates. As a result, there is a lower gas-liquid interfacial surface area for oxygen mass transfer resulting in smaller values of K_La.

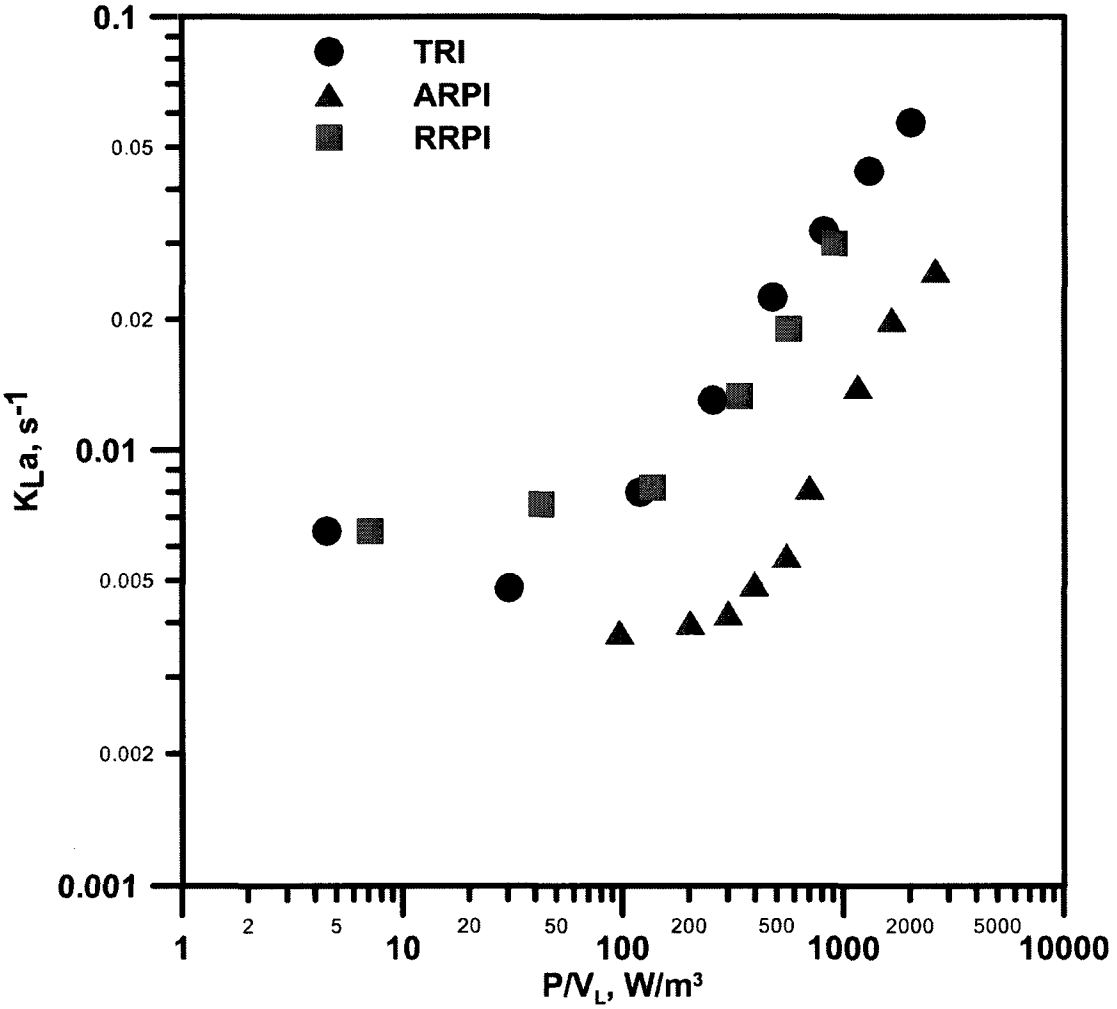

Figure 5.7 K_La versus the power input per unit volume for three types of impellers in water at 0.75 vvm aeration rate.

When dealing with highly viscous media, the TRI is not able to circumvent the non-uniform mixing problem. Dead zones still exist even if three Rushton turbines are used together. The problem would be even more pronounced for large scale systems. The DO as well as K_La would significantly vary throughout the fermentation vessel. In determining K_La experimentally, one would be faced with the problem of determining a local K_La associated to the location of the DO probe. As a result, only the ARPI and the RRPI were compared to each other when a 10 g/L CMC solution was used. In general, K_La for the 10 g/L CMC solution is approximately one order of magnitude smaller than the one obtained in a water system. The K_La values obtained from both the ARPI and the RRPI systems are comparable to each other (Figure 5.8).

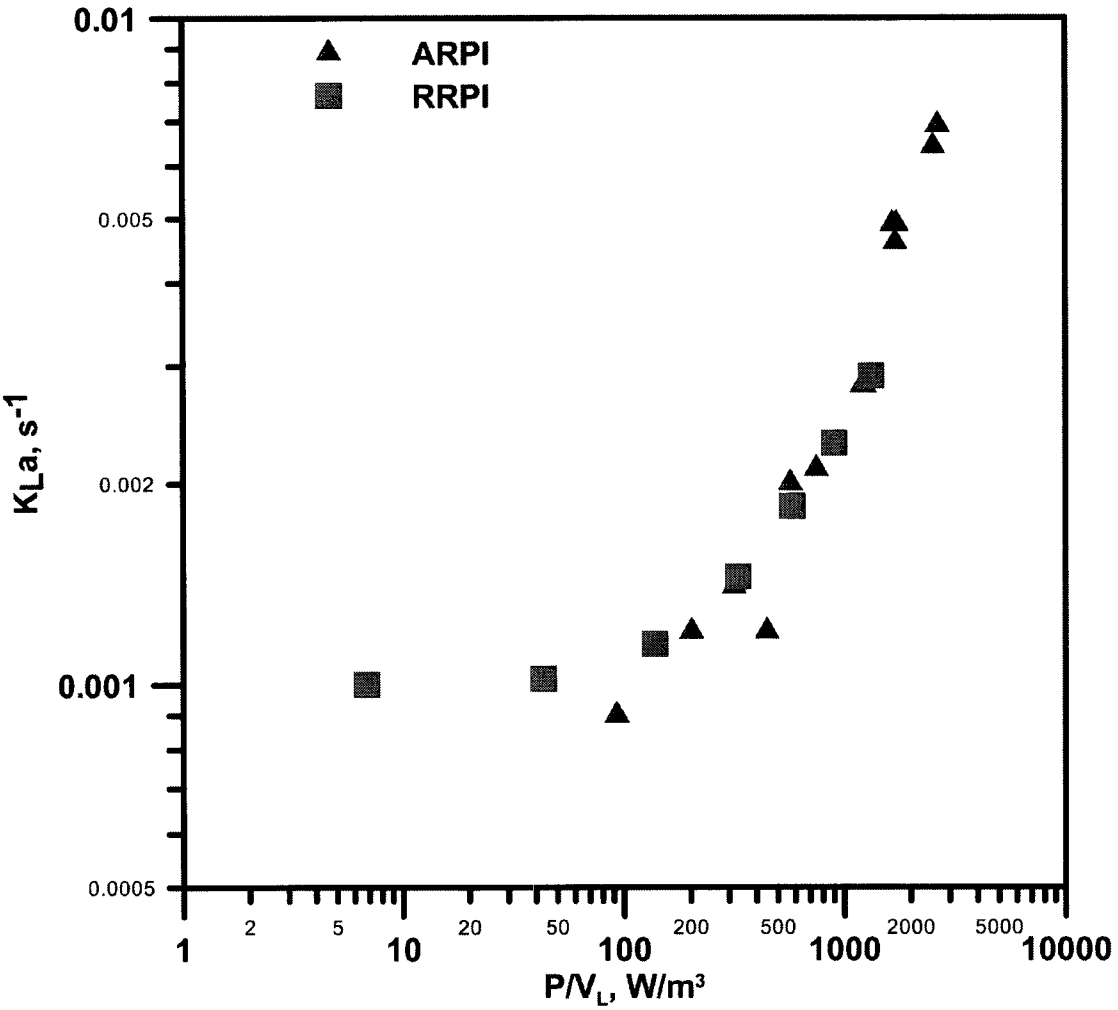

Figure 5.8 K_La versus the power input per unit volume for two types of impellers in 10 g/L CMC solution at 0.75 vvm aeration rate.

5.4 Conclusion

Based on the concept of the axial reciprocating plate impeller (ARPI), a new radial reciprocating plate impeller (RRPI) was designed to improve the mixing quality of fermentation broths experiencing a wide range of viscosities and more particularly for fluids showing shear thinning non-Newtonian behavior. Some of the shortcomings of the ARPI are overcome by changing the axial movement into an oscillatory rotation spanning a large fraction of the fermentation broth. The power input per unit liquid volume and K_La were determined for the RRPI and two other mixing devices in model fluids having a wide range of viscosities. The performance of the RRPI was compared to that of the triple Rushton impeller (TRI) and the ARPI. In water, the RRPI showed similar performance as the TRI, whereas the ARPI provided lower oxygen mass transfer rate probably due to the higher coalescence rate of bubbles. In a 10 g/L CMC solution, the RRPI was found to be as good as the ARPI. It can safely be concluded that the RRPI is a good candidate as a mixing device to handle fermentations that have rheologically-evolving broth.

5.5 References

Anonymous (2009). http://www.mitcalc.com/doc/tbelts/help/en/tbeltstxt.htm.

Aravamudan, K., Baird, M. H. I. (1999). Effects of Mass Transfer on the Hydrodynamic Behavior of a Karr Reciprocating Plate Column. Ind. Eng.Chem. Res., 38 (4), 1596-1604.

Audet, J., Lounes, M., and Thibault, J. (1996a). Pullulan fermentation in a reciprocating plate bioreactor. Bioprocess Engineering, 15(4), 209-214.

Audet, J., Thibault, J., and Leduy, A. (1996b). Polysaccharide concentration and molecular weight effects on the oxygen mass transfer in a reciprocating plate bioreactor. Biotechnology and Bioengineering, 52(4), 507-517.

Audet, J., Gagnon, H., Lounes, M., and Thibault, J. (1998). Polysaccharide production: Experimental comparison of the performance of four mixing devices. Bioprocess Engineering, 19(1), 45-52.

Dohi, N., Takahashi, T., Minekawa, K., and Kawase, Y. (2004). Power consumption and solid suspension performance of large-scale impellers in gas-liquid-solid three-phase stirred tank reactors. Chemical Engineering Journal, 97(2-3), 103-114.

Dohi, N., Takahashi, T., Minekawa,K., and Kawase,Y. (2006). Gas-liquid mass transfer characteristics of large-scale impellers: Empirical correlations of gas holdups and volumetric mass transfer coefficients in stirred tanks. Chemical Engineering Communications, 193(6), 689-701.

Espinosa-Solares, T., Brito-De la Fuente,E., Tecante,A., and Tanguy,P.A. (2001). Flow patterns in rheologically evolving model fluids produced by hybrid dual mixing systems. Chemical Engineering & Technology, 24(9), 913-918.

Espinosa-Solares, T., Brito-De la Fuente, E., Tecante, A., Medina-Torres, L., and Tanguy, P.A. (2002). Mixing time in rheologically evolving model fluids by hybrid dual mixing systems. Chemical Engineering Research & Design, 80(A8), 817-823.

Espinosa-Solares, T., Brito-De la Fuente, E., Tecante, A., and Tanguy, P.A. (2002). Gas dispersion in rheologically-evolving model fluids by hybrid dual mixing systems. Chemical Engineering & Technology, 25(7), 723-727.

Karr, A. E. (1959). Performance of Reciprocating Plate Extraction Columns. AIChE Journal, 5, 446-452.

Lin, Y. (2010). Improving the Production of High Molecular Weight Pullulan using a New Radial Reciprocating Plate Impeller. Ph.D. Thesis, University of Ottawa, Ottawa, Canada.

Lounes, M. and Thibault, J. (1993). Hydrodynamics and Power-Consumption of A Reciprocating Plate Gas-Liquid Column. Can. J. Chem. Eng., 71(4), 497-506.

Lounes, M., Audet, J., Thibault, J., and Leduy, A. (1995). Description and Evaluation of Reciprocating Plate Bioreactors. Bioprocess Engineering, 13(1), 1-11.

Perez, J. F., Sandall, O. C. (1974). Gas Adsorption by Non-Newtonian Fluids in Agitated Vessels. AIChE Journal, 20(4), 770-775.

Schugerl, K. (1981). Oxygen Transfer into Highly Viscous Media. In: Advances in Biochemical Engineering Biotechnology (Ed.: A. Fiechter), Springer-Verlag 19, 71-174.

CHAPTER 6

Modeling a new radial reciprocating plate impeller using computational fluid dynamics

Yun Lin, Zisheng Zhang, and Jules Thibault
Department of Chemical and Biological Engineering
University of Ottawa
Ottawa, Ontario, K1N 6N5, Canada

Abstract

A new impeller, the radial reciprocating plate impeller (RRPI), designed to handle highly viscous fermentation broth was modeled using computational fluid dynamics (CFD) to gain more insight into its performance. A standard Rushton turbine was first simulated using CFD software Fluent® for validation purposes. Under experimental conditions, the prediction of the power number using an existing correlation agrees qualitatively with both the experimental data and single phase simulation results. Multiphase simulation was used to better represent the gas-liquid interactions using Eulerian multiphase model. The radial reciprocating movement of the RRPI was approximated using small time steps, each of which has a different rotation speed. Water and carboxymethyl cellulose (CMC) solutions were used as model fluids to represent the different stages of a typical fermentation with a rheologically-evolving broth. By comparing the simulation results to experimental data, the efficiency of the toothed belt used to drive the Rushton turbine impeller was confirmed to be high as expected, while the efficiency of the three-arm linkage system used to achieve the radial reciprocation of the RRPI was estimated to be around 80%. The uniformity of mixing with the 3-Rushton impeller and the RRPI was compared to each other by investigating the distribution of liquid velocity, shear rate, and broth viscosity. The simulation results proved that the RRPI eliminated the dead zones that usually form when the Rushton turbines are used in viscous medium.

Keywords

Computational fluid dynamics (CFD), Design, Mixing, Multiphase, Stirred tank, Radial reciprocation

Nomenclature

a	volumetric superficial gas-liquid area, m^{-1}
A	amplitude of rotation speed, rpm
C	Cross model time constant, s
d_0	orifice diameter of gas distribution plate, m
d_B	bubble diameter, m
D	impeller diameter, m
	diffusivity, m^2/s
f	reciprocation frequency, Hz
g	gravitational acceleration, 9.81 m/s^2
K	power law consistency coefficient, $Pa \cdot s^n$
K_L	overall mass transfer coefficient defined on the liquid side, m/s
l	eddy length, m
m	Cross model rate constant
n	power law index
P	power, W
N	impeller speed, revolutions/s
N_P	power number
Re	Reynolds number
Sc	Schmidt number
t	time, s
	thickness of impeller blades, m
t_e	exposure time, s
T	vessel diameter, m
v'	root mean square of fluctuation velocity, m/s
v_0	friction velocity, m/s

Greek symbols

τ	torque, N·m
	shear stress, Pa
ρ	density, kg/m^3

η	viscosity, Pa·s
η_0	zero shear viscosity, Pa·s
η_∞	infinite shear viscosity, Pa·s
$\dot{\gamma}$	shear rate, s^{-1}
ω	angular speed, rpm or Hz
σ	surface tension, N/m
μ	viscosity, Pa·s
ε	energy dissipation rate per unit mass, W/kg

Subscripts

G	gas phase
L	liquid phase

6.1 Introduction

For conducting aerobic fermentations in stirred tank bioreactors, Rushton turbines are the most popular mixing devices to provide agitation and aeration to the fermentation broth. However, when the fermentations result in highly viscous shear-thinning broth, dead zones may form due to lack of mixing at the periphery of the bioreactor (Thibault and LeDuy, 1999). The presence of stagnant zones may significantly reduce the effective fermentation volume, and thus, the overall efficiency of fermentation. The quality of mixing throughout the fermentation broth is particularly important to achieve high volumetric oxygen mass transfer coefficient (K_La) and to prevent dissolved oxygen (DO) limitations. The use of a mixing device that can reduce or even eliminate the dead zones in the fermenter will have a chance to provide better volumetric oxygen transfer rate to the fermentation broth and, in addition, create more homogeneous operating conditions throughout the fermentation vessel. When dealing with highly viscous fermentation broths, close-clearance mixing devices, such as the axial reciprocating plate impeller (ARPI) (Lounes et al., 1995), the Maxblend system (Hiruta et al., 1997; Hasegawa et al., 1999),

the helical ribbon mixer (Audet et al., 1998), and the helical ribbon screw mixer (Brito-De La Fuente et al., 1997) can be used.

A new close-clearance mixing mechanism, the radial reciprocating plate impeller (RRPI), has been designed to mainly satisfy two objectives: to provide good mixing throughout the fermenter vessel and to give high K_La values by promoting good gas-liquid contact. The design of the RRPI was inspired by another close-clearance impeller, the ARPI. This ARPI has demonstrated some benefits as a mixing device in bioreactors, such as a more uniform distribution of the local mixing energy (Lounes et al., 1995). Promising results were obtained in several viscous fermentations which were carried out using this impeller (Audet et al., 1996, 1998). The main design constraint of the ARPI is the difficulty to ensure sterility because a part of the reciprocating shaft during its axial motion is continuously exiting and re-entering the fermentation vessel. Therefore, in the design of the RRPI, the axial reciprocating movement of the perforated plates was changed to an oscillatory partial radial rotation of the perforated plates. The radial back and forth rotation of this mixer, akin to the motion of a clothes washing machine, is more compatible with existing industrial equipments that are designed to handle rotating mixing devices. This new design has been tested experimentally to assess its mass transfer characteristics and then used in a 22-L laboratory scale bioreactor to optimize the pullulan production (Lin, 2010).

In this work, this new impeller was modeled using CFD software Fluent® in order to gain a deeper insight of its performance. Two mediums, having greatly different viscosities, were used as model fluids to represent the different stages of a rheologically-evolving fermentation broth. The results of the power input predicted from simulations were compared to experimental data, not only to validate the simulation procedure, but also to estimate the efficiency of the three-arm linkage system used to achieve the radial reciprocating movement. The distribution of the liquid velocity, the shear rate, and the viscosity were monitored to evaluate the uniformity of mixing. A stirred tank bioreactors equipped with Rushton turbines was also investigated for validation and comparison purposes.

6.2 Experimental setup

The bioreactor used in this investigation was designed and constructed in our laboratory. It has a height of 55 cm and an internal diameter of 22.8 cm, giving a total volume of 22 L. The working volume used in all experiments was 12 L. At the bottom of the bioreactor, a plate perforated with 100 small 1-mm diameter orifices is used as the air sparger. The perforations are evenly allocated along three concentric rings, which contain 16, 32 and 52 holes, respectively. The diameters of these rings are 7.6, 13.25 and 18.75 cm, respectively. In this investigation, the gas flow rate was controlled at 12 L/min, which is one volume of gas per volume of liquid per minute (vvm). This bioreactor was used for evaluating the performance of three mixing devices: a single Rushton turbine, a triple Rushton impeller (TRI), and the new RRPI. The experimental data of the last two have been reported in our previous work (Lin, 2010).

The Rushton turbines have a diameter of 10 cm. They are mounted on a 1-cm diameter shaft. When only a single Rushton turbine is used, it is located at the middle plane between the bottom of the bioreactor and the liquid surface, which is 14.7 cm from the bottom. When three Rushton turbines are used, the locations of the Rushton turbines, measured from the bottom of the bioreactor, were 4.9, 14.7 and 24.5 cm, respectively. A toothed belt was used to connect the motor shaft and the Rushton impeller shaft.

Figure 6.1 shows that the structure of the RRPI is very similar to a typical Rushton turbine impeller. Two sets of mixer blades are used with six equally-spaced blades mounted on each of the two hubs. The blades are however much larger than Rushton impeller blades. Each blade is a rectangular plate with a width of 9 cm and a height of 12 cm, and is perforated with 2-cm diameter holes arranged in an equilateral triangle pitch. The distance between the centers of each adjacent hole is 3 cm. The mixing assembly is comprised of two such hubs, which are positioned with a 30^{o} angle relative to each other. The diameter of the impeller assembly is 21.5 cm. With this diameter, the spacing between the tips of the blades and the internal wall of the vessel is 0.65 cm. Two of the blades on the upper hub are cut at appropriate locations to accommodate for the fermentation probes (temperature, pH and dissolved oxygen).

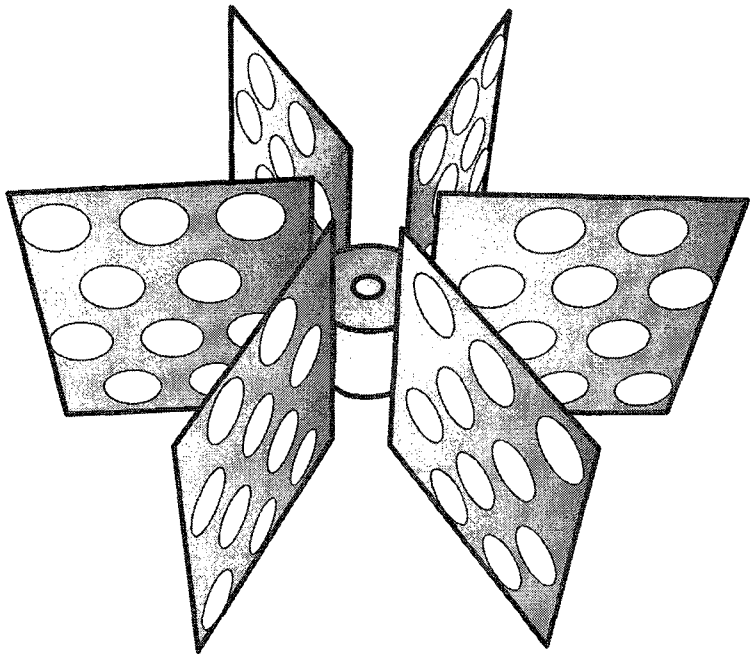

Figure 6.1 Schematic diagram of the RRPI's bottom hub.

The back and forth displacement is achieved using a simple three-arm linkage system (Figure 6.2). One arm is fastened to the bioreactor shaft and another to the motor shaft. The third arm connects the first two arms together. The effective length of the first (R), second (r), and third arm (L) are 10.4 cm, 2.5 cm and 13.2 cm, respectively. The distance between the two shafts (l) is 14 cm. While the motor shaft rotates at a constant speed in one direction, the bioreactor shaft rotates back and forth such that each impeller blade covers a region of the bioreactor that spans an angle of approximately 46^{o} (Lin, 2010).

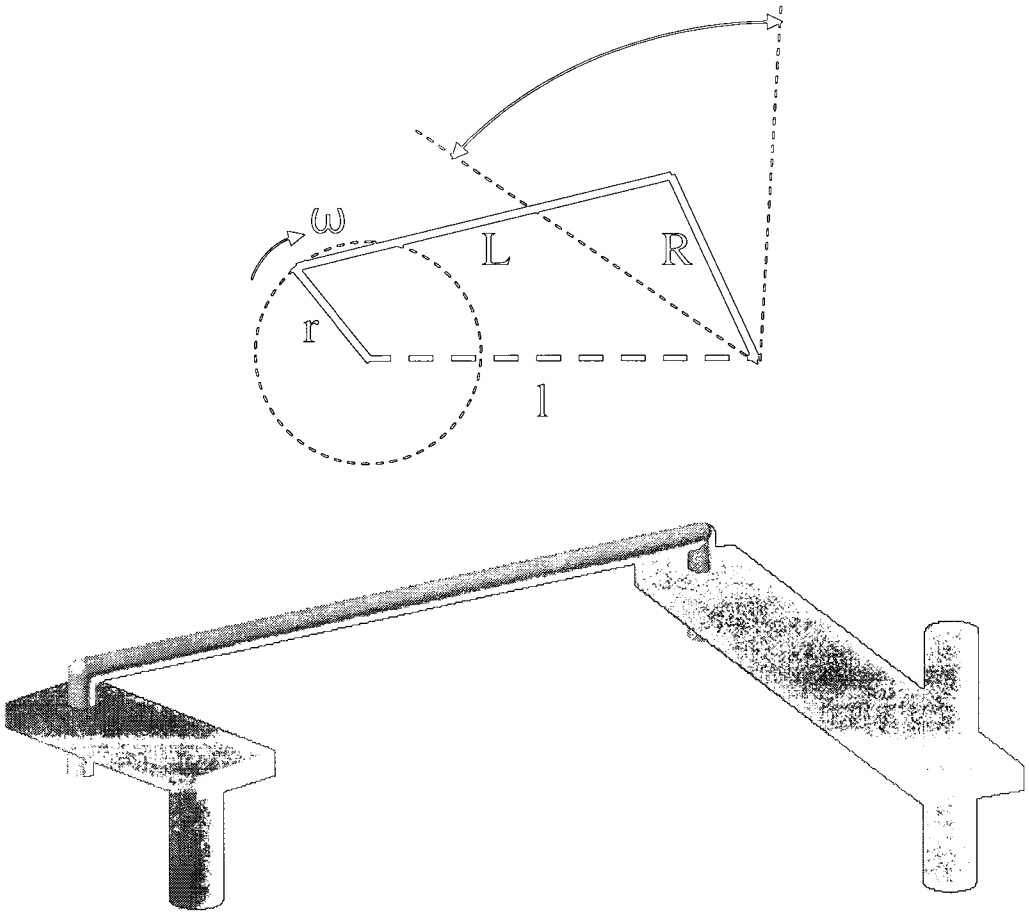

Figure 6.2 2D and 3D schematic diagram of the RRPI drive mechanism.

The motor that was used to drive the Rushton impellers and the RRPI is a 140 W variable speed motor (Heidolph's RZR 2102 control, Schwabach, Germany). Given the motor rotation speed and the torque data, the power provided by the motor can be calculated using Equation 6.1. In order to get the portion of the mixing power imparted to the fluid, the power required to drive an empty bioreactor is subtracted from the power when the bioreactor, which is agitated under the same rotation speed, is filled with the fluid. Since the speed and torque data reported by the motor are values at the motor shaft, the efficiency of both the toothed belt gear system and the three-arm linkage system are assumed to be 100%. In reality, the efficiency of a toothed belt, which is used for both the single Rushton turbine and the TRI system, is very high, typically over 97% (Anonymous, 2009). However, the efficiency of the three-arm linkage system used for the RRPI system

should be further away from 100%. One would need to measure the torque directly on the shaft of the bioreactor to have a more accurate appreciation of the actual power input consumed for mixing in this system. However, if it is technically impossible to achieve higher efficiency with this three-arm linkage system, the power input results obtained using the motor values are still more useful for practical purposes. The power number is then calculated using Equation 6.2.

$$P = 2\pi N\tau \tag{6.1}$$

$$N_P = \frac{P}{\rho N^3 D^5} \tag{6.2}$$

Two model fluids were tested: distilled de-ionized water and 10 g/L aqueous CMC (Hercules type 7H3SXF) solution. The temperature of the medium was maintained at 28°C for all experiments using water bath through a jacket on the outside of the bioreactor. The viscosities of the model fluids were determined using Anton Paar's Physica M301 rheometer with a double gap concentric cylinder measuring system (DG42). The viscosity of water was found to be 0.00089 Pa·s at 28°C. The 10 g/L CMC solution shows non-Newtonian shear-thinning behavior. Its viscosity in the shear rate range of 0.1 to 1000 s^{-1} is represented very well using the Cross rheological model (Equation 6.3). The corresponding parameters were determined to be: η_0 = 0.691 Pa·s, η_∞ = 0.0116 Pa·s, C = 0.0456 s, and m = 0.658.

$$\eta = \frac{\eta_0 - \eta_\infty}{1 + (C\dot{\gamma})^m} + \eta_\infty \tag{6.3}$$

6.3 Modeling

Commercial CFD software Fluent® 6.3.26 was used to carry out the simulation. Since many of the simulations represent a major computation challenge on a normal desktop computer, the majority of the calculations were performed using High Performance Computing Virtual Laboratory (HPCVL) supercomputers located in Kingston, Ontario, Canada. In most simulations, 16 CPUs were used in parallel mode as a compromise between the speed of computation and the parallel efficiency, as recommended by Kerdouss et al. (2008).

Unstructured tetrahedral cells were used for all cases. When the Rushton turbine is used in water, the Reynolds number (estimated using Equation 6.4) is over 10 000 under most rotation speeds, indicating that it is operated in the fully turbulent regime. And thus, the realizable k-epsilon turbulence model was used for these cases. For the other cases, the conventional Reynolds number, as defined for a mixing impeller rotating at constant speed and in a medium with constant viscosity, does not apply directly. In the RRPI system, the rotation speed and the direction of rotation continuously varies with time. When the CMC solution is used, the viscosity depends on the shear rate. An instant Reynolds number was estimated using the instant rotation speed of the RRPI at each time step, and an overall Reynolds number was estimated for each reciprocation speed using averaged absolute rotation speed at each time step within a cycle of reciprocation. When the CMC solution is used, a liquid volume weighted average viscosity is used as the effective viscosity for each time step to determine the corresponding Reynolds number. And the mean value of viscosities at all time steps within a cycle of reciprocation is used as the final effective viscosity to estimate the overall Reynolds number for that reciprocation speed. These effective viscosities of the CMC solution are much greater than that of water, so the estimated Reynolds number is usually smaller than 1000. However, it is unlikely that it is really in the laminar regime especially when the reciprocation speed is high, so the realizable k-epsilon turbulent model was still used in all simulations.

$$\mathrm{Re} = \frac{\rho N D^2}{\mu} \tag{6.4}$$

The multiple reference frame (MRF) method was used for all simulations performed with Rushton turbines because of the presence at the periphery of the bioreactor of four equally-spaced stationary baffles, each having a length of 23 cm and a width of 2.5 cm. The MRF method itself is a steady state approach. When it was used for the single phase simulation, the scaled residuals of all variables and the torque of the impeller were usually used to detect convergence. In order to compare simulation results with predictions from existing correlations, the system with a single Rushton turbine was simulated using the single phase model. Four different mesh sizes were tested initially to ensure grid independency.

When the gas-liquid interaction is modeled using the Eulerian multiphase model, the MRF can also be used, however, it is carried out using an unsteady state approach. The gas inlet was modeled using the mass flow rate boundary condition to ensure that gas is fed into the bioreactor at a rate of 12 L/min. The gas outlet is modeled using the pressure outlet boundary condition. Provided that a sufficiently large number of time steps are calculated, the simulation should reach steady state. In this work, it was shown that 500 time steps, each having a Δt of 0.02 s, were sufficient to obtain the correct flow features such as the velocity field. It was therefore used for all cases.

For simulating the bioreactor system with the RRPI where there were no baffles, the single reference frame (SRF) method was used because the impeller is the only geometrical physical element inside the simulation domain. The use of the SRF also avoids the difficulty of having to divide, as in the case of the MRF method, the small gap between the impeller tip and the tank wall while trying to keep the cell skewness small and the number of cells at a manageable level. Even with this difficulty removed, the smallest number of cells generated was almost 1.5 million. Since the rotation speed of the RRPI is changing continuously both in direction and speed, the simulation is intrinsically unsteady state.

The angular position of the RRPI was obtained analytically by solving the geometrical relationships between the three arms of the linkage system. Then, the rotation speed of the impeller shaft was derived using the finite difference method based on its analytical angular position. The rotation speed was then approximated using a basic sine wave function (Equation 6.5) evaluated for each reciprocating speed that was investigated. The corresponding parameters of Equation 6.5 for each reciprocating speed are listed in Table 6.1. Since t_0 only influences the phase at the start of the reciprocating motion, it was omitted from the table. In order to start each reciprocation cycle at the same phase, t_0 was set to be $1/(4f)$, such that the beginning of each cycle corresponds to the maximum negative speed when t equals zero. In Fluent®, 50 time steps were used to simulate one complete reciprocation cycle. The time increment Δt was thus varied depending on the reciprocation speed. The rotation speed of the moving zone was changed using journal files, which contain all necessary text user interface (TUI) commands for automatic execution.

$$\omega(t) = A\sin(2\pi f(t - t_0)) + A_0 \tag{6.5}$$

Table 6.1 Sine wave function parameters (Equation 6.5) used to represent the rotation speeds of the RRPI.

Motor speed	30	60	90	120	140	160	180
Reciprocating frequency	0.5	1	1.5	2	2.33	2.67	3
A, rpm	11.99	23.85	35.73	47.62	55.77	63.42	71.41
$2\pi f$	3.20	6.31	9.44	12.58	14.67	16.76	18.86
A_0, rpm	-0.0745	-0.0407	-0.0307	-0.0266	-0.1290	-0.0551	-0.0244

For each reciprocation speed, the simulation was first carried out for five cycles of reciprocation in order to reach a periodical steady state by the end of the fifth cycle, as was indicated by the cyclic torque results obtained. Then, the data obtained during the sixth reciprocation cycle were analyzed and averaged to get the final results for each reciprocating speed.

For a more accurate representation of the real situation where gas-liquid mixture is involved, the population balance model (PBM) should be used (Kerdouss et al., 2005; Moilanen et al., 2007, 2008; Gimbun et al., 2009). Unfortunately, this model is not included in a standard Fluent® license and it is therefore not available at HPCVL. It is also not very practical using the PBM locally on a normal desktop computer. Because, as suggested by Laakkonen et al. (2007), more than 80 bins should be used to minimize the discretization errors, this would require 80 more equations to be solved in addition to the momentum, multiphase, and turbulent equations. It would make it impossible to obtain useful results in a reasonable time scale. Usually, a smaller number of bins are used to relieve the calculation burden. Thirteen bins were found to be satisfactory by Kerdouss et al. (2008). However, 16 computer nodes were still recommended in order to handle the PBM efficiently.

Due to these limitations, single bubble size was used throughout the simulations performed in this investigation. Since the bubble diameter at the orifice of the gas plate distributor is predicted by the correlation presented in Equation 6.6 to be 3.55 mm (Moo-Young and Blanch, 1981), the air bubble diameter was set to 3 mm for all simulations using water as model fluid. When viscous medium is used, Moilanen et al. (2006) found

that small bubbles do not separate from the solution. For all simulations performed for the CMC solution, a 6 mm bubble diameter was used. However, the effect of using different bubble sizes will be further investigated.

$$d_B = \left(\frac{6\sigma d_0}{g(\rho_L - \rho_G)} \right)^{\frac{1}{3}} \tag{6.6}$$

The impeller torque can be directly reported by Fluent®. The power consumption can then be calculated using Equation 6.1. For the simulations performed for the single Rushton turbine and the assembly of three Rushton turbines (TRI), the torque data reached a stabilized value at the end of each simulation. For the RRPI simulations, since the angular velocity of the impeller is changing following the corresponding sine wave function, the torque data also show a cyclic behavior. The continuously changing angular velocity and torque result in the value of the power being different at all time steps. The averaged power consumption was obtained by integrating the instantaneous power over a complete cycle of reciprocation. For simulations performed with the TRI, the calculated power was first divided by the number of turbines (i.e. 3) in order to evaluate the averaged power number for each turbine. By comparing the simulated power consumption to the data obtained experimentally, the efficiency of the transmissions can be estimated.

Since unstructured mesh was used, cells do not have identical volume. As a result, Fluent®'s build-in histogram function cannot accurately reflect the distribution of selected simulation parameters. Therefore, the values for each of the desired parameters at all cell centers were exported to an ASCII file for further processing. The distributions of the liquid velocity, shear rate, and viscosity were obtained by sorting the cells into 50 bins which cover the range of interest for each parameter. The interested ranges are 0-0.7 m/s and 0-90 s^{-1} for the liquid velocity and the shear rate, respectively. Since the apparent viscosity of the CMC solution is already limited by the Cross model parameter η_0, the whole range of apparent viscosity is used. Then, the sum of the cell volume and the corresponding volume percentage were calculated for each bin. These calculations were carried out using a program executed in Compaq Visual Fortran standard edition 6.1.0.

6.4 Results and Discussion

6.4.1 Single phase simulations

6.4.1.1 Grid independency test

Prior to performing a large series of CFD simulations, exploratory simulations were done using the single phase method to conduct a grid independency test. For this test, simulations were performed for the stirred tank bioreactor equipped with a single Rushton turbine. The liquid surface was modeled using a symmetrical boundary. Four meshes with different cell numbers were generated using Gambit 2.3.16, the pre-processor for Fluent®. Each simulation usually required approximately 2500 iterations to reach convergence, which is determined by achieving almost constant values for the scaled residuals of all variables and the impeller torque. All four meshes gave almost the same torque results when the impeller was rotating at 400 rpm, and thus, the calculated power number was similar. The results of this test are presented in Table 6.2.

Table 6.2 Grid independency test for a single Rushton turbine running at 400 rpm.

Number of cells	Torque, N·m	Power, W	Power number
191535	0.2440	10.219	3.474
260508	0.2436	10.204	3.469
508974	0.2488	10.420	3.542
1401246	0.2486	10.413	3.540

The mesh with a cells number of 261k was used for all simulations performed using the single phase method at various rotation speeds with the single Rushton turbine. The mesh used for other more complex cases was generated in the same way with a similar level of details. However, the number of cells was significantly increased because in one case the mixing assembly has three Rushton turbines, and in the other case the impeller diameter of the RRPI is much larger. When the multiphase model was used, the number of mesh cells was further increased because it is necessary to represent with sufficient accuracy the 100 small gas inlets on the gas distributor at the bottom of the

bioreactor. In fact, the smallest mesh used for the multiphase simulation for the three Rushton turbines has a number of cells in excess of 1.2 million. For all these cases, it was verified that grid independency prevailed.

6.4.1.2 Power input at various rotation speeds

6.4.1.2.1 A single Rushton turbine

The stirred tank bioreactor equipped with a single Rushton turbine was investigated because it is the system that has been the subject of a great number of studies, and thus, many correlations exist in the literature to estimate the numerous parameters. For instance, one such correlation predicts the power number (N_P) when the mixing is in the fully turbulent regime as given in Equation 6.7 (Bujalski et al., 1987; Beshay et al., 2001). In the laboratory experimental system used in this investigation, the impeller diameter D of the six-blade Rushton turbine is 0.1 m, the thickness of the Rushton blades t is 0.001 m, and the vessel diameter T is 0.228 m. The theoretical correlation predicts that the power number of this bioreactor system is 5.62 when it is operated in the turbulent regime where the impeller Reynolds number is greater than 10 000. The impeller Reynolds number is calculated using Equation 6.4. The experimental values of the power number are smaller than those predicted by the correlation of Equation 6.7 and lie between 4 and 4.5. The simulation results, as represented in Figure 6.3, are even smaller with values close to 3.5 for almost all rotation speeds. However, although the values of the experimental power number are significantly different than the predicted and simulated values, the trend showing that the power number remains almost constant is in agreement with the correlation and previously published experimental results (Nagata, 1975; Beshay et al., 2001).

$$N_P = 2.512\left(\frac{t}{D}\right)^{-0.195}\left(\frac{T}{T_0}\right)^{0.063} \tag{6.7}$$

where $T_0 = 1$ m

6.4.1.2.2 The triple Rushton impeller (TRI)

For the case using the assembly of three Rushton turbines, the simulated power number is slightly smaller than the simulated power number for the single Rushton turbine (Figure 6.4). This estimated decrease is due to the relative contribution of the three

turbines to agitate the liquid medium. It is hypothesized that each turbine imparts less energy to the fluid to agitate the medium because the zones located further away of a given turbine are already agitated by nearby turbines. Nevertheless, the simulated power number remains almost identical at the various rotation speeds. On the other hand, the experimentally determined values of the power number show a decreasing trend as the speed of rotation is increased. This decrease in power number is caused by surface aeration. Despite the presence of baffles at the periphery of the mixing tank, it was visually observed that surface aeration occurred due the vortex generated by the top Rushton turbine, located near the liquid surface. The surface aeration was more important at higher rotation speed and the air entrained into the liquid medium transforms the single phase system into a gas-liquid dispersion, resulting in the observed decrease in the power number. The different trends observed in the experimental data and those generated by CFD for the single phase simulation indicate clearly that the multiphase model is necessary when gas entrainment occurs.

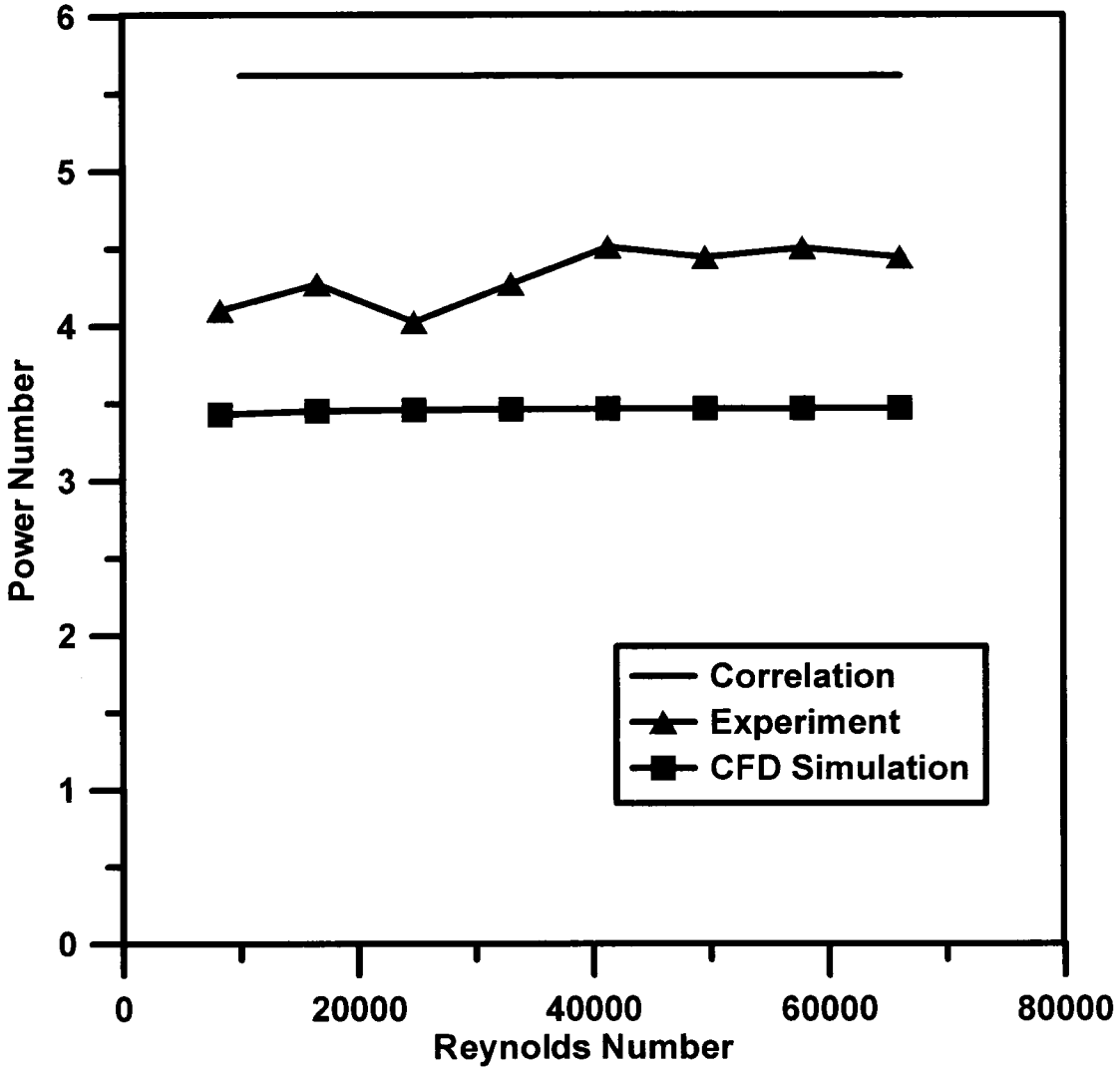

Figure 6.3 The power number versus Reynolds number for a system with a single Rushton turbine.

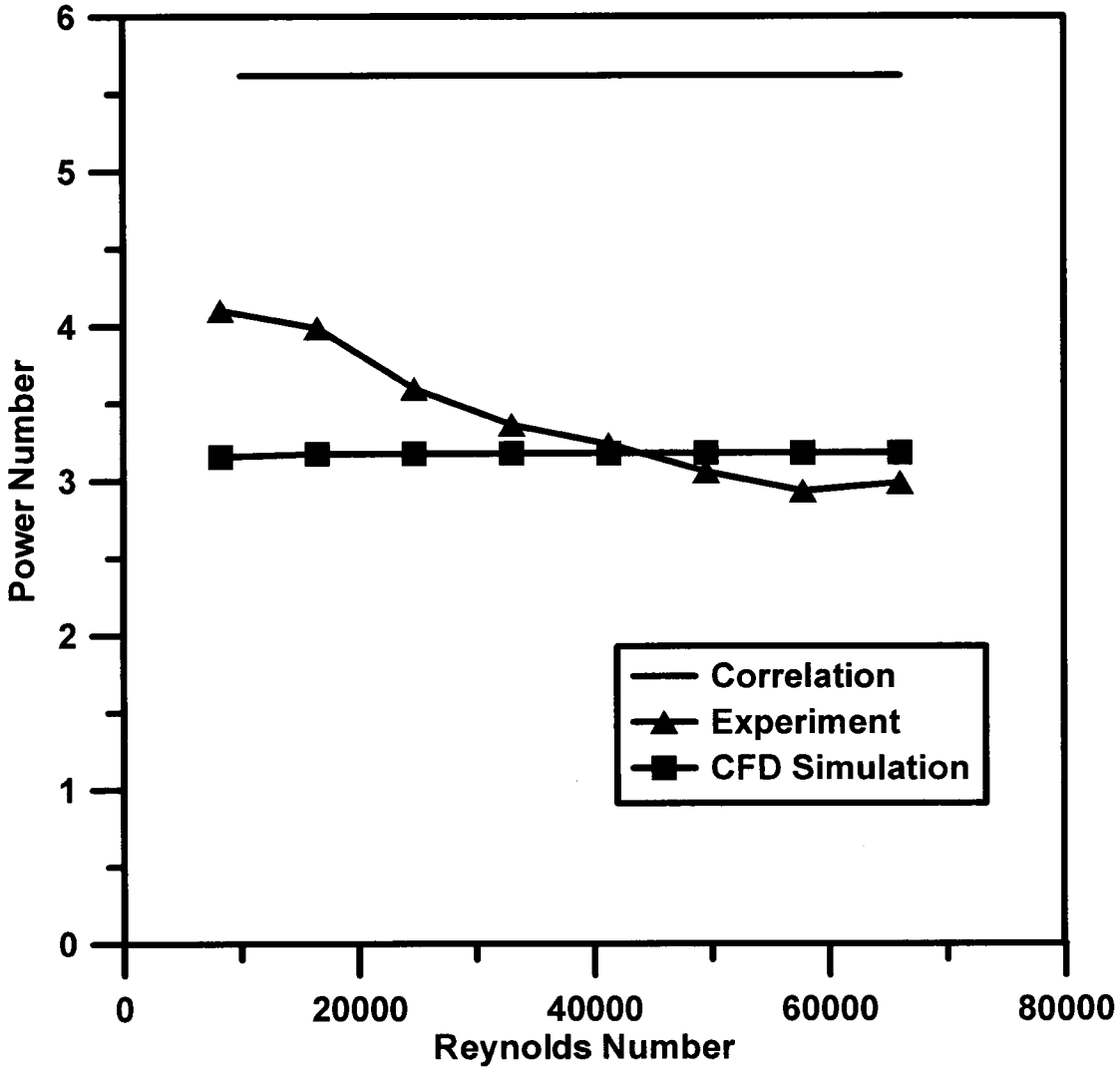

Figure 6.4 The power number versus Reynolds number for the TRI system.

6.4.2 Multiphase simulations

The use of multiphase model is essential to properly simulate the gas-liquid interaction that is usually encountered in an aerobic fermentation. Instead of modeling the portion of the bioreactor that was occupied by the liquid, as it was done with the single phase simulations, the whole bioreactor volume was modeled. The fine gas inlet orifices were also simulated as close to its exact geometry as possible together with the top gas outlet. The additional modeling requirements have significantly increased the number of

mesh elements to over one million. The large number of mesh elements makes the computation time required to carry out the simulation a factor that must be carefully considered.

6.4.2.1 Power consumption

6.4.2.1.1 Power input per unit volume in water

Power input per unit volume is an important criterion for the design of a reactor where mixing is involved. The results obtained for the stirred tank bioreactor using the TRI are shown in Table 6.3, while those obtained from the same bioreactor using the RRPI are shown in Table 6.4. In the TRI bioreactor system, since a toothed belt gear system was used to connect the motor shaft and the impeller shaft, the efficiency of the gear system should also be considered. In practice, the efficiency of the toothed belt system is usually reported to be over 97% (Anonymous, 2009). This is qualitatively supported by simulations and the experimental results for the cases where the agitation speed was higher than 150 rpm. For lower agitation speeds, the observed difference is partially caused by the relative accuracy of the motor torque measurement. Because at lower agitation speeds, the torque reading is small and the variation in the measured data is relatively large, the accuracy under these conditions is therefore compromised. In the RRPI bioreactor system, the prior knowledge on the efficiency of the three-arm linkage system does not exist. It seems that at lower reciprocation speeds, the torque measurement also suffered from the same accuracy problem. When the reciprocation speed is higher than 1.5 Hz, the efficiency of the linkage system is in the vicinity of 80% assuming that the simulated results are exact.

Table 6.3 Experimental and simulated power inputs per unit volume for the TRI system in water with 1vvm aeration.

Agitation speed (bioreactor shaft), rpm	P/V, W/m^3		Efficiency
	Experiment	CFD simulation	
50	8.8	4.1	46%
100	51	31	60%
150	139	102	73%
200	285	266	93%
250	535	452	84%
300	882	847	96%
350	1255	1265	101%
400	1772	1626	92%

Table 6.4 Experimental and simulated power inputs per unit volume for the RRPI system in water with 1vvm aeration.

Reciprocating speed, Hz	P/V, W/m^3		Efficiency
	Experiment	CFD simulation	
0.5	3.8	4.6	120%
1	30	32	106%
1.5	114	108	95%
2	284	253	89%
2.33	497	401	81%
2.67	778	588	76%
3	1199	837	70%

6.4.2.1.2 Power input per unit volume in the 10 g/L CMC solution

For highly viscous medium, mixing using Rushton turbines is not efficient because adequate mixing only prevails in the vicinity of the mixing impellers and stagnant zones in the periphery of the mixing vessel are created. Nevertheless, both experiments and simulations were carried out to investigate the effect of viscosity on the power input per unit volume (Table 6.5). The corresponding experimental and simulated results for the RRPI bioreactor system are shown in Table 6.6. Under most rotation speeds in the TRI system, the power input per unit volume for the 10 g/L CMC solution was about 15%

lower that the values obtained in water. This decrease is most likely due to a smaller effective volume that is being mixed because of the presence of dead zones. However, the opposite trend was observed for the RRPI system. Indeed, under most reciprocating speeds, the power input requirement to mix the 10 g/L CMC solution increased approximately 10-15% compared to that required to mix water. The diameter of RRPI is large enough to cover most of the liquid volume, such that an increase in viscosity will result in an increase in the power input per unit volume. One would have expected to observe a much greater increase in the power requirement when CMC solution is used. However, the relatively low increase in power input per unit volume is probably caused by the fact that the fluid is being actively agitated and the CMC solution is a shear thinning fluid, so the apparent viscosity is not as high as if it were being accelerated from liquid at rest.

Table 6.5 Experimental and simulated power input per unit volume as a function of agitation speed for the TRI in 10 g/L CMC solution with 1vvm aeration.

Agitation speed (bioreactor shaft), rpm	P/V, W/m^3		Efficiency
	Experiment	CFD simulation	
50	8.6	6.3	74%
100	39	28	71%
150	120	88	73%
200	250	206	82%
250	397	390	98%
300	649	661	102%
350	1006	1033	103%
400	1454	1519	105%

Table 6.6 Experimental and simulated power inputs per unit volume as a function reciprocating speed for the RRPI in the 10 g/L CMC solution with 1vvm aeration.

Reciprocating speed, Hz	P/V, W/m^3		Efficiency
	Experiment	CFD simulation	
0.5	6.5	8.4	128%
1	43	45	105%
1.5	132	128	97%
2	313	269	86%
2.33	556	426	77%
2.67	873	584	67%
3	1312	862	66%

6.4.2.2 Uniformity of mixing

6.4.2.2.1 Mixing in water

The uniformity of mixing can be evaluated by examining the distribution of the liquid velocity and the shear rate throughout the volume of the liquid. This information can be easily obtained using CFD whereas it would be very difficult to obtain experimentally. Because the meshes used for both mixing device assemblies are unstructured and the cells do not have the same volume, a meaningful distribution can only be obtained by making a histogram based on the cell volumes whose interested parameters at the cell center fall into different ranges. In order to compare the two different bioreactor systems, it is desired to have similar power input per unit volume for both systems. According to Tables 6.3 and 6.4, both the experimental and CFD simulation results of the power input per unit volume have approximately the same value when the TRI system is operated at 200 rpm and the RRPI system is running at 2 Hz. These two conditions were therefore compared to each other.

For the case where the TRI system is operated at 200 rpm, the steady state distribution of the liquid velocity and shear rate are shown in Figure 6.5. The bar at the extreme right of the range in each histogram shows the volume fraction that has a velocity or shear rate that are higher than 0.7 m/s or 90 s^{-1}, respectively. The liquid velocity has a maximum value of 1.44 m/s. The maximum shear rate was found to be 10360 s^{-1}. However, the majority of the liquid volume has a velocity that lies between 0.1 to 0.3 m/s,

and a shear rate that lies between 5 to 30 s^{-1}. Overall, the liquid volume weighted velocity of liquid and shear rate were found to be 0.215 ± 0.121 m/s and 17.2 ± 21.0 s^{-1} (mean ± standard deviation (SD)), respectively.

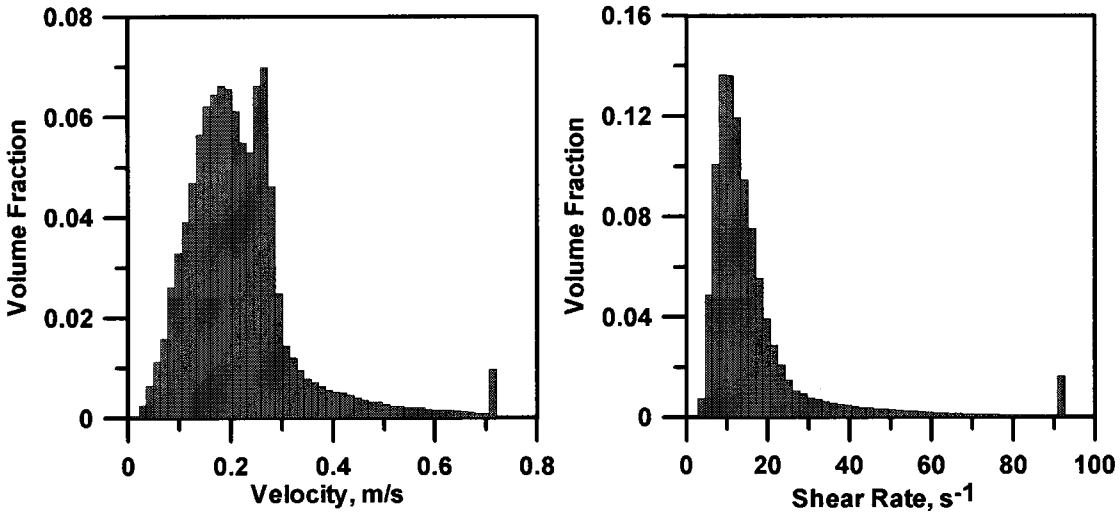

Figure 6.5 Volume weighted histogram of liquid velocity and shear rate when the TRI system operating at 200 rpm was used in water.

For the RRPI bioreactor system, being intrinsically unsteady, the distribution of the liquid velocity has to be analyzed for each of the 50 steps used to represent a cycle of reciprocation. The histograms of two representative steps are shown in Figure 6.6. Step 12 corresponds to a rotation speed that is closest to 0. Step 35 corresponds to a rotation speed that is 2/3 of the maximum value of the oscillatory rotation speed. Histograms obtained at other time steps were also found to be similar. The velocity for the majority of the liquid volume lies between 0.1 to 0.3 m/s, and the shear rate of the majority of the liquid volume lies between 5 to 30 s^{-1}, which correspond to the same values that were prevailing in the TRI system. Additional statistical data on the velocity and shear rate fields at all 50 time steps are given in Figure 6.7. Both the mean and SD data of liquid velocity and shear rate show cyclic behavior, although not exactly in phase with each other. The overall mean and SD over one complete cycle of reciprocation was found to be 0.170 ± 0.089 m/s and 20.38 ± 23.01 s^{-1} for the liquid velocity and shear rate, respectively.

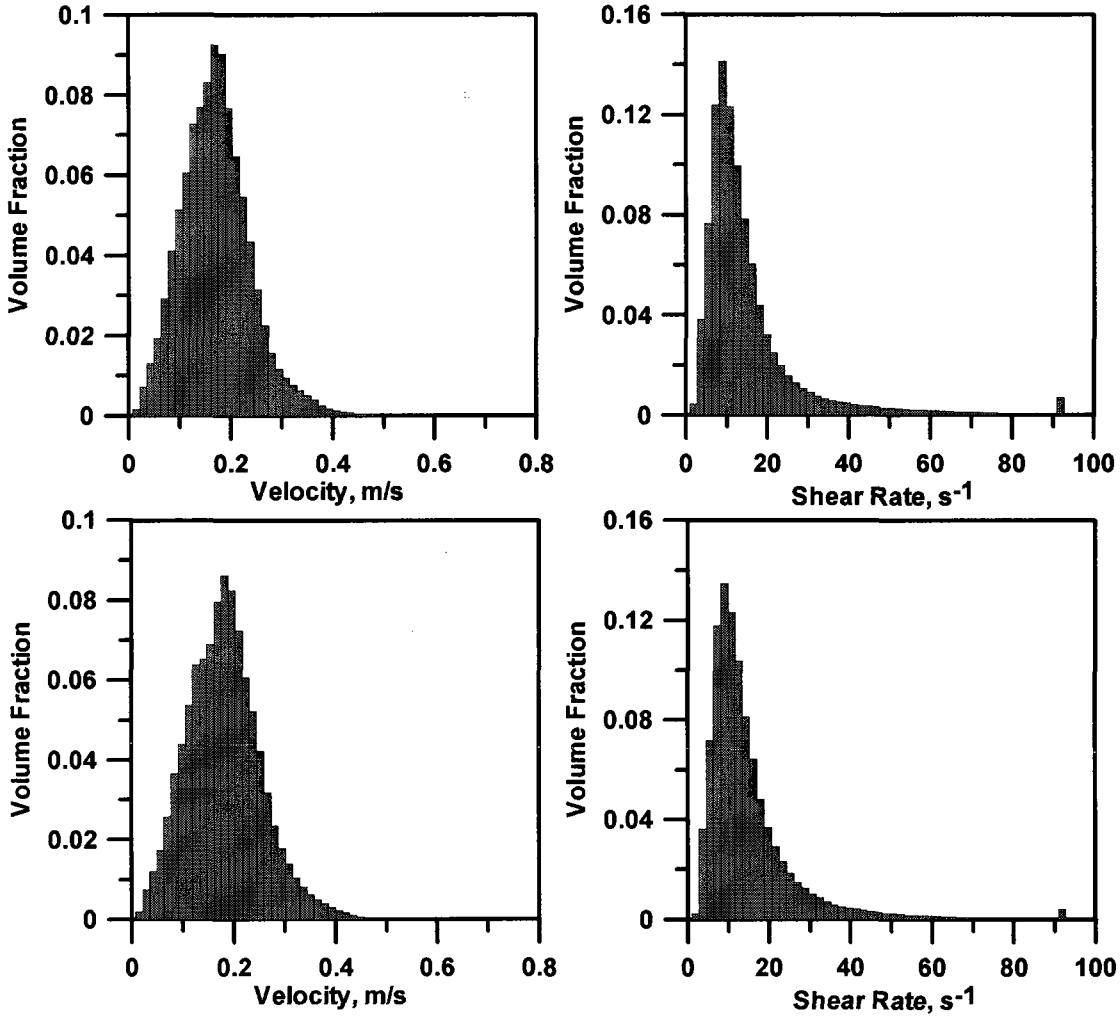

Figure 6.6 Volume weighted histogram of liquid velocity and shear rate when the RRPI system running at 2 Hz was used in water. (Top: Step 12; Bottom: Step 35)

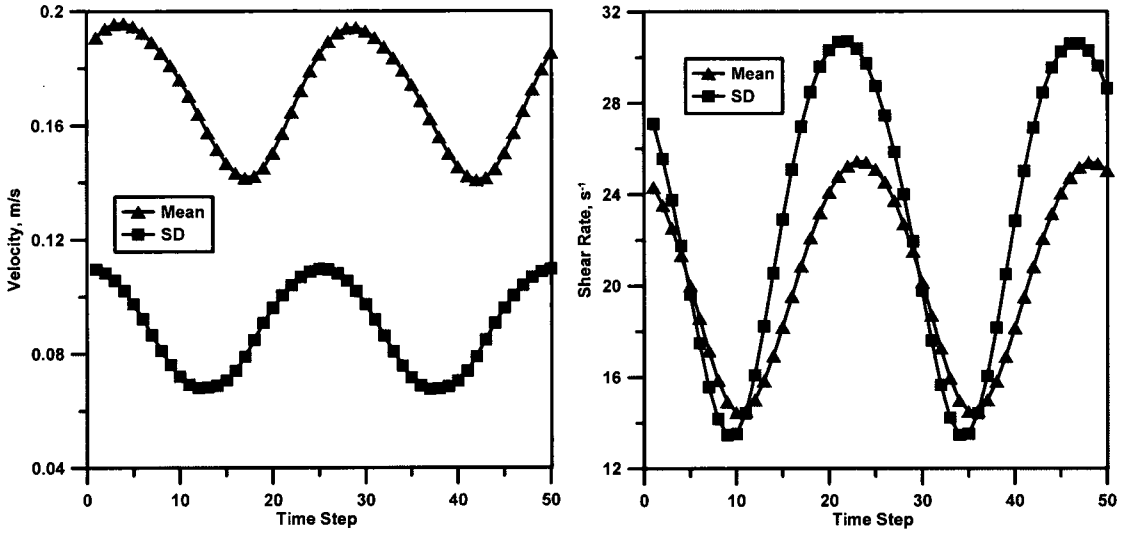

Figure 6.7 Velocity and shear rate statistics for the RRPI reciprocating at 2 Hz in water.

6.4.2.2.2 Mixing in 10 g/L CMC solution

For the non-Newtonian CMC solution, the uniformity of mixing was also evaluated by the distribution of the liquid velocity and the shear rate. In addition, the distribution of the liquid apparent viscosity throughout the liquid volume was also used. The steady state distributions of the liquid velocity, shear rate and apparent fluid viscosity, for the TRI system operated at 200 rpm, are shown in Figure 6.8. The shape of the velocity distribution is different from that obtained in water. The maximum volume fraction lies very close to 0 m/s. If less than 0.014 m/s (2% of 0.7 m/s) is used to judge the presence of dead zones, the first bar in the graph corresponds to a dead zone. Similar approach was used by Moilanen et al. (2007) to detect the presence of dead zones. In this case, 7.0% of the total liquid volume experiences a null velocity and would be considered as a stagnant zone. The apparent viscosity distribution also shows that a noticeable portion of the liquid has a maximum apparent viscosity, indicating that it is motionless. This maximum apparent viscosity only occurs for about 0.3% of the total liquid volume. When the scale of the bioreactor is larger, this volume percentage could be much greater. Overall, the liquid volume weighted velocity of liquid, shear rate, and apparent viscosity were found to be 0.147 ± 0.127 m/s, 11.8 ± 17.7 s^{-1}, and 0.441 ± 0.074 Pa·s, respectively.

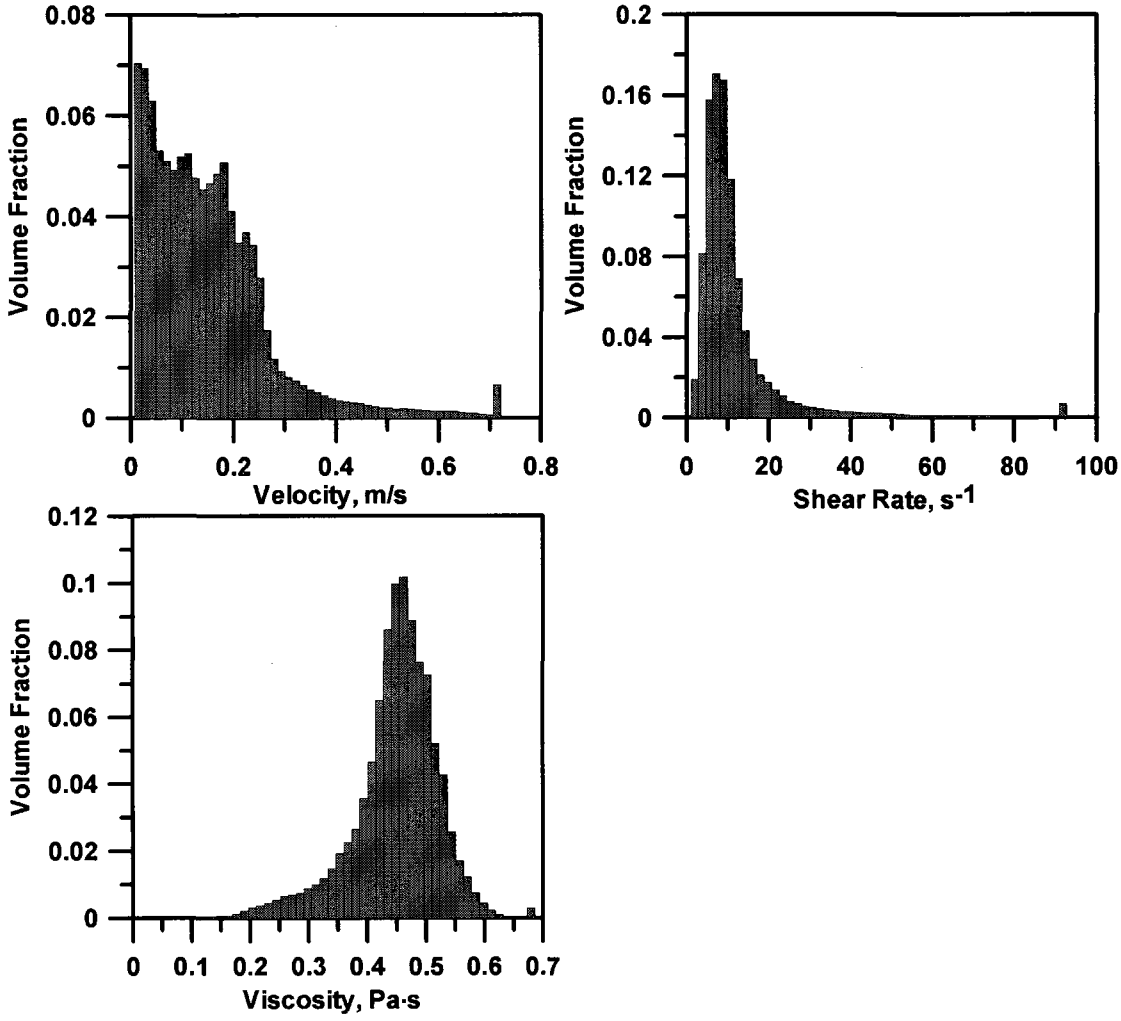

Figure 6.8 Volume weighted histogram of liquid velocity, shear rate, and apparent viscosity when the RTI system operated at 200 rpm is in the 10 g/L CMC solution.

The volume weighted liquid velocity, shear rate and apparent viscosity distributions for the RRPI system operated at 2 Hz are presented in Figure 6.9 for Step 12 of the reciprocation cycle. The maximum velocity probability density function (PDF) is now located further away from 0 m/s. In addition, the zone with the maximum apparent viscosity has disappeared which indicates that there are no significant stagnant zones in the liquid medium. Similar results were obtained for other time steps. Additional statistical data on the liquid velocity, shear rate fields, and apparent viscosity at all 50 time steps are given in Figure 6.10. The overall mean and SD over one complete cycle of reciprocation were found to be 0.118 ± 0.081 m/s, 13.98 ± 18.43 s^{-1} and 0.435 ± 0.091 Pa·s for the liquid

velocity, shear rate, and apparent viscosity, respectively. However, the determination of the actual stagnant zone should be based on other methods instead of using the 0.014 m/s limit, since the velocity of the fluid inside may be momentarily very close to 0 due to the reciprocation movement of the impeller. This was done by checking the liquid velocity at all cell centers for all 50 time steps over one cycle of reciprocation. The portion of cells that always have very small velocities can be regarded as the actual dead zone that is subjected to very small agitation. As expected, negligible volume fraction was found to be located in a dead zone when the RRPI is used to mix the 10 g/L CMC solution.

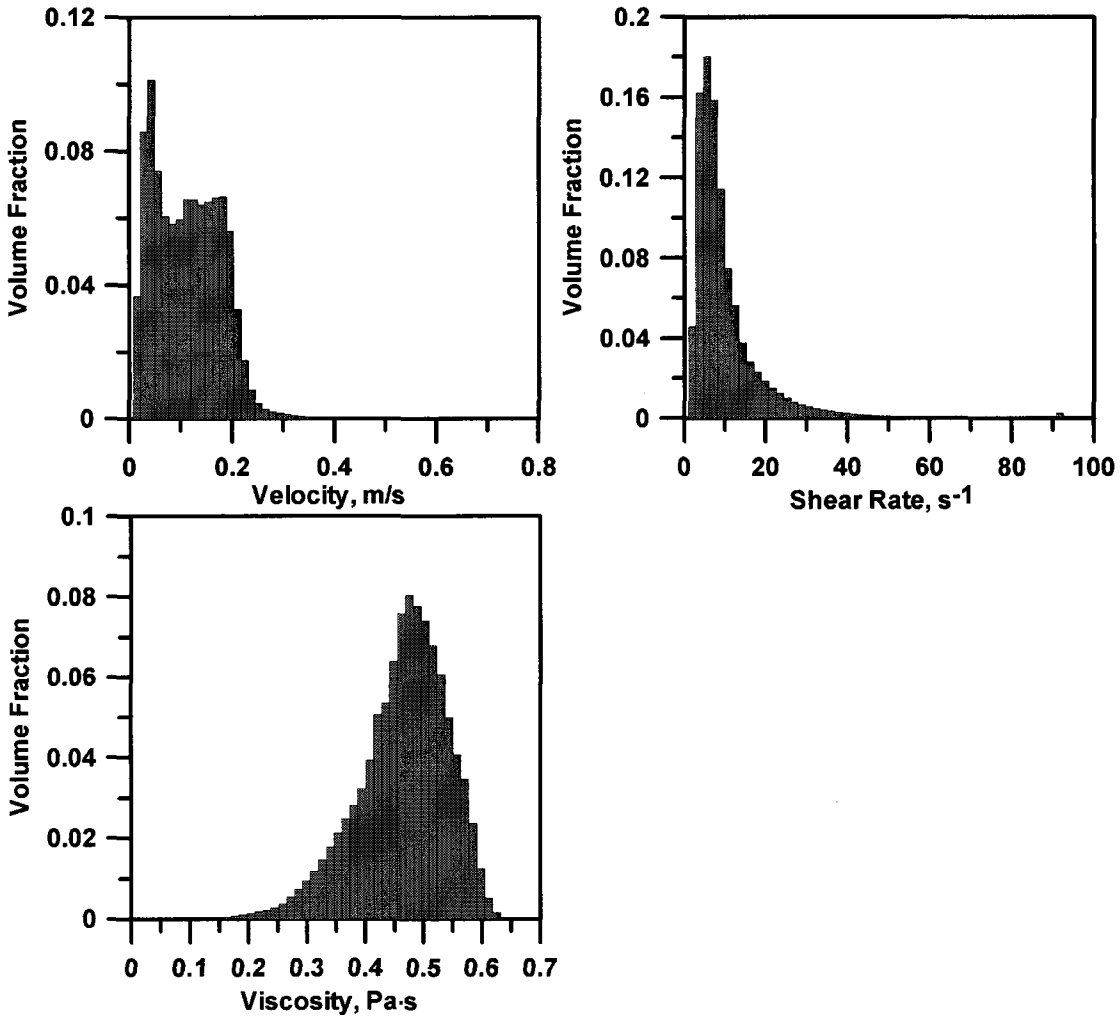

Figure 6.9 Volume weighted histogram of liquid velocity, shear rate, and apparent viscosity when the RRPB is running at 2 Hz in 10 g/L CMC (Time step 12).

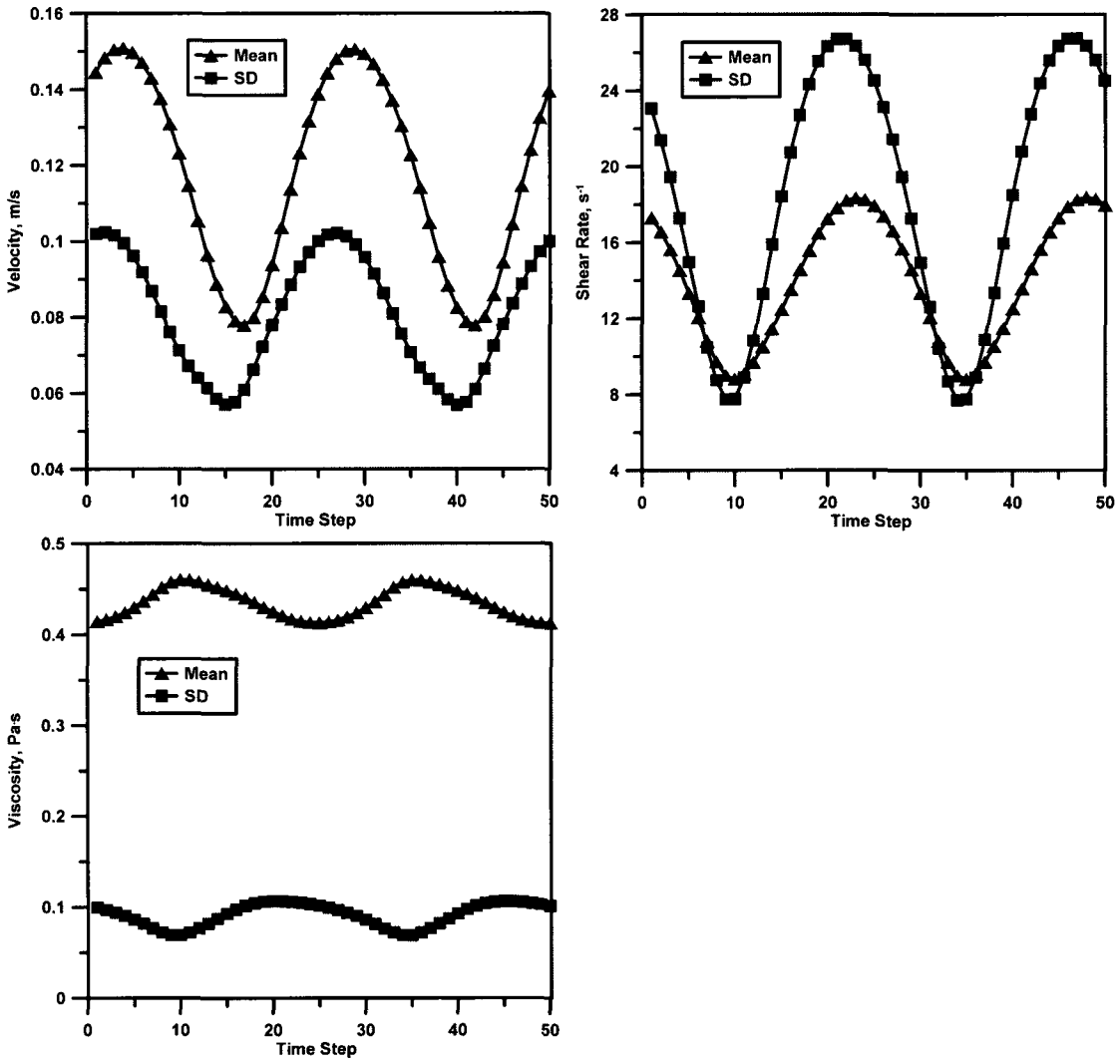

Figure 6.10 Liquid velocity, shear rate and viscosity statistics when the RRPI is running at 2 Hz in 10g/L CMC.

Based on the results presented above with the TRI bioreactor system and the RRPI bioreactor system, it is evident that RRPI system is more efficient in mixing highly viscous non-Newtonian medium. The new stirrer is superior to the TRI because it can provide more uniform mixing, and thus it eliminates the dead zones when the broth viscosity is high.

6.4.2.3 Overall mass transfer coefficient (K_La)

The initial intent in determining the power requirement was to predict the power input per unit volume and K_La correlation in order to test and improve the design of any

new impeller. However, several difficulties were encountered on the course of pursuing this goal.

First, the PBM was not available at the HPCVL. K_La prediction is usually done by predicting the overall mass transfer coefficient K_L and the superficial gas surface area a, separately. Using the PBM model is critical for an accurate estimation of a. The surface area of each bubble depends on the bubble size used. For a given gas holdup, the value of a will be different when different bubble sizes are used. In fact, the gas holdup was found to be influenced by the bubble size when single bubble size was used for simulation.

Then, K_L prediction is based on semi-empirical correlations. When water is used as the model fluid, it can be estimated using Equation 6.8.

$$K_L = C_1\sqrt{D_L}\left(\frac{\varepsilon\rho_L}{\mu_L}\right)^{0.25} \tag{6.8}$$

In previous works, two expressions for the proportionality constant C_1 used were: $2/(\pi^{-0.5})$ or 0.301(Kawase and Moo-Young, 1990). However, a factor of 3.75 is observed in the prediction of K_L when using these two values of C_1.

Since CMC is non-Newtonian, the K_L correlation has to be modified correspondingly. There exists a correlation for power law non-Newtonian fluids using Higbie penetration theory (Equation 6.9), which is derived in the same way as Equation 6.8 for water (Kawase et al., 1987). However, the power law viscosity model can only represent the viscosity of the CMC solution at very limited range of shear rate.

$$K_L = C_1\sqrt{D_L}\left(\frac{\varepsilon\rho_L}{K}\right)^{\frac{1}{2(1+n)}} \tag{6.9}$$

Following a similar derivation method, another correlation was derived for any non-Newtonian fluid provided that the local parameters, such as the shear stress and viscosity, are known from the CFD simulations.

Since the fluctuation velocity has been known to be close to the frictional velocity, it is calculated using Equation 6.10.

$$v' \approx v_0 = \sqrt{\tau/\rho} \tag{6.10}$$

The length scale is calculated using Equation 6.11.

$$l = \frac{(v')^3}{\varepsilon} \tag{6.11}$$

Then Kolmogoroff's time scale is given by Equation 6.12:

$$t_e = \frac{l}{v'} \tag{6.12}$$

Finally, according to Higbie's penetration theory, the liquid-phase mass transfer coefficient is given by Equation 6.13.

$$K_L = C_1 \sqrt{\frac{D_L}{t_e}} \tag{6.13}$$

The diffusivity of oxygen (D_L) in the liquid needs also to be considered carefully. The influence of the viscosity on the diffusivity may be neglected, such that the diffusivity in water can be used as was done by Moilanen et al. (2007). As an alternative, the variation of the diffusion coefficient with temperature and viscosity can be approximated using Equation 6.14. This equation is based on the Stokes-Einstein equation. Since the temperature was maintained at 28°C for all cases, the mass transfer coefficient only depends on viscosity. The diffusivity in water and the water viscosity can be used as the reference (Equation 6.15). However, with respect to the choice of C_1, more research needs to be done to see which value should be used or to find a more representative value.

$$\frac{D_{T_1}}{D_{T_2}} = \frac{T_1}{T_2}\frac{\mu_{T_2}}{\mu_{T_1}} \tag{6.14}$$

$$D = \frac{D_{water}\mu_{water}}{\mu} \tag{6.15}$$

As a result, the prediction of K_L for simulations with non-Newtonian fluid can have a relative wide range of values and will influence the results obtained through CFD.

In addition, it took over 1 hour to reach a steady state gas holdup in non-Newtonian fluids (Moilanen et al., 2006). It is still not practical to simulate a time on that scale even using the HPCVL.

6.5 Conclusion

In order to model the new mixing mechanism, the radial reciprocating plate impeller (RRPI), that was designed to handle highly viscous fermentation broth, a standard Rushton turbine was first simulated using computational fluid dynamics (CFD) with Fluent©. The experimental and predicted results for single phase simulations qualitatively agree with an existing correlation that predicts the power number under experimental conditions. Multiphase simulation was used to better represent the gas-liquid interactions using Eulerian multiphase model. The special movement of the new RRPI was simulated in Fluent© using journal files to change the speed of the impeller automatically. By comparing the simulation results to the experimental data, the high efficiency of the toothed belt used to drive the Rushton turbine impeller was confirmed, while the efficiency of the three-arm linkage system used to achieve the radial reciprocation for the RRPI was estimated to be around 80%. The uniformity of mixing with the 3-Rushton impeller and the RRPI was compared to each other by investigating the distribution of the liquid velocity, shear rate, and apparent viscosity when the non-Newtonian medium was used. Simulation results proved that the RRPI eliminated the presence of dead zones that usually form when the Rushton turbines were used in viscous medium.

6.6 References

Anonymous (2009). http://www.mitcalc.com/doc/tbelts/help/en/tbeltstxt.htm.

Audet, J., Lounes, M., and Thibault, J. (1996). Pullulan fermentation in a reciprocating plate bioreactor. Bioprocess Engineering, 15(4), 209-214.

Audet, J., Gagnon, H., Lounes, M., and Thibault, J. (1998). Polysaccharide production: Experimental comparison of the performance of four mixing devices. Bioprocess Engineering, 19(1), 45-52.

Beshay, K. R., Kratena, J., Fort, I., and Bruha, O. (2001) Power input of high-speed rotary impellers. Acta Polytechnica, 41(6), 18-23.

Brito-De La Fuente, E., Choplin, L., and Tanguy, P. A. (1997). Mixing with helical ribbon impellers: effect of highly shear thinning behaviour and impeller geometry. Chemical Engineering Research and Design, 75(A1), 45-52.

Bujalski, W., Nienow, A. W., Chatwin, S., and Cooke, M. (1987). The dependency on scale of power numbers of Rushton disc turbines. Chemical Engineering Science, 42(2), 317-326.

Gimbun, J., Rielly, C. D., and Nagy, Z. K. (2009). Modelling of mass transfer in gas-liquid stirred tanks agitated by Rushton turbine and CD-6 impeller: A scale-up study. Chemical Engineering Research & Design, 87(4A), 437-451.

Hasegawa, S., Nagatsuru, M., Shibutani, M., Yamamoto, S., and Hasebe, S. (1999). Productivity of concentrated hyaluronic acid using a Maxblend® fermentor. Journal of Bioscience and Bioengineering, 88(1), 68-71.

Hiruta, O., Yamamura, K., Takebe, H., Futamura, T., Iinuma, K., and Tanaka, H. (1997). Application of Maxblend Fermentor® for microbial processes. Journal of Fermentation and Bioengineering, 83(1), 79-86.

Kawase, Y., Halard, B., and Moo-Young, M. (1987). Theoretical prediction of volumetric mass transfer coefficients in bubble columns for Newtonian and non-Newtonian fluids. Chemical Engineering Science, 42(7), 1609-1617.

Kawase, Y., and Moo-Young, M. (1990). Mathematical models for design of bioreactors: applications of Kolmogoroff's theory of isotropic turbulence. The Chemical Engineering Journal, 43, B19-B41.

Kerdouss, F., Kiss, L., Proulx, P., Bilodeau, J. F., and Dupuis, C. (2005). Mixing characteristics of an axial-flow rotor: Experimental and numerical study. International Journal of Chemical Reactor Engineering, 3, 1-16.

Kerdouss, F., Bannari, A., Proulx, P., Bannari, R., Skrga, M., and Labrecque, Y. (2008). Two-phase mass transfer coefficient prediction in stirred vessel with a CFD model. Computers & Chemical Engineering, 32(8), 1943-1955.

Laakkonen, M., Moilanen, P., Alopaeus, V., and Aittamaa, J. (2007). Modelling local bubble size distributions in agitated vessels. Chemical Engineering Science, 62(3), 721-740.

Lin, Y., (2010) Improving the Production of High Molecular Weight Pullulan Using a New Radial Reciprocating Plate Impeller. Ph.D. Thesis, University of Ottawa, Ottawa, Canada.

Lounes, M., Audet, J., Thibault, J., and Leduy, A. (1995). Description and Evaluation of Reciprocating Plate Bioreactors. Bioprocess Engineering, 13(1), 1-11.

Moilanen, P., Laakkonen, M., and Aittamaa, J. (2006). Modeling aerated fermenters with computational fluid dynamics. Industrial & Engineering Chemistry Research, 45(25), 8656-8663.

Moilanen, P., Laakkonen, M., Visuri, O., and Aittamaa, J. (2007). Modeling local gas-liquid mass transfer in agitated viscous shear-thinning dispersions with CFD. Industrial & Engineering Chemistry Research, 46(22), 7289-7299.

Moilanen, P., Laakkonen, M., Visuri, O., Alopaeus, V., and Aittamaa, J. (2008). Modelling mass transfer in an aerated 0.2 m^3 vessel agitated by Rushton, Phasejet and Combijet impellers. Chemical Engineering Journal, 142(1), 95-108.

Moo-Young, M., and Blanch, H. W. (1981). Design of biochemical reactors, mass transfer criteria for simple and complex systems. Advances in Biochemical Engineering/Biotechnology , Eds., Springer, Berlin / Heidelberg, 19, 1-69.

Thibault, J., and LeDuy, A. (1999). Pullulan, microbial production methods. in Flickinger, M. C. and Drew, S. W. (Eds.), Encyclopedia of bioprocess technology: fermentation, biocatalysis, and bioseparation. New York: John Wiley & Sons; 2232-2247

CHAPTER 7

Optimization of *Aureobasidium pullulans* fermentation using a prototype radial reciprocating plate impeller

Yun Lin, Zisheng Zhang, and Jules Thibault
Department of Chemical and Biological Engineering
University of Ottawa
Ottawa, Ontario, K1N 6N5, Canada

Abstract

A prototype radial reciprocating plate impeller has been developed for fermentations characterized by highly viscous non-Newtonian broth. With this new impeller, the operating levels of several factors were determined in order to optimize pullulan production with *Aureobasidium pullulans* ATCC 42023 in a 22-L bioreactor using experimental designs. Because both high molecular weight (MW) and high concentration of pullulan were desired, the exopolysaccharide (EPS) concentration and the broth viscosity were used as optimization objective functions to be maximized. A 6-run uniform design was used in the screening stage. The best operating conditions found among the 6 runs were used as the starting point for further optimization. The two most influential factors for EPS concentration, the pH and the agitation speed, were further investigated in the second phase of the optimization. A minimal run-number D-optimal design that investigates up to second order effects was used in the optimization stage. Although the number of experiments performed was relatively small, the prediction accuracy of the model was satisfactory. An optimal zone of operating conditions for high MW pullulan production was identified. Under the validation condition to test the models at the predicted optimal point, 23.25 g/L EPS was produced at 78 h. This is equivalent to an EPS productivity of 0.30 $gL^{-1}h^{-1}$. The corresponding apparent viscosity of the broth was 0.38 Pa·s at the shear rate of 10 s^{-1}.

Keywords

Pullulan fermentation, Design of experiments, Radial reciprocating plate impeller, Oscillatory, Optimization

7.1 Introduction

Pullulan is a polysaccharide produced extracellularly by *Aureobasidium pullulans* through fermentation. It is a linear polymer of maltotriose subunits connected by α-(1→6) linkages (Catley and Whelan, 1971). Pullulan has several desirable properties such as water-soluble, edible, and biodegradable. And thus, it has many existing and potential applications in various industries (LeDuy et al., 1988; Singh, 2008). Pullulan has been mainly used as food additive for decades (Yuen, 1974). The relatively high price of this biopolymer has prevented its widespread utilization. Only until recently, it has found more applications in the biomedical and pharmaceutical industry where the price is of less concern (Leathers, 2003).

One of the many difficulties associated with pullulan fermentation is its highly viscous non-Newtonian broth. In fact, the high viscosity is the source of many other problems that are encountered in process monitoring, sampling, mixing and downstream separation (Thibault and LeDuy, 1999). Both pullulan concentration and its molecular weight (MW) are contributing factors to the broth viscosity (Leduy et al., 1974). There are certainly ways to control the viscosity to a relatively low level if only low MW pullulan is desired as the final product, however, pullulan yield may also be influenced (Sugimoto, 1978). When high concentration of high MW pullulan is desired, high viscosity is unavoidable.

Rushton turbine is the most popular mixing device for aerobic fermentations. It is efficient in providing a good oxygen mass transfer with relatively low energy consumption when the liquid viscosity is low. However, if the fermentation results in highly viscous shear-thinning broth, significant dead zones may exist, especially at large scale operations (Thibault and LeDuy, 1999). This would significantly reduce the effective fermentation volume, and thus, the overall efficiency of fermentation. One approach to solve this problem is to use close-clearance impellers, such as an axial reciprocating plate impeller (ARPI). Promising results were obtained in *A. pullulans* fermentations using a laboratory scale bioreactor equipped with an ARPI (Lounes et al., 1995; Audet et al., 1996, 1998; Gaidhani et al., 2003, 2005). However, its adaptation to a large-scale industrial

bioreactor could be difficult because of its characteristic oscillatory axial movement of a stack of perforated plates.

A new radial reciprocating plate impeller (RRPI) was designed to overcome this problem while trying to maintain most of the characteristics and benefits of the ARPI. The relationship between the power input per unit liquid volume and the overall oxygen mass transfer coefficient (K_La) was determined in our previous work using water and aqueous CMC solutions (Lin, 2010). In this work, the RRPI was used in a 22-L laboratory scale bioreactor to conduct *A. pullulans* fermentation in search of optimal operating conditions for the mass production of high MW pullulan.

There are many factors that could influence the pullulan fermentation process, such as strain (Gibson and Coughlin, 2002), substrate (Goksungur et al., 2003), dissolved oxygen level (Gibbs and Seviour, 1996), and mixing device (Audet et al., 1998). The most efficient method to find the optimal operating conditions is using design of experiments (DOE) (Goksungur et al., 2005; Singh et al., 2009). Usually, there are two stages: screening and optimization. In the screening stage, several potential factors are investigated together in order to find a few factors that are most influential. Then, these factors are further analyzed in the optimization stage to find the optimal operating conditions, usually using response surface methodology. However, there exists a myriad of choices with respect to the selection of experimental designs for both stages. In this work, it is desired to keep the number of runs to a minimum given the duration of an experiment. Therefore, a 6-run uniform design was used to investigate 5 factors in the screening stage. Then, a 6-run (excluding the duplicate at the center point) D-optimal design investigating the two most influential factors, which were identified during the screening stage, was used in the optimization stage.

7.2 Materials and Methods

7.2.1 Experimental designs

7.2.1.1 Uniform design

Uniform designs (UD) do not assume any model ahead of experiments, but try to allocate experimental points uniformly scattered in the experimental domain (Fang, 1980; Wang and Fang, 1981). A type $U_n(n^s)$ UD can investigate *s* factors with *n* experiments, where *n* can be any integer greater than *s*. In the screening stage, a 6-run UD was used to investigate 5 factors: $(NH_4)_2SO_4$ (nitrogen source) concentration, pH, agitation speed, aeration rate, and temperature (Columns 2-6 of Table 7.1).

7.2.1.2 D-optimal design

Optimal designs have several variants based on A-, D-, G-, and V-optimality. D-optimal design is more popular than the others. It is generated by seeking the maximum of the determinant of the information matrix of the design, based on a pre-determined model and the researcher's requirement on the number of experiments (NIST/SEMATECH, 2009).

In the optimization stage, the best operating conditions from the UD results were used as the center point of the D-optimal design. The D-optimal design was generated using JMP IN software (Sall et al., 2001) by specifying the two most influential factors as the independent variables and choosing the minimal number of runs (6 in this investigation) to investigate up to 2^{nd} order effects. The factor levels of the two most influential process variables, the pH and agitation speed, as well as the experimental results, are presented in Table 7.2.

Table 7.1 The $U_6(6^5)$ uniform design matrix and the experimental results at 102 h.

Run #	X_1 Nitrogen Concentration, gL^{-1}	X_2 pH	X_3 Agitation Speed, rpm (motor speed)	X_4 Aeration Rate, $Lmin^{-1}$	X_5 Temperature, °C	EPS, gL^{-1}	Ln(Viscosity), mPa·s	DCW, gL^{-1}
1	0.5	4.5	125	11	29	29.00	5.42	7.28
2	0.3	7.0	95	9	31	3.95	0.93	2.15
3	0.7	6.0	110	7	26	12.55	2.71	4.44
4	0.9	5.0	65	8	27	11.83	3.43	4.00
5	0.1	5.5	50	10	27	12.88	3.81	2.80
6	1.1	6.5	80	12	28	8.34	1.48	6.58

Table 7.2 The D-optimal design matrix and the experimental results at 78 h.

Run #	X_2 pH	X_3 Agitation Speed, rpm (motor speed)	EPS concentration, gL^{-1}	Ln (Viscosity), mPa·s	DCW, gL^{-1}
1	4.5	125	22.33	5.70	6.20
7	4.5	125	24.43	5.63	6.23
8	5.5	150	25.08	3.94	5.68
9	3.5	100	15.65	5.52	4.90
10	5.5	100	10.39	2.33	3.30
11	3.5	150	22.85	6.11	7.05
12	4.5	100	19.83	5.86	5.95

7.2.2 Microorganism and culture conditions

Among the two strains of *A. pullulans* that were tested in Erlenmeyer flasks (Lin et al., 2007), ATCC 42023 was selected for the bioreactor experiments due to better pullulan production performance. Freeze-dried culture was purchased from ATCC. It was then revived following the accompanying instructions. The first generation of ATCC 42023 from the freeze-dried culture was incubated in malt extract solution (Blakeslee's formula without agar). After 1 day of incubation, the resulting culture was dispensed into dozens of 2 ml microtubes. These microtubes were stored in a -80°C refrigerator for long-term storage. The inoculums for the bioreactor experiments were prepared in 1 L flasks containing 600 mL medium (5% of the production medium volume). The inoculum medium has the same composition as the production medium used in the bioreactor, and the initial pH is the same as the controlled pH in the bioreactor. Each time, one microtube was thawed quickly and used to inoculate the 600 mL medium. The inoculums were incubated for 48 h in an orbital shaker (Barnstead/Lab-Line Max^{Q} 5000) running at 200 rpm and at the same temperature at which the associated bioreactor experiments were conducted.

7.2.3 Bioreactor and the radial reciprocating plate impeller

The bioreactor, constructed in our laboratory, has an inner diameter of 22.8 cm and a height of 55 cm, which gives a total volume of 22 L. The working volume used in all experiments was 12 L. At the bottom of the bioreactor, a plate perforated with 100 1-mm diameter holes was used as air sparger. The perforations are evenly allocated along three concentric rings, which contain 16, 32 and 52 holes, respectively. The diameters of these rings are 7.6, 13.25 and 18.75 cm, respectively. A jacket for water circulation is built on the outside of the bioreactor to maintain the fermentation broth at a constant temperature.

The RRPI was designed to combine the advantages of the reciprocating perforated plates of the ARPI and the rotational motion of a typical Rushton turbine by adopting a reciprocating partial rotation of perforated blades spanning a portion of the cylindrical tank. The design of this mixer was inspired by the oscillatory movement of a clothes washing machine. The back and forth displacement is achieved using a simple three-arm linkage system (Figure 7.1). One arm is fastened to the bioreactor shaft and another to the motor shaft. The third arm connects the first two arms together. The effective lengths of the first (R), second (r), and third arms (L) are 10.4 cm, 2.5 cm and 13.2 cm, respectively. The distance between the two shafts (l) is 14 cm. While the motor shaft rotates at a constant speed in one direction, the bioreactor shaft rotates back and forth such that each impeller blade covers a region of the fermenter that spans an angle of approximately 46° (Lin, 2010).

The mixing assembly of the RRPI is comprised of two hubs, which are positioned with a 30° angle relative to each other. Six equally-spaced blades are mounted on each hub. Figure 7.2 shows the schematic diagram of the bottom hub of the RRPI which is very similar to a typical Rushton turbine. The blades are however much larger than those of a Rushton turbine and each blade is perforated with a series of 2-cm diameter holes arranged in an equilateral triangle pattern. The distance between the centers of each adjacent hole is 3 cm. Each blade is a rectangular plate with a width of 9 cm and a height of 12 cm. The diameter of the impeller assembly is 21.5 cm which leaves 0.65 cm spacing between the tips of the blades and the internal wall of the bioreactor. Two of the blades on

the upper hub were cut at appropriate locations to accommodate the fermentation probes (temperature, pH and dissolved oxygen).

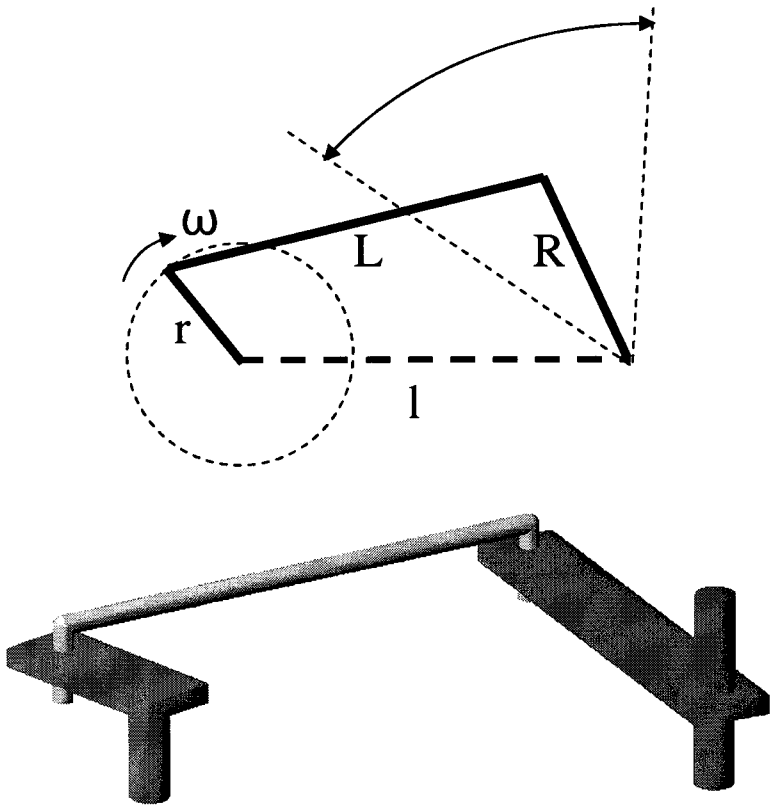

Figure 7.1 2D and 3D illustration of the RRPI drive mechanism.

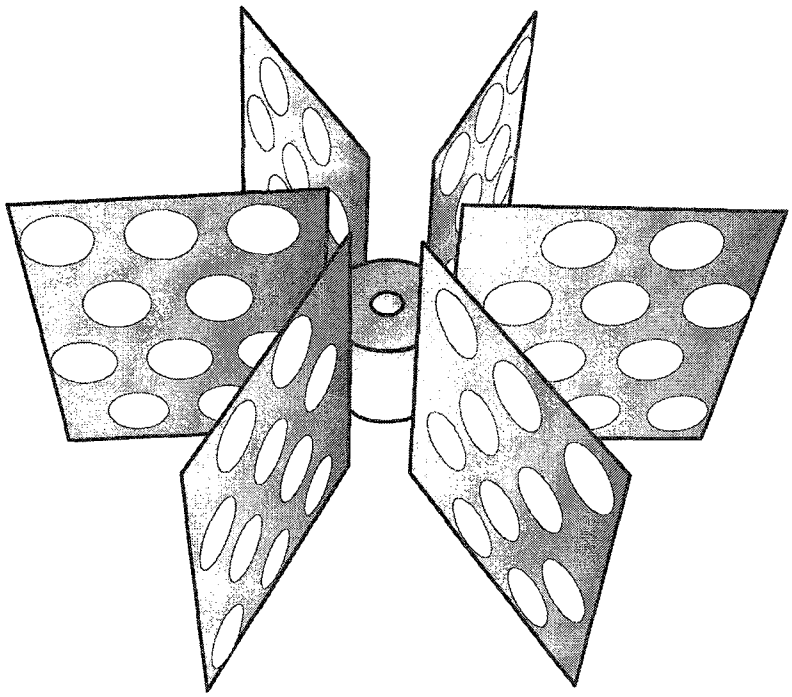

Figure 7.2 Schematic diagram of the bottom hub of the RRPI.

7.2.4 Fermentation conditions

In the screening stage, the production medium had the following composition (gL^{-1}): sucrose 50.0, yeast extract 0.2, K_2HPO_4 5.0, $MgSO_4.7H_2O$ 0.2, NaCl 1.0 and varying concentration of $(NH_4)_2SO_4$ as listed in Table 7.1. The pH was adjusted to the set value using 5M HCl before autoclaving the medium. Agitation, aeration and temperature were controlled at the desired values according to Table 7.1. During the fermentation, the pH of the broth was monitored and maintained at the set value by supplying 2M NaOH.

In the optimization stage, the $(NH_4)_2SO_4$ concentration, aeration, and temperature were fixed at the best operating conditions found in the screening stage: 0.5 gL^{-1}, 11 $Lmin^{-1}$, and 29°C, respectively. The pH and agitation speed were varied according to the values given in the experimental design as shown in Table 7.2.

7.2.5 Analytical techniques

Approximately 30 mL sample was taken from the bioreactor every 12 h except that the second sample was taken at 6 h after inoculation. Eight mL out of the 30 mL sample were centrifuged at 14100 g for 15 min to separate the biomass and the supernatant. However, if the viscosity of the sample was very high, only 4 mL were used and it was diluted with 1 volume of distilled de-ionized (DD) water prior to centrifuging. The supernatant was conserved. The cell pellets were washed with 4 mL DD water, and centrifuged again. The second supernatant was combined with the first one for exopolysaccharide (EPS) precipitation by adding the equivalent of 2 volumes (24 mL) of 99% ethanol. The cells were suspended and transferred to a pre-dried and pre-weighted aluminum dish, and dried in an oven at 105°C overnight before weighting again. The precipitated EPS together with the mother liquor were kept at 4°C in a refrigerator for 24 h before filtration through a pre-dried and pre-weighted glass microfiber filter (Whatman type GFA). The filtered EPS was also dried at 105°C for 24 h and then weighted.

About 12 mL of the sample were used to determine the viscosity of the broth using a rheometer (Anton Paar's Physica M301) with a double-gap concentric cylinder measuring system (Anton Paar's DG42). The shear rate was varied and controlled between 0.1 and 1000 s^{-1}. The temperature was controlled at 28°C regardless of the bioreactor temperature.

For monitoring purposes, the concentrations of sucrose, glucose, and fructose in the broth supernatant were analyzed using a Waters' Sugar-PAK I column in a Waters' Breeze HPLC system. The column was maintained at 90°C. The recommended mobile phase, 50 mg/L calcium disodium ethylene diamine tetraacetate (calcium disodium EDTA), was running at 0.5 mL/min. The broth supernatant was diluted 4 times with the mobile phase before filtration through 0.45 μm membrane filter (Millipore). After filtration, a 20 μL sample was injected into the HPLC system. Various concentrations of ACS reagent sucrose, glucose, and fructose (Sigma-Aldrich) were used to construct the calibration curves.

7.3 Results and Discussion

7.3.1 Screening using a uniform design

Like many other processes, pullulan production is influenced by multiple factors. Five potential factors were selected, based on the literature and prior experiments, to be investigated in the screening stage (Table 7.1): $(NH_4)_2SO_4$ concentration, pH, agitation speed, aeration rate, and temperature. Even though there are recommended values for each of these factors in the literature (Goksungur et al., 2003; Lacroix et al., 1985; Gibbs and Seviour, 1996; Madi et al., 1996; Chi and Zhao, 2003), they may not be the optimal values in a different experimental setup. In fact, some conflicting recommendations are reported (Youssef et al., 1999). This is probably because the influence of factors may change under different operating conditions, which is usually explained as factor interactions. In this work, since a new mixing mechanism was used, no prior knowledge on the best agitation speed of the new impeller existed. As a result, one of the objectives of this study was to find a suitable agitation speed for this new impeller. In addition, it is possible that using this new mixing mechanism may change the influence of other factors. It was therefore decided to use experimental designs to identify the most influential factors, and to hopefully reveal the directions leading to better pullulan productivity in the screening stage.

Screening is usually done with 2-level fractional factorial designs. For a 5-factor problem, the minimum number of runs is 8 in order to estimate the influence of all main factors and ignore any higher order effects and interactions. Although fractional factorial design is a powerful technique, it is not very informative until a sufficient number of runs are carried out in order to estimate the 2-factor interactions together with the main factor effects. For a 5-factor problem, it requires 16 runs. This is still a large number, considering that only one experiment can be done at once in the bioreactor, and each experiment takes a minimum of 8 days. As an alternative, uniform design was chosen due to its smaller number of runs and its ability to better cover the interior region of the experimental domain (Lin et al., 2009). To investigate 5 factors, the minimum number of uniform design runs is 6. In addition, since it is based on the principle of distributing the

design points uniformly over the experimental domain, the best condition found among the uniform design results should make a good starting point for the subsequent optimization stage, even if it cannot detect meaningful main effects and interactions of factors.

The 6-run uniform design that was used in the screening stage is tabulated online (Anonymous, 2009). The design and the corresponding pullulan production results are shown in Table 7.1. The viscosity of most broth samples showed non-Newtonian behavior. The apparent viscosity measured at the shear rate of 10 s^{-1} was used as one of the responses. The data obtained at 102 h was used for analysis, because the sugar content was almost depleted at that point, and afterwards, the EPS concentration remained almost the same for the best experiment (Run 1) among the 6 runs (Figure 7.3).

Assuming there are only main factor effects, that is no factor interactions and higher order effects, the factor effects on the EPS concentration, the broth viscosity and the dry cell weight (DCW) are listed in Table 7.3. A high positive value implies that an increase in the associated factor, which is scaled between -1 to 1 for analysis, will lead to a significant increase of the output variable, and vice-versa.

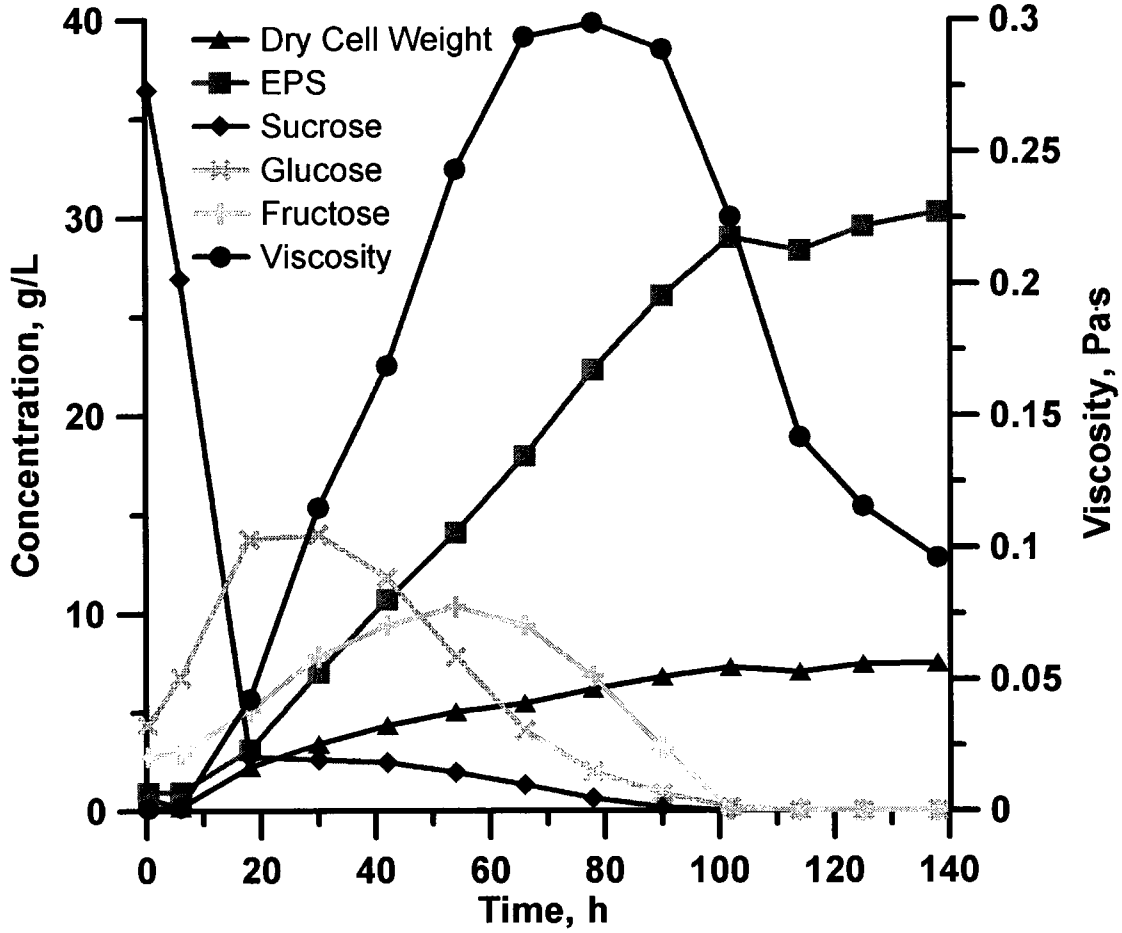

Figure 7.3 Fermentation kinetics of Run 1.

Table 7.3 The main factor effects on the responses

Factor	EPS concentration, g/L	Ln (Viscosity), mPa·s	DCW, g/L
X_1	-1.58	-0.480	1.326
X_2	-9.02	-2.033	1.006
X_3	5.09	0.261	1.235
X_4	2.97	0.209	1.453
X_5	-1.49	-0.300	-0.546

7.3.2 Optimization using a D-optimal design

As expected, the influence of the various factors on the two responses that are to be optimized, the EPS concentration and the broth viscosity, is not the same (Table 7.3).

Although it is desired to optimize both parameters at the same time, the EPS production has a higher priority if there is conflict. Since pH (X_2) and the agitation speed (X_3) are the most influential effects on the EPS concentration, these two factors are further investigated using surface response methodology with a D-optimal design. Using the custom design feature of the JMP IN 4.0.4 academic version (Sall et al., 2001), a 6-run D-optimal design was generated by specifying that 2 factors are to be investigated up to their 2^{nd} order effects with the minimum number of runs. A replicate at the center point is added to the design to estimate the pure error of the experiments. Since Run 1 of the uniform design showed the best results for all three responses, it was used as the center point for this D-optimal design. The upper level of the agitation speed was chosen to be 150 rpm mainly due to the mechanical strength limitation of the three-arm linkage system. In fact, the two runs that were operated at 150 rpm did not last the intended 102 h fermentation time without the failure of the connecting rod (the third arm of the linkage system) occurring. The fatigue of the connecting rod is probably caused by the high frequency oscillatory movement. Although 150 rpm is not a high rotation speed, it corresponds to a 2.5 Hz oscillation of the perforated blades. As a result, the experimental results were analyzed at 78 h instead. The responses are listed in Table 7.2 together with the design matrix.

Fitting the data of this 7-run D-optimal design to a second degree polynomial model, the model for EPS concentration at 78 h was found to be:

$$C_{EPS} = 23.38 - 0.758X_2 + 5.473X_3 - 6.81X_2^2 + 1.923X_3^2 + 1.873X_2X_3 \quad (7.1)$$

and the model representing the broth apparent viscosity at the shear rate of 10 s^{-1} at 78 h was found to be:

$$Ln(\text{Viscosity}) = 5.663 - 1.341X_2 + 0.550X_3 - 1.938X_2^2 + 0.752X_3^2 + 0.255X_2X_3 \quad (7.2)$$

The predicted surface responses of both models as a function of pH and agitation speed exhibit saddle points. However, the contour plots indicate that within the experimental domain tested, both EPS concentration and the viscosity of the broth will increase to a higher value at the operating conditions where the pH is 4.5 (level 0) and the agitation speed is 150 rpm (level 1) (Figures 7.4 and 7.5).

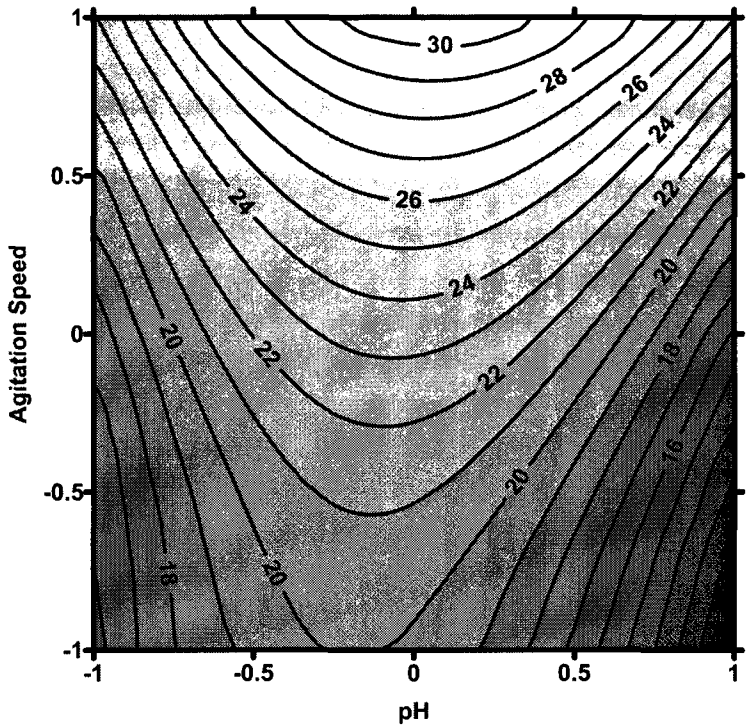

Figure 7.4 Contour plot for EPS concentration based on the model from 7-run D-optimal design. Axes are scaled as follows: Agitation speed [100-150 rpm] and pH [3.5-5.5]

To validate the model for its ability to identify the optimal operating conditions within the explored domain, a validation run was carried out at a pH of 4.5 and an agitation speed of 150 rpm. At 78 h, 23.25 g/L of EPS was produced and the broth viscosity at the shear rate of 10 s^{-1} was 0.380 Pa·s (ln(viscosity) = 5.94 mPa·s). These values were significantly lower than the model predicted EPS of 30.78 g/L and broth viscosity of 1.054 Pa·s (ln(viscosity) = 6.96 mPa·s), indicating that the models are satisfactory for rough estimation only. The prediction discrepancy of the models is mainly caused by the small number of experiments carried out. A standard central composite design (CCD) for 2 factors requires at least 9 runs. In our D-optimal design, which is actually a reduced on-face CCD, only 6 design points were investigated to determine the 6 parameters of the second degree polynomial model.

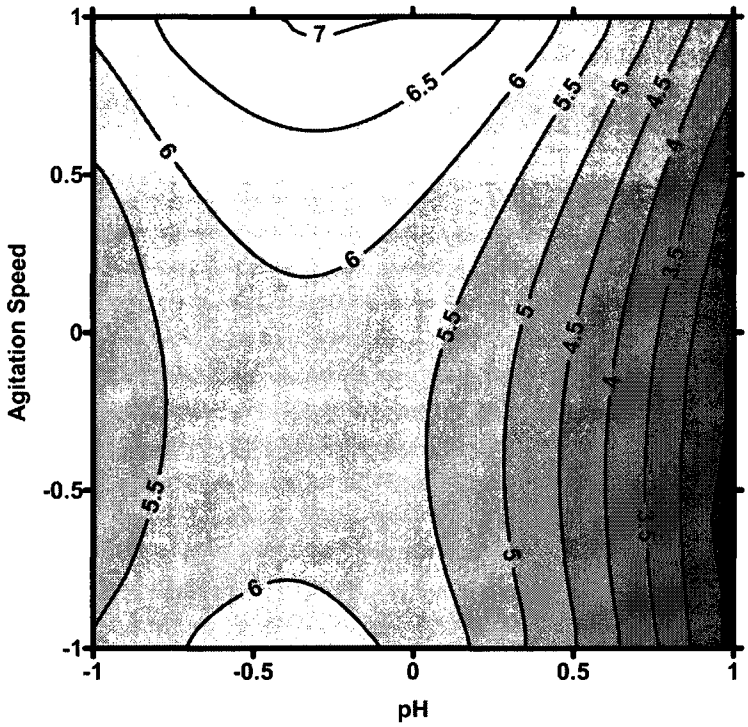

Figure 7.5 Contour plot for broth logarithm apparent viscosity at the shear rate of 10 s^{-1} based on the model from 7-run D-optimal design. Axes are scaled as follows: Agitation speed [100-150 rpm] and pH [3.5-5.5]

As suggested by our previous investigation on the efficiency of DOE, the inclusion of a few additional data points into the design is quite useful for better model prediction when the number of runs is small (Lin et al., 2009). So this validation point, which is also one of the star points for an on-face CCD, is included to fit the second degree polynomial model for better prediction. Thus, the following models are obtained:

$$C_{EPS} = 23.38 - 0.758X_2 + 4.218X_3 - 3.048X_2^2 - 1.84X_3^2 + 1.873X_2X_3 \quad (7.3)$$

$$Ln(\text{Viscosity}) = 5.663 - 1.341X_2 + 0.379X_3 - 1.425X_2^2 + 0.239X_3^2 + 0.255X_2X_3 \quad (7.4)$$

The contour plots of the new responses indicate that the shape of the response surface is very similar. However, the magnitude of the responses is decreased significantly (Figures 7.6 and 7.7). The predicted surface response of the broth viscosity model remains a saddle point, whereas the EPS concentration model exhibits a maximum of 25.98 g/L at pH 4.77 (level 0.27) and at an agitation speed of 157 rpm (level 1.28). The corresponding prediction of the broth viscosity is 0.478 Pa·s (ln(viscosity) = 6.17 mPa·s). However, the

condition for the maximum EPS concentration is not too far away from the validation condition, and so are their corresponding model predictions (Table 7.4). The slightly higher EPS prediction is obtained by compromising on the viscosity.

In addition, the experimental results of both the EPS concentration and the broth viscosity obtained at the validation point were quite close to those obtained at the two center points. This indicates that both conditions are on a plateau of optimal high concentration and high MW pullulan production. This is also observed from the contour plots, because the iso-lines are located far apart in that region for both the EPS concentration and the broth viscosity (Figures 7.6 and 7.7). This plateau is probably formed due to the important impact of the highly viscous non-Newtonian broth on the microorganisms. When the viscosity is very high, the transfer of nutrients to the cells and the removal of wastes from the cells are hindered. Thus, the production of pullulan may be limited to the availability of nutrients. An increase of the agitation speed from 100 rpm to 125 rpm may have helped to relieve this problem, but a further increase of the speed to 150 rpm probably did not bring additional improvement. As a result, the microorganisms produce similar quantity of pullulan under the two higher agitation speeds.

For this reciprocating radial mixing mechanism, varying the rotation speed is not the only way to change the power input for mixing in the bioreactor. There is another parameter that can be adjusted, the amplitude of the oscillatory movement. This can be done by changing the lengths of the three arms in the linkage system. If higher power input for mixing is required for a better productivity of pullulan, increasing the amplitude is an alternative to increasing the rotation speed. In addition, using larger oscillation amplitude, instead of higher rotation speed, may have lower physical requirement on the whole system's mechanical strength due to lower oscillatory frequency created.

Table 7.4 Comparison of experimental data and the model predictions.

Run #	X_2 pH	X_3 Agitation Speed, rpm	Experimental data		Model prediction	
			EPS concentration, gL^{-1}	Ln(Viscosity), mPa·s	EPS concentration, gL^{-1}	Ln(Viscosity), mPa·s
1	0	0	22.33	5.70	23.38	5.66
7	0	0	24.43	5.63	23.38	5.66
8	1	1	25.08	3.94	23.83	3.77
9	-1	-1	15.65	5.52	16.90	5.69
10	1	-1	10.39	2.33	11.64	2.50
11	-1	1	22.85	6.11	21.60	5.94
12	0	-1	19.83	5.86	17.32	5.52
Validation	0	1	23.25	5.94	25.76	6.28
Max EPS	0.27	1.28	-	-	25.99	6.17

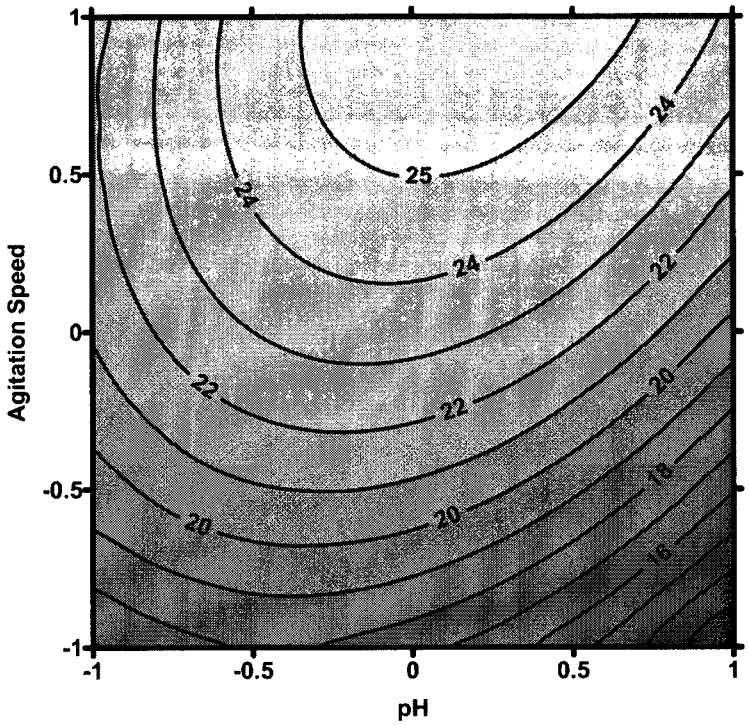

Figure 7.6 Contour plot for EPS concentration based on the model from 8-run D-optimal design. Axes are scaled as follows: Agitation speed [100-150 rpm] and pH [3.5-5.5]

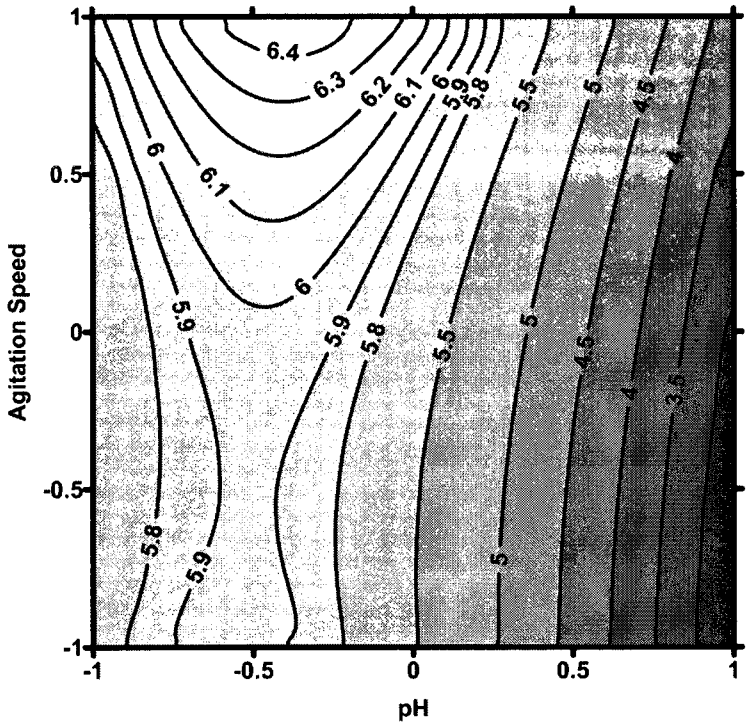

Figure 7.7 Contour plot for broth logarithm apparent viscosity at the shear rate of 10 s^{-1} based on the model from 8-run D-optimal design. Axes are scaled as follows: Agitation speed [100-150 rpm] and pH [3.5-5.5]

7.4 Conclusions

A prototype radial reciprocating plate impeller was designed to handle fermentations with highly viscous non-Newtonian broth. It was tested for pullulan production using *A. pullulans* in a laboratory scale bioreactor. In the screening stage, five factors were investigated using a 6-run uniform design. The best condition found in the screening was used as the center point of a D-optimal design for further investigation on the two most influential factors in the optimization stage. Since high concentration of high MW pullulan is desired, both the EPS concentration and the broth viscosity were optimized at the same time. An optimal plateau for high MW pullulan production was found. Under the validation conditions at 78 h, 23.25 g/L EPS was produced with a broth apparent viscosity of 0.38 Pa·s at the shear rate of 10 s^{-1}. This is equivalent to an EPS productivity of 0.30 $gL^{-1}h^{-1}$.

7.5 References

Anonymous, (2009). The Uniform Design. http://www.math.hkbu.edu.hk/UniformDesign/.

Audet, J., Lounes, M., and Thibault, J. (1996). Pullulan fermentation in a reciprocating plate bioreactor. Bioprocess Engineering, 15(4), 209-214.

Audet, J., Gagnon, H., Lounes, M., and Thibault, J. (1998). Polysaccharide production: Experimental comparison of the performance of four mixing devices. Bioprocess Engineering, 19(1), 45-52.

Catley, B. J. and Whelan, W. J. (1971). Observations on Structure of Pullulan. Archives of Biochemistry and Biophysics, 143(1), 138-142.

Chi, Z. M. and Zhao, S. Z. (2003). Optimization of medium and cultivation conditions for pullulan production by a new pullulan-producing yeast strain. Enzyme and Microbial Technology, 33(2-3), 206-211.

Fang, K. T. (1980). The Uniform Design: Application of Number-theoretic Methods in Experimental Design. Acta Math. Appl. Sin. 3, 363-372.

Gibbs, P. A. and Seviour, R. J. (1996). Does the agitation rate and/or oxygen saturation influence exopolysaccharide production by *Aureobasidium pullulans* in batch culture? Applied Microbiology and Biotechnology, 46(5-6), 503-510.

Gibson, L. H. and Coughlin, R. W. (2002). Optimization of high molecular weight pullulan production by *Aureobasidium pullulans* in batch fermentations. Biotechnology Progress, 18(3), 675-678.

Goksungur, Y., Dagbagli, S., Ucan, A., and Guvenc, U. (2005). Optimization of pullulan production from synthetic medium by *Aureobsidium pullulans* in a stirred tank reactor by response surface methodology. Journal of Chemical Technology and Biotechnology, 80(7), 819-827.

Goksungur, Y., Ucan, A., and Guvenc, U. (2004). Production of pullulan from beet molasses and synthetic medium by *Aureobasidium pullulans*. Turkish Journal of Biology, 28(1), 23-30.

Lacroix, C., Leduy, A., Noel, G., and Choplin, L. (1985). Effect of pH on the Batch Fermentation of Pullulan from Sucrose Medium. Biotechnology and Bioengineering, 27(2), 202-207.

Leathers, T. D. (2003). Biotechnological production and applications of pullulan. Applied Microbiology and Biotechnology, 62(5-6), 468-473.

LeDuy, A., Choplin, L., Zajic, J. E., and Loung J. H. T. (1988). Pullulan. In H. F. Mark, N. M. Bikales, C. G. Overberger, G. Menges, and J. I. Kroschwitz (Eds.). Encyclopedia of polymer science and engineering (Vol. 13, pp. 650-660). New York: John Wiley & Sons.

Leduy, A., Marsan, A. A., and Coupal, B. (1974). Study of Rheological Properties of A Non-Newtonian Fermentation Broth. Biotechnology and Bioengineering, 16(1), 61-76.

Lin, Y., Zhang, Z. S., and Thibault, J. (2007). *Aureobasidium pullulans* batch cultivations based on a factorial design for improving the production and molecular weight of exopolysaccharides. Process Biochemistry, 42(5), 820-827.

Lin, Y., Zhang, Z. S., and Thibault, J. (2009). Comparison of experimental designs using neural networks. The Canadian Journal of Chemical Engineering, 87(6), 965-971.

Lin, Y., (2010) Improving the Production of High Molecular Weight Pullulan Using a New Radial Reciprocating Plate Impeller. Ph.D. Thesis, University of Ottawa, Ottawa, Canada.

Lounes, M., Audet, J., Thibault, J., and Leduy, A. (1995). Description and Evaluation of Reciprocating Plate Bioreactors. Bioprocess Engineering, 13(1), 1-11.

Madi, N. S., McNeil, B., and Harvey, L. M. (1996). Influence of culture pH and aeration on ethanol production and pullulan molecular weight by *Aureobasidium pullulans*. Journal of Chemical Technology and Biotechnology, 65(4), 343-350.

NIST/SEMATECH (2009). e-Handbook of Statistical Methods. www.itl.nist.gov/div898/handbook.

Sall, J., Lehman, A., and Creighton, L. (2001) JMP Start Statistics. Duxbury, Pacific Grove, CA, USA

Singh, R. S., Saini, G. K., and Kennedy, J. F. (2008). Pullulan: Microbial sources, production and applications. Carbohydrate Polymers, 73(4), 515-531.

Singh, R. S., Singh, H., and Saini, G. K. (2009). Response Surface Optimization of the Critical Medium Components for Pullulan Production by *Aureobasidium pullulans* FB-1. Applied Biochemistry and Biotechnology, 152(1), 42-53.

Sugimoto, K. (1978). Pullulan: Production and Applications. Fermentation and Industry, 36(2), 98-108.

Thibault, J., and LeDuy, A. (1999). Pullulan, microbial production methods. In Flickinger, M. C. and Drew, S. W. (Eds.), Encyclopedia of bioprocess technology: fermentation, biocatalysis, and bioseparation. New York: John Wiley & Sons; 2232-2247

Wang, Y., and Fang, K. T. (1981). A Note on Uiform Distribution and Experimental Design. Kexue TongBao (Chin. Sci. Bull.), 26, 485-489.

Youssef, F., Roukas, T., and Biliaderis, C. G. (1999). Pullulan production by a non-pigmented strain of *Aureobasidium pullulans* using batch and fed-batch culture. Process Biochemistry, 34(4), 355-366.

Yuen, S. (1974). Pullulan and Its Applications. Process Biochemistry, 9(9), 7-9 & 22.

CHAPTER 8

Conclusions

This research project had a main objective to improve the mass production of high MW pullulan through fermentations. The general fermentation and analysis procedures were established with experiments in Erlenmeyer flasks. Influential operating factors were revealed for this small scale system using 2-level fractional factorial designs. Useful information was also obtained for further investigation in a laboratory scale bioreactor. In order to find an efficient experimental design, popular designs were compared for their performance using artificial neural networks. Uniform designs were found to be more efficient when the process shows significant non-linear behavior. And thus, it was used in the screening stage of the bioreactor investigations. In order to adequately mix the highly viscous non-Newtonian broth that is usually encountered in typical *A. pullulans* fermentation, a new mixing mechanism, the radial reciprocating plate impeller, was designed, built and tested. This new impeller provides equivalent or better mass transfer rate at a given power input per unit volume than the other two impellers that were used in this investigation: the triple Rushton impeller and the axial reciprocating perforated plates. So this new impeller was shown to be able to handle rheologically evolving broth better than both the triple Rushton impeller and the axial reciprocating plate impeller. This finding is also supported by the simulations performed using computational fluid dynamics. A series of fermentation runs were then performed in the laboratory scale bioreactor equipped with the RRPI for the optimization of the production of high MW pullulan. Although the number of experiments performed was relatively small, the prediction accuracy of the prediction model was found to be satisfactory. More importantly, the best exopolysaccharide productivity found (0.30 $gL^{-1}h^{-1}$) is significantly higher than the best result (0.19 $gL^{-1}h^{-1}$) obtained from Erlenmeyer flasks while keeping the MW of pullulan or, equivalently, the broth viscosity at a relatively high level. This represents an increase of 58% in productivity.

8.1 Recommendations

CFD is a powerful technique that allows gaining a deeper insight into the mixing of complex medium in a cost effective manner. For the best representation of the actual situation, the population balance model (PBM) should be used especially when the medium is non-Newtonian.

Prediction of mass transfer coefficients (K_La) using CFD has already been demonstrated (Bakker 1992; Moilanen et al., 2006, 2007; Kerdouss et al., 2008; Gimbun et al., 2009). It is usually done by predicting K_L and a separately. However, there are a number of issues related to the prediction of K_L using existing correlations, which may raise some doubts on the validity of its prediction and particular data related to this parameter should be examined carefully as it does not possess the same accuracy as other parameters predicted by CFD. Nevertheless, the capability of predicting K_La is very important.

The new impeller, as designed in this investigation, is by no means the optimal design. It should be further improved. CFD simulations can be used to test the influence of blade perforation sizes, position of the blades, diameter of the impeller assembly on the power requirement, mixing uniformity and K_La.

In this study, the frequency of the RRPI was changed to vary the power input. Under high frequencies, a significant stress was imposed on the bioreactor system especially on the three-arm linkage system. This has created some problems in conducting bioreactor experiments. One possible solution to this problem is changing the reciprocating amplitude by using different arm lengths on the three-arm linkage system alone or together with changing the frequency.

In this research project, all the fermentations were performed in batch mode. Fed-batch mode is also a promising method, although it has not been used in commercial production of pullulan. Several researches have been carried out using this method (Shin et al., 1987; Youssef et al., 1999). Much higher exopolysaccharide productivity, 0.90 $gL^{-1}h^{-1}$, was achieved by Moscovici et al. (1996).

8.2 References

Bakker A. (1992). Hydrodynamics of Stirred Gas-Liquid Dispersions. Ph.D. Thesis, Delft University of Technology, Delft, The Netherlands.

Gimbun, J., Rielly, C. D., and Nagy, Z. K. (2009). Modelling of mass transfer in gas-liquid stirred tanks agitated by Rushton turbine and CD-6 impeller: A scale-up study. Chemical Engineering Research & Design, 87(4A), 437-451.

Kerdouss, F., Bannari, A., Proulx, P., Bannari, R., Skrga, M., and Labrecque, Y. (2008). Two-phase mass transfer coefficient prediction in stirred vessel with a CFD model. Computers & Chemical Engineering, 32(8), 1943-1955.

Moilanen, P., Laakkonen, M., and Aittamaa, J. (2006). Modeling aerated fermenters with computational fluid dynamics. Industrial & Engineering Chemistry Research, 45(25), 8656-8663.

Moilanen, P., Laakkonen, M., Visuri, O., and Aittamaa, J. (2007). Modeling local gas-liquid mass transfer in agitated viscous shear-thinning dispersions with CFD. Industrial & Engineering Chemistry Research, 46(22), 7289-7299.

Moscovici, M., Ionescu, C., Oniscu, C., Fotea, O., Protopopescu, P., and Hanganu, L. D. (1996). Improved exopolysaccharide production in fed-batch fermentation of *Aureobasidium pullalans*, with increased impeller speed. Biotechnology Letters, 18(7), 787-790.

Shin, Y. C., Kim, Y. H., Lee, H. S., Kim, Y. N., and Byun, S. M. (1987). Production of Pullulan by a Fed-Batch Fermentation. Biotechnology Letters, 9(9), 621-624.

Youssef, F., Roukas, T., and Biliaderis, C. G. (1999). Pullulan production by a non-pigmented strain of *Aureobasidium pullulans* using batch and fed-batch culture. Process Biochemistry, 34(4), 355-366.